



<https://theses.gla.ac.uk/>

Theses Digitisation:

<https://www.gla.ac.uk/myglasgow/research/enlighten/theses/digitisation/>

This is a digitised version of the original print thesis.

Copyright and moral rights for this work are retained by the author

A copy can be downloaded for personal non-commercial research or study,
without prior permission or charge

This work cannot be reproduced or quoted extensively from without first
obtaining permission in writing from the author

The content must not be changed in any way or sold commercially in any
format or medium without the formal permission of the author

When referring to this work, full bibliographic details including the author,
title, awarding institution and date of the thesis must be given

Enlighten: Theses

<https://theses.gla.ac.uk/>
research-enlighten@glasgow.ac.uk

**DEVELOPMENT AND APPLICATION OF TWO NEW
BRUSHLESS RELUCTANCE MOTOR DRIVES.**

Alan J. Hutton

**Submitted for the degree of
Master of Science**

**Department of Electronics and
Electrical Engineering
University of Glasgow**

November 1990

© Alan J. Hutton B.Eng 1990

ProQuest Number: 11007597

All rights reserved

INFORMATION TO ALL USERS

The quality of this reproduction is dependent upon the quality of the copy submitted.

In the unlikely event that the author did not send a complete manuscript and there are missing pages, these will be noted. Also, if material had to be removed, a note will indicate the deletion.



ProQuest 11007597

Published by ProQuest LLC (2018). Copyright of the Dissertation is held by the Author.

All rights reserved.

This work is protected against unauthorized copying under Title 17, United States Code
Microform Edition © ProQuest LLC.

ProQuest LLC.
789 East Eisenhower Parkway
P.O. Box 1346
Ann Arbor, MI 48106 – 1346

ACKNOWLEDGEMENTS

I would like to thank Professor J. Lamb for the provision of the research and computing facilities in the Department of Electronics and Electrical Engineering.

I would also like to express my gratitude to Professor T.J.E. Miller, my supervisor, for all his guidance throughout this project and also for his valuable assistance in the preparation of this thesis. Grateful acknowledgement is made to the financial support made available through the Glasgow University Scottish Power Electronics and Electric Drives (SPEED) consortium.

Sincere thanks are also due to my fellow colleagues Mr C. Cossar and Mr M. McGilp with whom I had many stimulating and helpful discussions and to Mr I. Young of the Power Electronics group for all his advice and assistance throughout the duration of this work.

I would also like to thank Mr H. Anderson, Mr J. Kelly and Mr A. MacLaren of the Mechanical workshop for all the mechanical support during my time at the University.

Finally, I wish to thank my fiancée Elaine and my family for all their moral support and for making the past two years so enjoyable.

CONTENTS

	PAGE
ABSTRACT	7
CHAPTER 1 INTRODUCTION	
1.1 Introduction	9
1.2 Review of Published Literature	11
CHAPTER 2 HIGH SPEED SWITCHED RELUCTANCE MOTOR FOR FOOD PROCESSOR.	
2.1 Introduction	22
2.2 Basic Principles of SR Motor	25
2.3 System Design	35
2.3.1 Motor Design	37
2.3.2 Control Circuit Design	41
2.3.3 Power Circuit Design	45
2.4 Comparison of Experimental Results	49
2.4.1 Torque/Speed Characteristics	49
2.4.2 Thermal Capability	51
2.5 Conclusions	56
2.6 Future Work	58
CHAPTER 3 FLUX SCREENING METHODS IN A SWITCHED RELUCTANCE MOTOR.	
3.1 Introduction	60
3.2 Fundamental Principles	61
3.2.1 Torque Production using Screening Methods	61
3.2.2 Transients in Coupled Circuits	65
3.3 Methods for Screen Evaluation	65

	PAGE	
3.3.1	Phase Current Expression for Rotor with Conducting Inserts.	67
3.4	Evolution of Different Rotor/Stator Configurations	69
3.4.1	Conducting Insert Rotor	70
3.4.2	Copper Bar Rotor	72
3.4.3	Conducting Stator Slot Screens	73
3.5	Finite-Element Analysis of Screen Concepts	74
3.6	Modelling of Diffusion Effects within Rotor Screen using Finite-Elements	80
3.7	Experimental Tests	85
3.7.1	DC Static Inductance Measurements	
3.7.2	Open Loop Torque/Speed Characteristics	86
3.8	Conclusions	89
3.9	Future Work	91
 CHAPTER 4 CONCLUDING DISCUSSION		
4.1	Discussion	93
 REFERENCES		95

APPENDICES	PAGE
APPENDIX 1.1 National Semiconductor SPEED SR Control Chip.	103
APPENDIX 2.1 Experimental Pulse Circuit for Flux Linkage versus Current Characteristics in SR Motor.	107
APPENDIX 2.2 Program for Measurement of Flux Linkage versus Current Curves using the Tektronics 7854 Digital Storage Scope.	108
APPENDIX 2.3 Stator/Rotor Laminations for 72mm SR Motor.	110
APPENDIX 2.4 Stator/Rotor Laminations for 88mm SR Motor.	111
APPENDIX 2.5a Control Circuit for 72mm & 88mm SR Motors.	112
APPENDIX 2.5b Half H Bridge 3 Phase Power Circuit.	113
APPENDIX 2.6a Theoretical Calculation of Heat Storage Capacity for 72mm SR Motor.	114
APPENDIX 2.6b Theoretical Calculation of Heat Storage Capacity for 88mm SR Motor.	115
APPENDIX 2.7 Theoretical Calculation of Phase Winding Temperature Rise in 72mm and 88mm SR Motors.	116
APPENDIX 2.8 Experimental System Efficiency versus Applied Torque for the Series AC Commutator Motor and the 72mm & 88mm SR Motors.	117
APPENDIX 3.1 Experimental SR Test Motor Lamination Cross Section.	118
APPENDIX 3.2 Sub-Transient Inductance Theory.	119

	PAGE
APPENDIX 3.3 Transients in Series RL Circuits	120
APPENDIX 3.4a Conventional SRM Rotor.	124
APPENDIX 3.4b Conducting Insert Rotor.	125
APPENDIX 3.4c Copper Bar Rotor.	126
APPENDIX 3.4d Conducting Stator Slot Screens.	127
APPENDIX 3.5 Copper Bar Rotor Construction.	128
APPENDIX 3.6 Command Procedure for Finite Element Package to Calculate Winding Inductance.	129
APPENDIX 3.7a Torque/Speed Characteristics for Normal Mode with Normal and Conducting Insert Rotors.	130
APPENDIX 3.7b Torque/Speed Characteristics for Long Dwell Mode with Normal and Conducting Insert Rotors.	131
PAPERS PUBLISHED :	
"An Axial Airgap Disk Motor", Hutton, A.J., Miller, T.J.E., 23rd University Power Engineering Conf., Nottingham, September 1988.	132
"Use of Flux Screens in Switched Reluctance Motors", Hutton, A.J., Miller, T.J.E., IEE Variable Speed Drives Conf., London, September 1989.	136
"Design of a Synchronous Reluctance Motor Drive", Miller, T.J.E., Cossar, C., Hutton, A.J., IAS 24th Annual Conf. on Electric Machines, October 1989.	141

ABSTRACT

The switched reluctance (SR) motor is a new form of brushless DC motor without permanent magnets, capable of low cost manufacture and a wide speed range.

Because of its simplicity, ruggedness and wide speed range, it is a candidate for a broad range of applications from domestic appliances to aerospace and automotive actuators.

In this thesis, two original aspects of the SR motor drive are explored.

First, the application of the SR motor to a domestic food processor is explored by designing, building and testing two prototype drives. This project provided experience on the entire system design. In particular, it permitted an evaluation of the SR drive at high speed with respect to its efficiency, thermal characteristics, power density and noise level in comparison with a conventional AC series commutator motor with triac control.

The second aspect of this thesis is an original investigation into the use of flux screens to improve the specific torque (torque per unit volume) of the switched reluctance motor. The torque of the SR motor is determined by the variation of self-inductance of the phase windings as the rotor rotates. Under dynamic operating conditions this variation can, in principle, be increased by dynamically decreasing the minimum self-inductance through the use of eddy current screens. Several configurations of screens are postulated, analyzed by finite-element techniques and tested in an experimental motor. Although the experimental results are inconclusive, this investigation introduces some interesting possibilities for future motors.

The work described in this thesis was entirely sponsored by industry, and particular acknowledgement is made to Kenwood Ltd. (food processor project); Lucas (disk motor project); and the SPEED consortium (flux screen project).

CHAPTER 1

1.1 Introduction

It is over 150 years since Wheatstone came up with the idea for a reluctance motor but it was not until 1982 that a commercially viable product first came on the market. The switched reluctance motor (SRM) has evolved in various forms over several decades and has many commercial applications in general industry.

Recently, the SR motor has emerged as a serious competitor to both brushless DC and induction motors in particular applications. The drive is under intense development for a wide range of industrial and domestic appliances in which low cost, high reliability, high efficiency, variable speed and long life are required. The increasing availability and progressive improvement of power semiconductor devices in the past few years have had a significant impact on the cost effectiveness of the SR motor since the power electronics have now become an integrated part of the drive itself.

The SR motor has, in recent years, established itself in particular niches of the market place. In particular, industrial pumps and small computer peripheral drives are just two recent applications of the switched reluctance motor in today's technology. However, much development work is required before the drive can be a serious replacement for existing DC and induction motor drives.

The SRM has a number of attractive features which include 1) simple construction 2) free of costly magnets 3) absence of copper on the rotor and 4) low rotor losses. Consequently, this gives the drive a number of

advantages over existing motor drives. In particular, the fault tolerant nature of the motor under almost all electrical fault conditions make the drive suitable for hazardous environments. The control performance of the drive makes it a candidate for a near-servo-quality motor which is often required in modern motion control systems. The aerospace and the automotive industries employ such systems where high reliability, reduced cost and weight for a drive are placed at a premium.

In Chapter 2 the basic principles governing the operation of the SR motor are discussed. Particular emphasis is placed on a four pole rotor, six pole stator motor geometry since extensive studies have been reported on the operation of this drive topology. The design of the control and power electronics are developed in the Chapter culminating in the presentation of a complete drive system for a domestic food processor. Two SR motor configurations are considered. Using torque/speed data and thermal transfer experimental information an engineering decision is taken to provide the most effective SR drive system for the food processor.

Chapter 3 is concerned with the use of flux barriers or screens applied to a conventional SR motor. The aim is to reduce the unaligned phase inductance and subsequently, increase the available specific output torque. The design, construction and performance of various flux screening concepts are described with conclusions drawn about the most effective screening methods employed.

Finally, Chapter 4 contains a concluding discussion on the results obtained throughout this project together with suggestions for further work in the field.

1.2 Review of Published Literature

There is an abundance of published literature on the switched reluctance motor drive and comprehensive reviews have been written by P.J. Lawrenson [1.1], T.J.E. Miller [1.2] and J.V. Byrne [1.3,1.4] to name a few. It is therefore the objective of this section to outline the history and concept of the SR motor and highlight the numerous publications which were relevant to its development over the years.

In 1841, Wheatstone devised an electromagnetic engine which used the fundamental principles of magnetic reluctance to provide rotation. The motor consisted of a set of horse-shoe magnets which were electrically energized and could be switched on and off in sequence so as to pull the 'keepers' on the rotor into alignment. Figure 1.1 shows the patent drawing for the first of Wheatstone's reluctance type motors. An issue of the *Electrician* published in 1882 carried an article by Robert Davidson of Aberdeen which described an electric motor which was constructed from two U shaped electromagnets. These were switched on alternately to attract one of three axial iron bars placed around the periphery of a wooden drum, i.e., the rotor. A number of years before the publication of Davidson's paper, he built a five ton car which was propelled by this motor [1.5] and in 1843 it made a number of successful trips on the Glasgow to Edinburgh railway link.

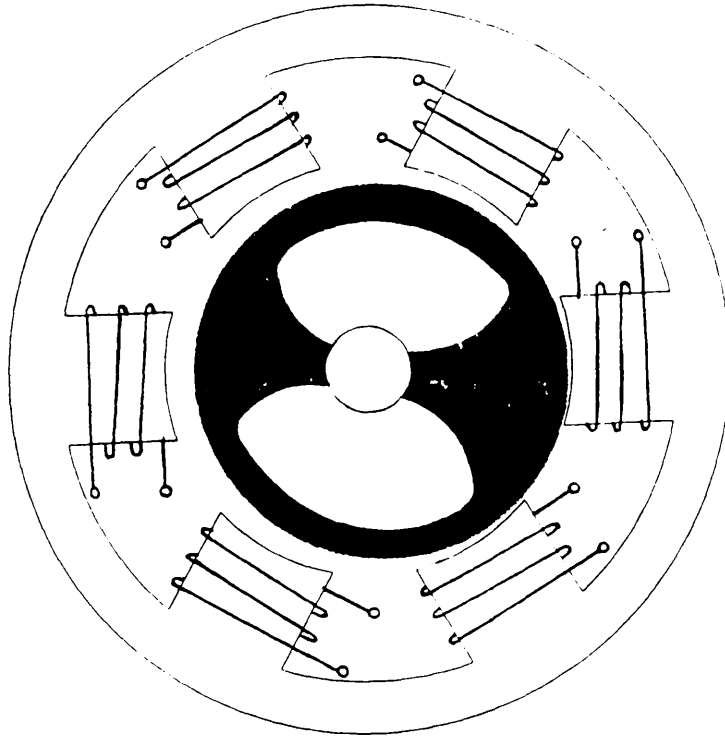


Figure 1.1 Wheatstone's Reluctance Type Motor

Other early inventors produced crude electric motors about this time which were based on the switched field concept. Most notable C. Page of Salem, Massachusetts produced a number of interesting motor designs. In particular, the switched field machine he designed in 1851 for traction purposes cost \$30,000 of Government funding, weighed twelve tons and travelled at a mere 19 miles an hour. This was technically disastrous for Page and was due to the lack of consideration for the complete drive system incorporating the electric motor.

These and other experiments with electrically operated cars were interesting, but none of them were practical because the motors were inefficient and the batteries required for power were very expensive.

During the decades after 1890, the attention towards switched field drive systems was significantly less and designers were turning their attention to a new breed of

AC motors. This was the direct result of the AC supply becoming widely available. Many years went by over which the induction motor was brought to a reasonable state of perfection and was found to be very versatile. Indeed, the induction motor still survives as the main work horse in many of today's industries.

At the start of the 1960's, interest was once again stirred in the switched field theory for machines [1.6]. Researchers started to take note of their potential and in 1961, Anderson and Cruickshank of Dundee published a patent [1.7] in which a three phase variable speed drive was built using new thyristor technology to create the switching field system. Due to interference problems and cash flow difficulties their research was discontinued although they saw the future potential of the SR motor with the advent of cheaper and less cumbersome electronics. It was pointed out in this article that in the design of this apparently simple motor many factors have to be considered and many precautions taken to ensure satisfactory operation. This motor design requires a high torque to inertia and torque per unit stator volume in order to compete with conventional state-of-the-art motor drives, and the time constant, the ratio of the phase winding inductance to its resistance, should be as small as is possible to attain a high speed of operation. Such problems still apply to motor design of today and are discussed in detail in Chapter 3.

In 1920, C.B. Chicken and J.H. Thain in Newcastle upon Tyne obtained a US patent [1.8] for the invention of a reluctance type motor which could produce a large torque per unit rotor volume. The longitudinal structure of this machine is shown in Figure 1.2. The remarkable feature of this motor is the motion of the soft steel rotor passing successively between the two opposite electromagnetic cores of the stator. This structure in

which the rotor teeth are sandwiched by the stator teeth is known to be the one geometry which can produce the largest torque from a unit volume of the rotor.

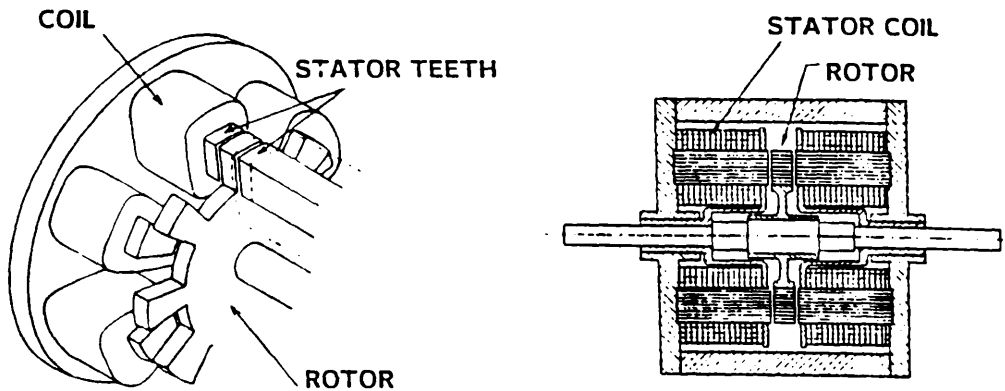


Figure 1.2 Variable Reluctance Motor invented by C.B. Chicken and J.H. Thain

In 1960, the axial air-gap disk motor concept was revived by Emil Ranseen of Chicago who patented an electric motor in which the rotor poles extended radially into axial alignment with the stator poles [1.11]. This design used one rotating disk per phase with each disk having twelve radial teeth.

In 1968 the manufacturer Icon/Fujitsu developed a commercial stepping motor [1.10] based on the original idea of Ranseen: Figure 1.3. It had five phases and twenty-four radial teeth in each rotating disk per phase. This design was a great improvement from Ranseen's motor because of the two extra phases and the reduction of the disk thickness. This resulted in an increased output torque for the same size of stator volume. Another advantage of the Fujitsu motor was the design of the disks which had magnetic sectors instead of teeth. This allowed more magnetic poles to be placed on each

disk giving an overall increase in the shearing area across the motor. In 1971, Fanuc Ltd. of Japan used the same idea to produce a multi-stack variable reluctance motor with five phases. This was primarily a power stepping motor and was used for numerically controlled (NC) machines such as milling machines and XY plotters.

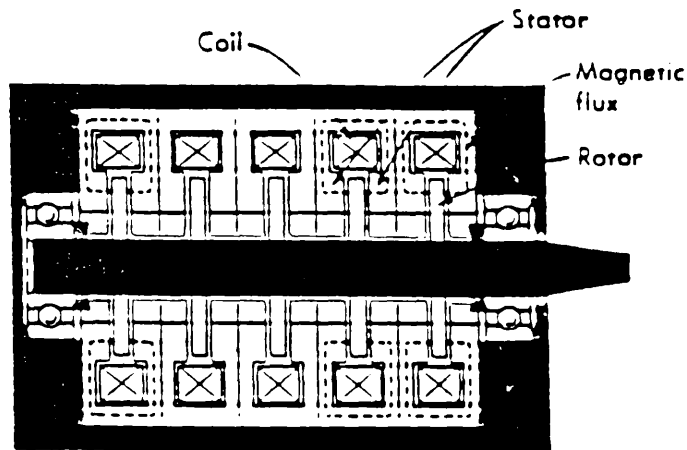


Figure 1.3 Variable Reluctance Stepping Motor designed by Icon/Fujitsu of Japan

In 1972, L. Unnewehr and W. Koch of the Ford Motor Company published a paper [1.11] which described a prototype variable reluctance disk motor which used a small number of thick disks per phase with seventeen magnetic sectors on each disk. The motor geometry is shown in Figure 1.4. The intended use for this type of motor was for traction and variable-speed drive applications. Their findings suggested that a disk motor with two rotating disks per phase and seventeen magnetic sectors could have the potential for an inexpensive and efficient variable-speed drive.

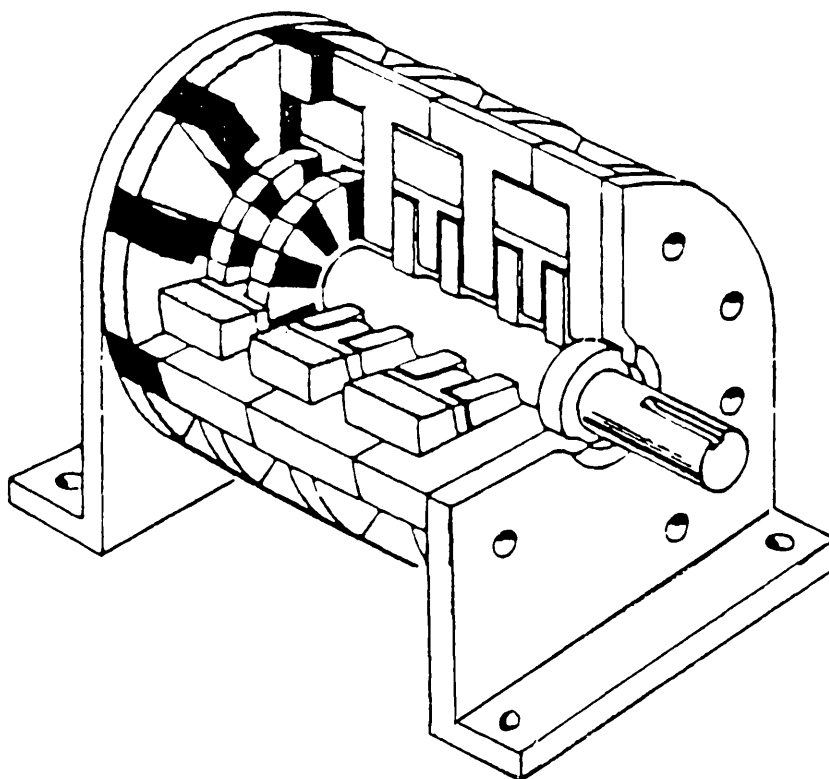


Figure 1.4 Axial air-gap Disk Motor designed by Unnewehr and Koch of the Ford Motor Company

Although practical applications of modern SR motors occurred in the early 1970's, their prototypes actually existed in earlier days. Indeed, P.French and A. Williams of TRW Inc. presented a report [1.12] to the American Institute of Aeronautics and Astronautics in July 1967 which concerned a reluctance motor with a rotating disk geometry of Figure 1.5. Their aim was to design a reluctance motor which could develop very high shaft powers without the need for high rotational speeds. The design was a 2-phase multi-disk machine with seven rotating disks per phase. Its purpose was for a torpedo motor drive and at the time of writing there were problems associated with control circuit operation

although both French and Williams saw no obstacles in developing the motor to its full potential.

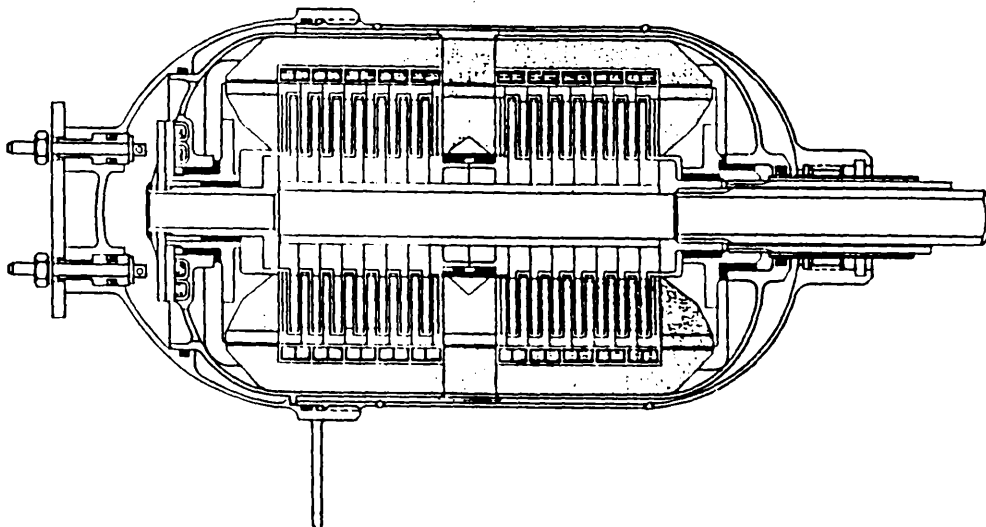


Figure 1.5 Torpedo Motor with disk geometry designed by P. French and A. Williams of TRW Laboratories.

In 1980, Bastos, Goyet and Lucidarme of the Laboratoire d'Electrotechnique at the University of Paris revived the disk motor concept. They carried out experimental studies on an interleaved disk reluctance motor [1.14]. Their design, as shown in Figure 1.6, incorporated a small number of rotating disks per phase with a multi-stack, three phase arrangement.

The July 1980 issue of the I.E.E. Proceedings carried the most notable paper by P.J. Lawrenson et al. on the theory and potential of SR motor drives under the title 'Variable-Speed Switched Reluctance Motors' [1.13]. This paper was concerned with the fundamental design considerations for an SR motor and its application to an electric vehicle drive. Lawrenson concluded that the SR motor was a very substantial variable-speed motor

drive and with commercial and technical development they could become very attractive.

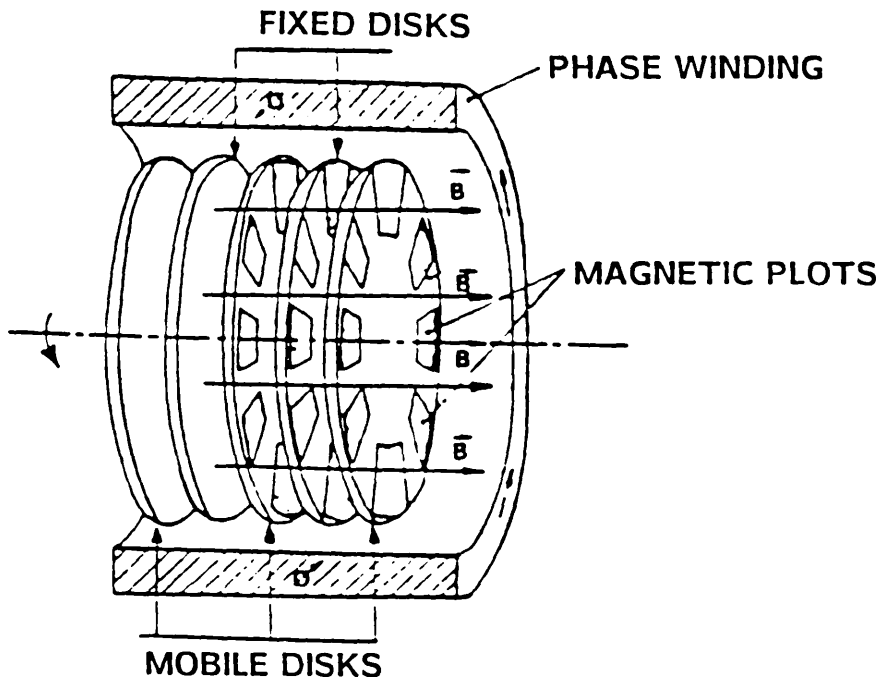


Figure 1.6 Disk Motor designed by J. Bastos et. al of University of Paris

Coinciding with the appearance of this paper, intensive research work aimed at improving the performance of SRM's was started in a few academic establishments. W. Ray and R. Davis of Nottingham University published a paper [1.14] in 1979 which considered the thyristor inverter design requirements for an SR motor in a traction application. The aim was to design a thyristor drive with an efficient control strategy to provide the optimum performance/cost ratio of the drive as a whole.

From the middle of the 1980's, general purpose drive manufacturers took note of the possible uses of SR motors as an alternative to the inverter-fed induction motor. One of the first industrial applications for the

SR motor was in high horse-power pump drives [1.15]. Another was the application of the SR motor to a traction drive system [1.16]. These companies promoted the development of reliable, high performance SR drive systems. One of the more recent developments in SR motor technology was an XY computer plotter drive [1.17]. The accelerating, steady running and braking operation of the motor combined with its low-cost implementation was ideally suited to this type of application.

With the advancement of the SR motor came the progressive improvements to the electronic and power controls. Technological progress in transistors and semiconductor devices advanced at such an alarming rate in the late 1950's and early 1960's. MOS transistors for a practical use appeared in 1964 and a year later digital integrated circuits were introduced onto the market. In subsequent years, development advanced to the stage of middle stage integration and further to very large scale integration. As a result, the logic circuit control of the SR drive system was miniaturized while ensuring reliability and lower product costs. Microprocessor technology is now rapidly taking control of the drives market and indeed, the realisation of a microprocessor controlled variable reluctance motor drive was achieved back in 1984 [1.18]. This was the milestone in microprocessor drives of the future and is now setting the trend for the 1990's.

Towards the end of the 1980's, SR motors with excellent dynamic performance have become available. The increased interest in this technology has created numerous prototype SR drive systems both at academic and industrial R and D establishments: Figure 1.7. This has also led to the recent mass production of the drive. In the USA, the manufacture of computer plotters using the variable reluctance servomotor drive has emerged as a marketable product. In the latter part of the 1980's, direct drive robot motors using a variable reluctance

motor with a large number of stator/rotor teeth and very small length/diameter ratios have appeared [1.19]. These are mainly slow speed motors and are used in direct drive applications for robot and factory automation.

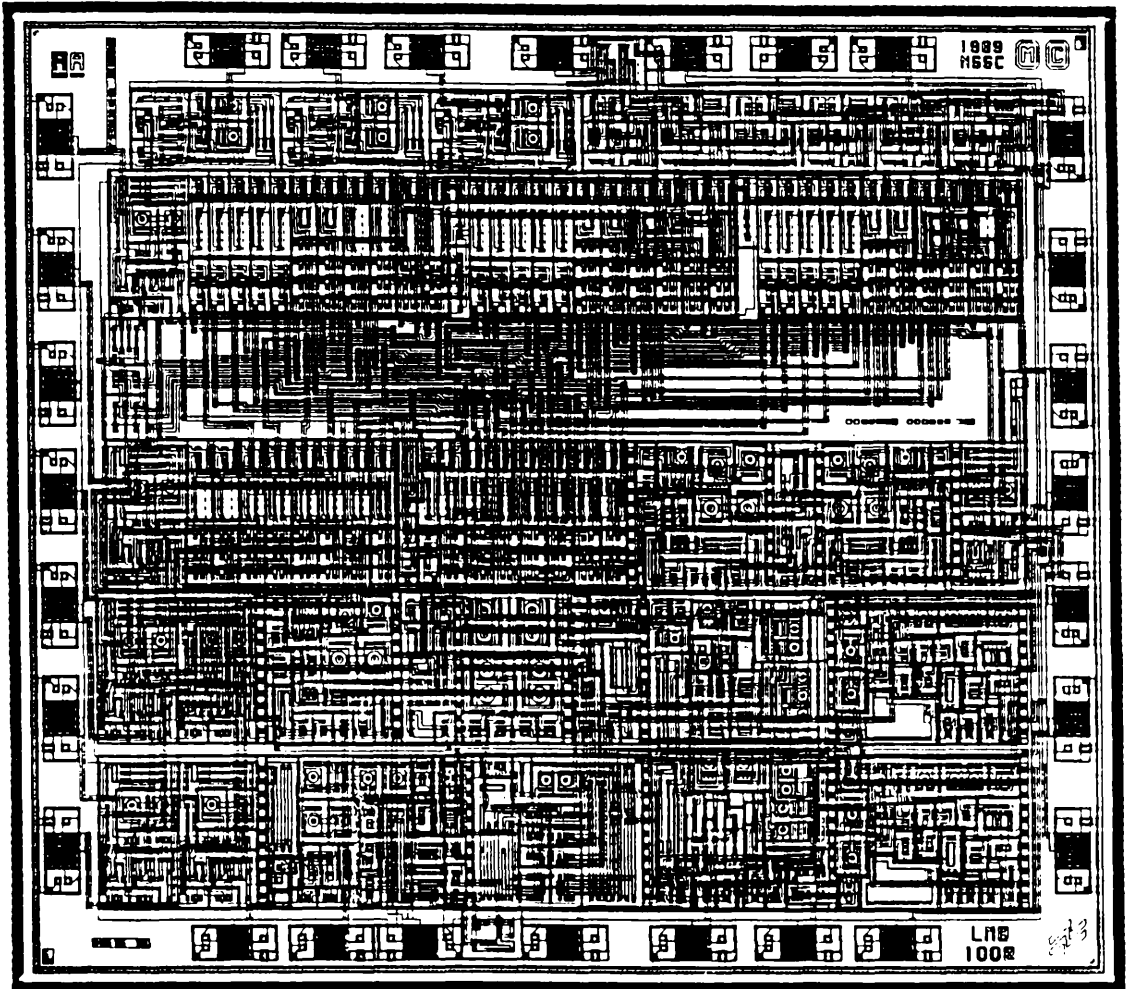


Figure 1.7 Multi-mode Commutation and Speed Control Circuit developed by SPEED and designed by National Semiconductor, UK as a monolithic integrated circuit: LMB1008.

Progress in SR technology also has its casualties. The axial air-gap disk motor used in NC machines [1.20] has nowadays been replaced due to two factors: first, the limitations that SR motors have with regard to a smooth finish, and second the advancements made in digital drive systems for DC servomotors. However, stand alone microprocessor drive systems along with the power semiconductor package will provide a cheap, reliable drive system for the SR motor which will, in turn, make it a strong competitor in the drives market of the 1990's.

CHAPTER 2

HIGH-SPEED SWITCHED RELUCTANCE MOTOR FOR FOOD PROCESSOR

2.1 Introduction

The first aspect of this thesis is the application of the switched reluctance motor to a domestic food processor by designing, building and testing two prototype drives.

Most domestic appliances such as food mixers, vacuum cleaners and power hand tools require only a unidirectional motor for their operation. To keep costs to a minimum the speed control techniques employed are of simple design and the power handling circuit usually consists of a single triac: [2.1]. A domestic food processor is a typical drive application which uses a series AC commutator motor. It is a brush commutated drive which is cheap to manufacture and is electrically robust. The control and power electronics are mature and a time proven product. Not only do they provide the highest power per pound (£) but also the combination of solid state devices and the motor itself provide an economical, controllable motor package. The main disadvantage associated with the commutator motor is the very noisy operation at high speed, poor efficiency and limited operational life due to brush wear. Many of today's drive systems now require good performance, long term reliability and cheap manufacturing costs. It is therefore reasonable to believe that domestic appliance manufacturers may look for an alternative drive system which will provide good speed control, quiet high speed operation, high efficiency and a motor which would be extremely simple, rugged and inexpensive to manufacture.

The switched reluctance motor may seem to be the right choice for this type of application: the motor is less expensive both in materials and in manufacturing than the series AC commutator motor, and even when the control electronics are added, it may prove to be the least expensive of all the brushless dc drive alternatives. Another candidate drive system is the permanent magnet brushless DC motor drive. However, the main drawbacks associated with these drives are the retention of the permanent magnets in the rotor under high speed operation and also the additional expense of the magnets. It can therefore be safely said that the SR motor could become a serious contender against a PM brushless DC drive in particular domestic applications if the decision is taken for an alternative drive.

The main advantages of the SR motor are;

- 1) Good speed control.
- 2) High efficiency.
- 3) Quieter high speed operation.
- 4) Low cost electronic components
- 5) Lower maintenance costs

There are a number of disadvantages associated with the SR motor which may hinder its widespread use in domestic applications. These are

- 1) Requirement for large DC link capacitor to smooth out ripple current.
- 2) A shaft position sensor may be required which adds cost to the system.

- 3) Few of the component parts of the motor are compatible with existing motor production so that there is an investment barrier to the SR motor exploitation.

The objective of this research is to assess the feasibility of using a switched reluctance drive in a domestic food processor by designing, building and testing two prototype systems. The design of the control and power electronics are also discussed in detail.

Two slightly different SR motors are considered. The first is a 72mm stator diameter motor which is built using a stiff aluminium and totally enclosed fan-cooled frame. The stack length is 55mm and is impregnated with a varnish coating to help bind the laminations together. The second SR motor has a larger 88mm stator diameter. It has been built into the existing series AC motor frame and fan construction. The stack length for this motor is 35mm. There is no varnish treatment on this stack although the laminations are held tightly together by a steel clamping brace. The torque/speed characteristics, efficiency, thermal capabilities and noise levels of both drives are measured and an engineering decision is made on the best SR drive system for the food processor. Initially, the aim is to match the performance of the switched reluctance motor drive systems with the series AC commutator motor with triac control.

The objective with the 72mm SR motor was to replace the AC motor with a smaller motor; the smallest that would meet the torque/speed requirements. The objective with the 88mm SR motor was to make the SRM the same size as the AC motor and see how the efficiencies, noise levels, etc compared.

2.2 Basic Principles of SR Motor

The switched reluctance motor is a doubly-salient, singly-excited motor which has copper windings on the stator and no copper present on the rotor. The rotor is also free of magnets or cage winding and is built up from a stack of silicon steel laminations. The stator and rotor arrangement is shown in Figure 2.1. The coils for each phase are wound on diametrically opposite stator pole pairs to form opposite magnetic polarities: (a North and South pole). The phase end-windings are kept short to reduce end-winding inductance and resistance and also to improve the active stack length of the motor compared to the overall length.

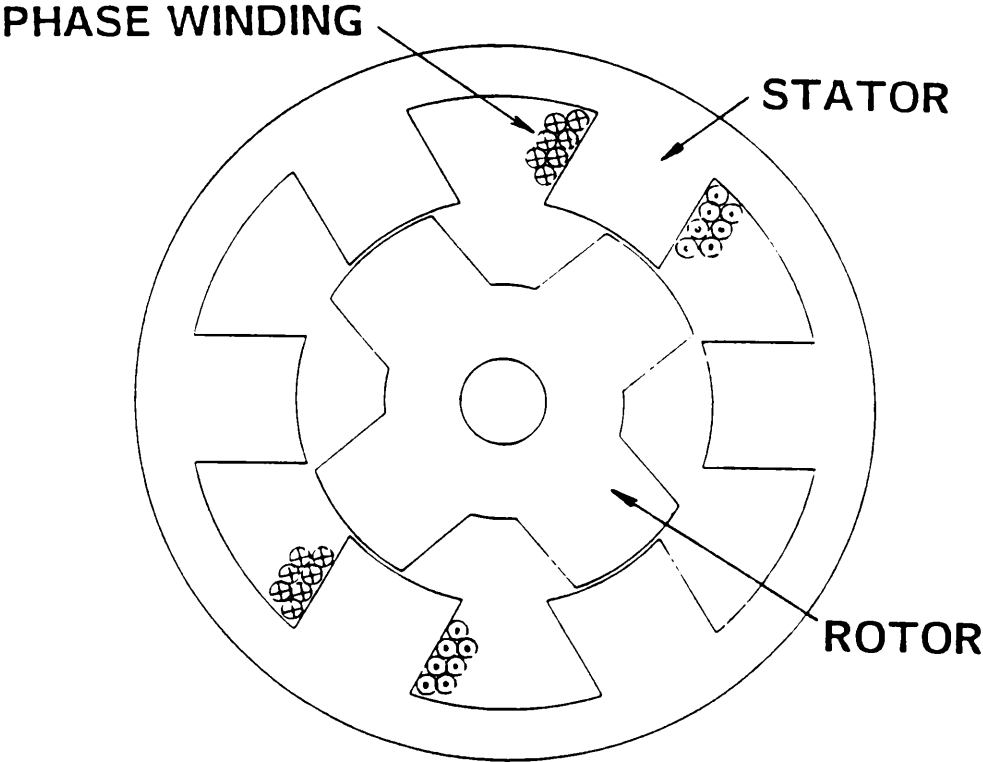


Figure 2.1 Stator and Rotor arrangement for Switched Reluctance Motor.

Currents in the stator circuit are switched on and off in accordance with the rotor position. By a sequence of magnetic attractions a rotation is set up. A rotor position sensor, together with the electronic control system of Figure 2.2 ensures that the phase windings are excited at the correct instant, i.e., the rotor pole angle with respect to the stator pole angle, to develop the required torque in the most efficient way.

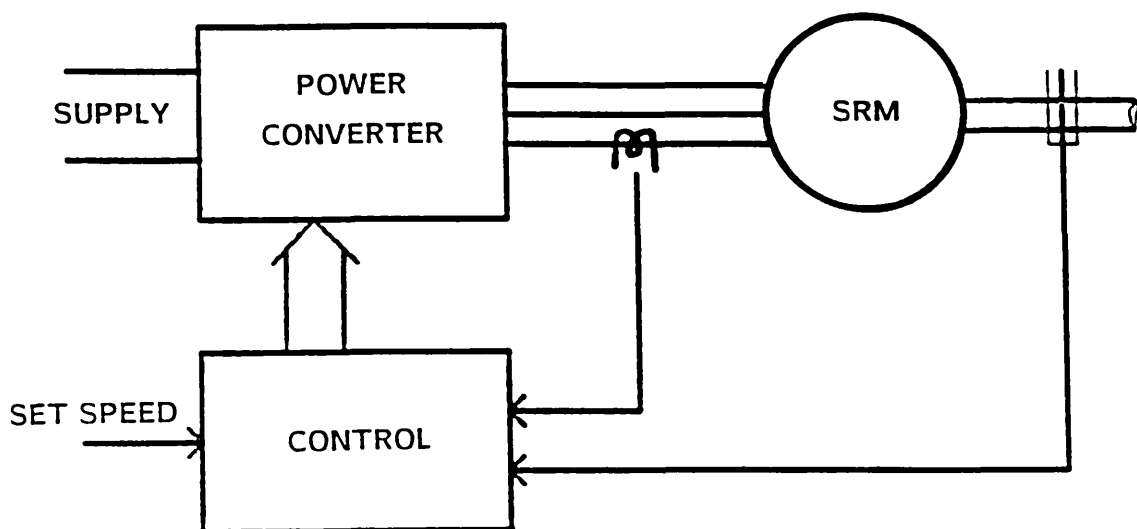


Figure 2.2 Schematic diagram for Electronic Control System

The torque in the motor is developed by the tendency for the magnetic circuit to adopt a configuration of minimum reluctance and to maximize the inductance of the excited phase winding. As the rotor moves from the unaligned to

the aligned position, i.e., a rotor pole aligns with a stator pole, the phase inductance varies between two extreme limits as shown in Figure 2.3. During one step or 'stroke' of the rotor pole, forward motoring occurs if current is fed into the phase winding during a period of rising inductance.

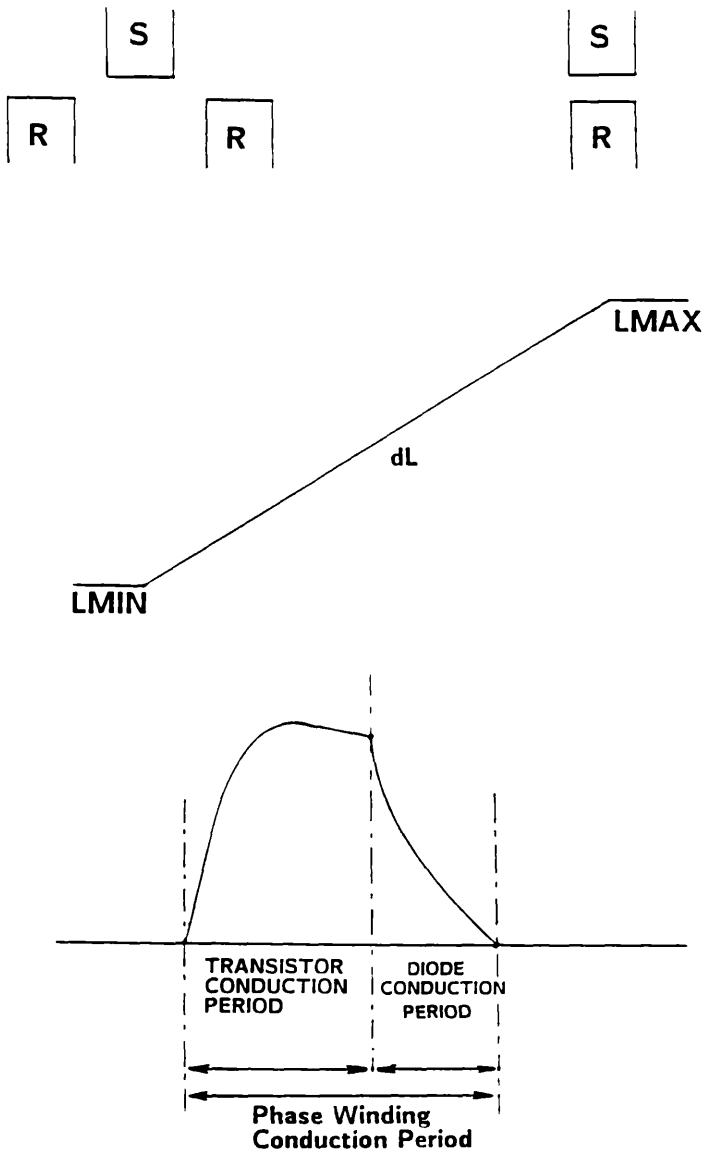


Figure 2.3 Inductance profile and Current Waveform for Motoring Condition.

Throughout this step the phase current and corresponding flux linkage follow a closed trajectory as shown in Figure 2.4. The ideal motoring condition would imply a square pulse of phase current which would coincide with the rising inductance period. The energy converted (W) from electrical to mechanical during one step is equal to the area enclosed by this trajectory. The average electromagnetic torque (T) is given by

$$T = \frac{qN_r}{2\pi} W \quad (\text{Nm}) \quad (2.1)$$

where qN_r is the number of steps per revolution and is the product of the number of phases q and the number of rotor poles N_r . In small motors only a fraction of the available 'conversion area' can be utilised due to thermal current limitations imposed on the motor.

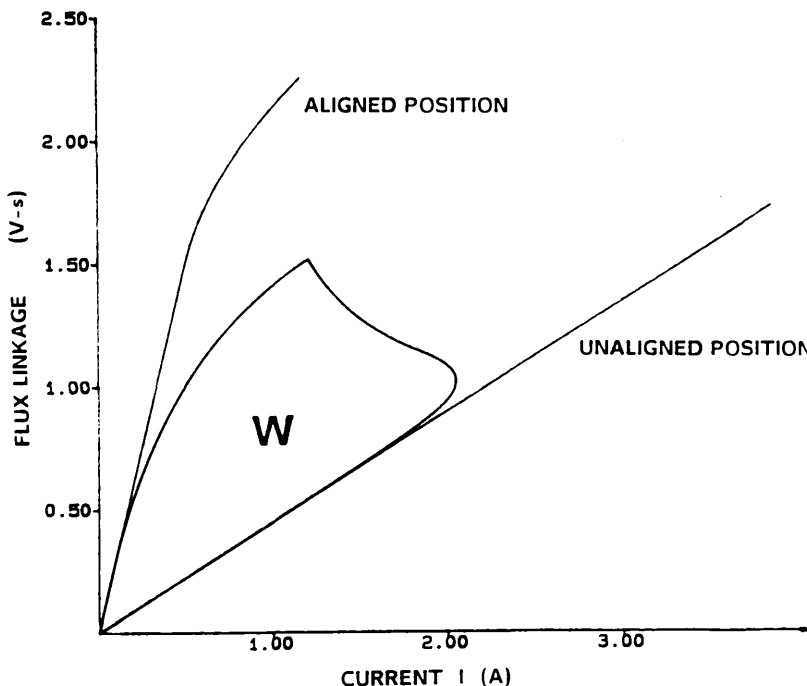


Figure 2.4 Flux Linkage/Current Trajectory

In order to achieve the greatest torque per ampere of phase current the conversion area must be maximised between the aligned and unaligned magnetization curves. There are three ways to achieve this; first, design the motor with a large aligned inductance implying a very small air-gap; secondly, design the motor for a small unaligned inductance implying a large interpolar arc between rotor poles and narrow stator poles; and thirdly, use a magnetic material for the laminations which possesses a very high saturation flux-density (B).

In the aligned position the flux linkage for a given phase current is maximised although their relationship is extremely non-linear due to magnetic saturation at the stator/rotor poles or the stator/rotor yoke. The incremental phase inductance is subsequently very high at low values of phase current and decreases as the rated current value is approached.

The flux linkage/current characteristic for the unaligned position is completely dominated by the large interpolar air-gap between the stator and the rotor poles. Local magnetic saturation on the pole tips does exist despite the linear relationship between the flux linkage and phase current. The incremental phase inductance for the unaligned position is therefore independent of the phase current.

The terminal voltage equation for one phase of the SR motor in terms of the current and flux linkage is given by

$$V = Ri + \frac{d\psi}{dt} \quad (V) \quad (2.2)$$

and since the flux linkage (Ψ) is a function of the phase current and rotor position then

$$V = Ri + \frac{\delta\Psi}{\delta i} \frac{di}{dt} + \frac{\delta\Psi}{\delta\theta} \frac{d\theta}{dt} \quad (2.3)$$

Since $\omega = \frac{d\theta}{dt}$ and $\frac{\delta\Psi}{\delta\theta} = i \frac{dL}{d\theta}$ only if i is constant and L does not depend on i then

$$V = Ri + L \frac{di}{dt} + i\omega \frac{dL}{d\theta} \quad (2.4)$$

where L is the incremental inductance. If resistance is negligible

$$V = L \frac{di}{dt} + i\omega \frac{dL}{d\theta} \quad (2.5)$$

Multiply both sides of the equation by i to give

$$i \frac{d\Psi}{dt} = iL \frac{di}{dt} + i^2 \omega \frac{dL}{d\theta} \quad (2.6)$$

The left hand side of this equation represents the electrical power supplied to the motor phase winding. The first component on the right hand side of this equation represents the inductive voltage drop across a fixed inductance. The second component is the self emf which is proportional to the phase current, motor speed and rate of change of phase inductance with rotor angle. The electrical power supplied (iV) is therefore

$$iV = \frac{d}{dt} \left[1/2 Li^2 \right] + 1/2 i^2 \omega \frac{dL}{d\theta} \quad (2.7a)$$

where the rate of change of stored magnetic energy is represented by

$$iV = \frac{d}{dt} \left[\frac{1}{2} Li^2 \right] \quad (2.7b)$$

This equation is only valid if L does not depend on i ie., the Ψ versus i curve has to be a straight line.

Subtracting equation (2.7a) from (2.6) gives

$$P_m = \omega_m T = \frac{1}{2} \omega i^2 \frac{dL}{d\theta} \quad (2.8)$$

From equation (2.8) the linear expression for the instantaneous torque is

$$T = \frac{1}{2} i^2 \frac{dL}{d\theta} \quad (2.9)$$

This equation reveals the nature of torque production in the switched reluctance motor if L is independent of i. Useful torque will be produced only if current is pulsed into the phase winding during a period of rising inductance ie., while the rotor pole moves from the unaligned to the aligned position with the stator pole.

2.2.1 Experimental Flux Linkage versus Current

Characteristics for SR Motor

It is important to have a thorough understanding of the flux distribution within the motor magnetic circuit since this influences the amount of available converted

mechanical energy. Indeed, Corda and Stephenson [2.2] have discussed in great detail the analytical estimations for the flux linkage versus current relationship. Equation 2.4 can be used to derive the voltage equation which can then be integrated in the form

$$\Psi = \int (V - Ri) dt \quad (2.10)$$

through one time step. Assuming that the speed (N) is constant then the integration can be done with respect to the rotor angle (θ). The experimental test circuit of Appendix 2.1 was designed to give a repetitive pulse of current into one phase winding of the switched reluctance motor. The phase current was measured using a current probe from a digital storage oscilloscope. The voltage dropped across the phase winding was measured using two voltage probes connected to the differential inputs of the scope. The scope was programmed with the sequence of commands listed in Appendix 2.2. This program sampled the voltage and phase current waveforms at any instant. These waveforms were then used to compute the flux linkage/current characteristics for a particular rotor pole position with respect to the excited stator pole. The experiment was carried out for the rotor pole fixed in the aligned and unaligned positions and also for every two degree steps between these upper and lower boundaries. An incremental resolver was used to give a measure of the two degree steps between the aligned and unaligned position. Figure 2.5a and 2.5b show the results obtained for the flux linkage versus phase current for both the 72mm SR motor and the 88mm SR motor.

The 88mm motor depicts a very non-linear nature for the flux linkage above phase currents of 1.5 amps. This is similar to the 72mm motor which experiences non-linearity at just around 1 amp. In both cases this can be explained

by considering the effects of saturation in the magnetic material. The stator yoke thickness in the 72mm motor is smaller than that of the 88mm motor and therefore experiences saturation at lower phase currents. Magnetic flux fringing also becomes more significant as the poles approach alignment.

Measured Rotor diameter (mean) = 1.51 inches
 Measured Stator diameter (mean) = 1.525 inches
 Measured Airgap (mean) = 0.020 inches

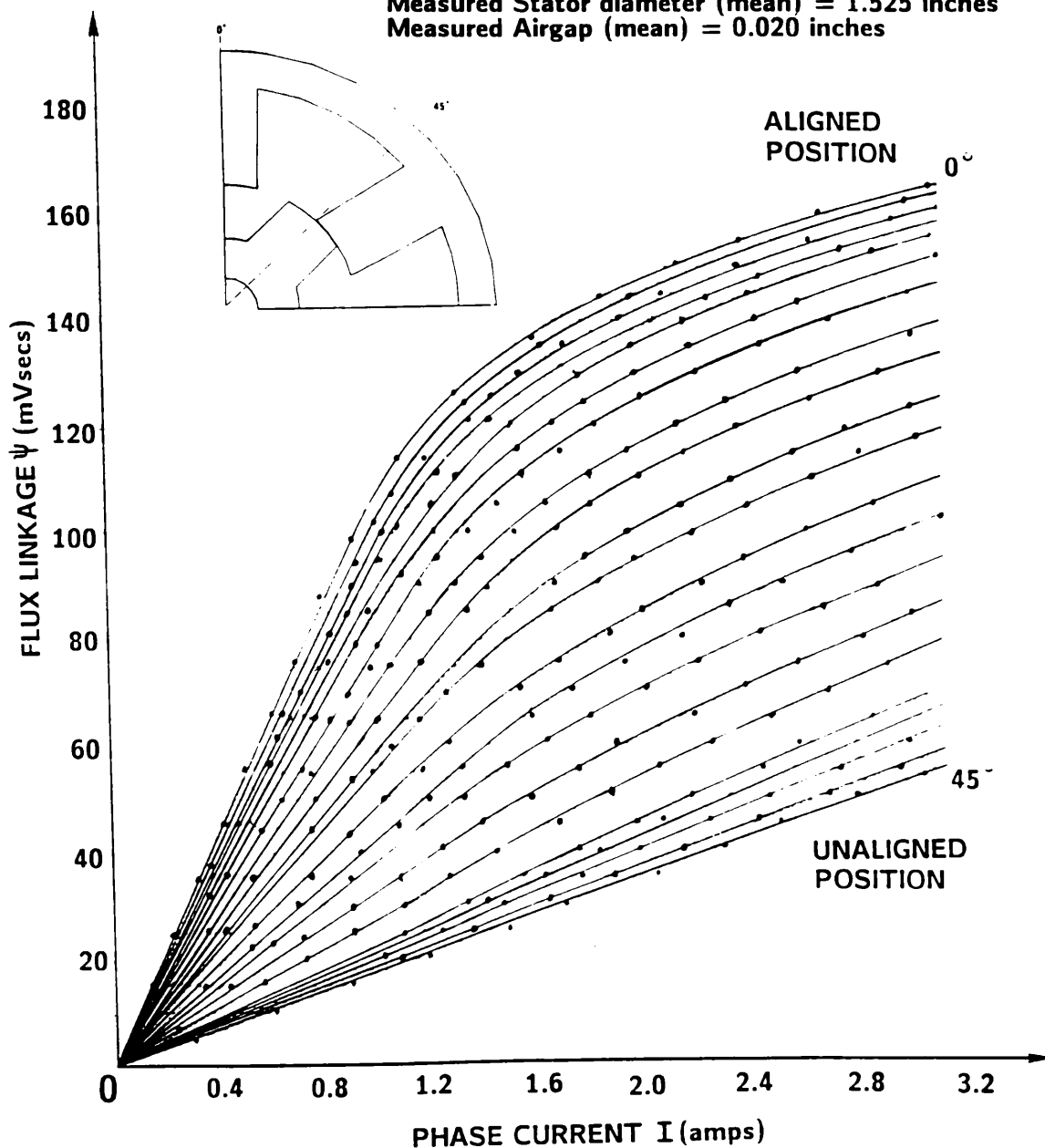


Figure 2.5a Flux Linkage versus Current Characteristics for 72mm SR motor.

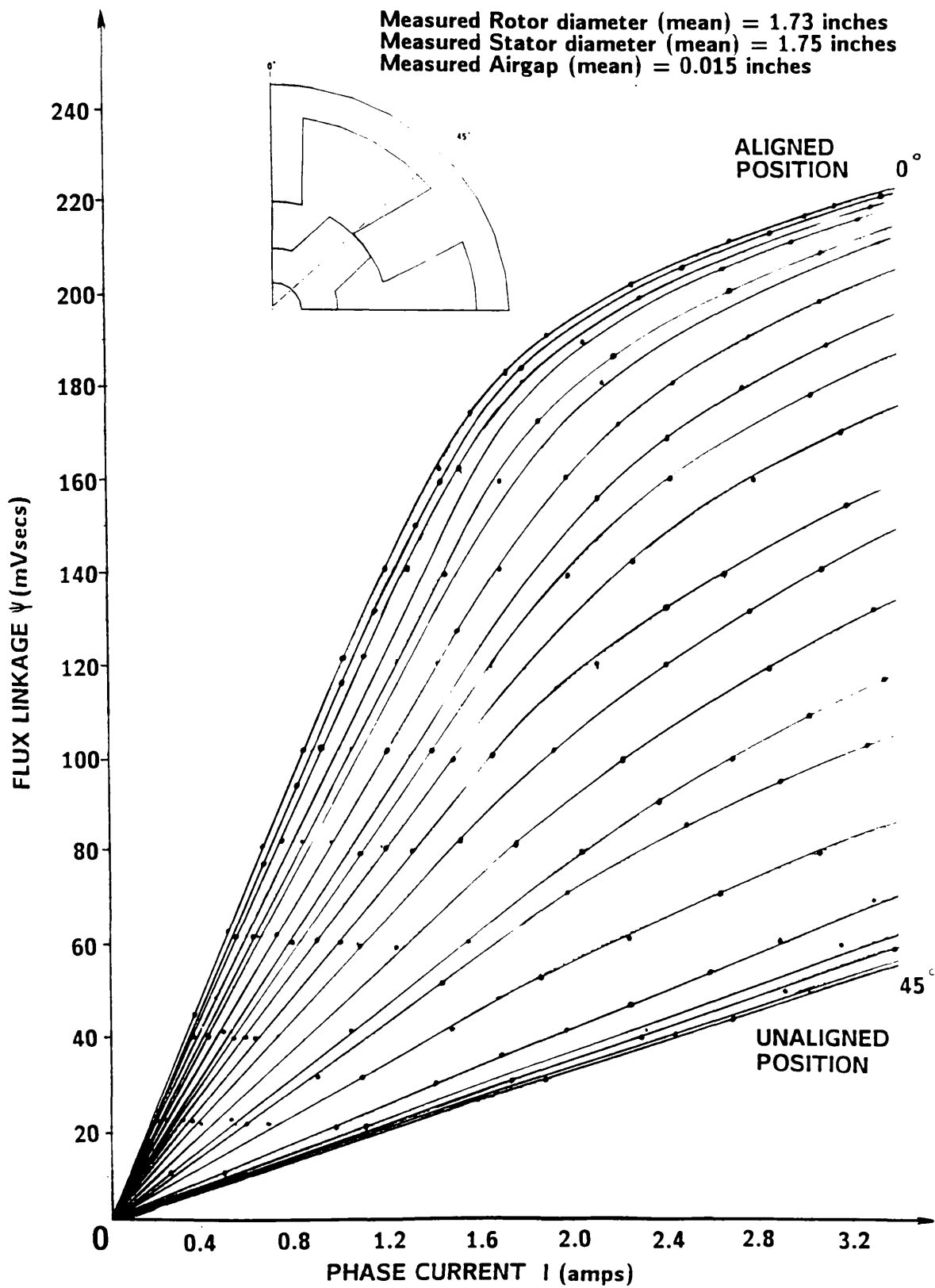


Figure 2.5b Flux Linkage versus Current Characteristics for 88mm SR motor.

2.3 System Design

The switched reluctance drive system for the food processor is schematically represented by Figure 2.6.

There are three main design areas incorporated within the overall drive system. These are :

- 1) Motor design
- 2) Control electronics design
- 3) Power electronics design

Clearly, a high level of integration will be required to maintain low system costs. This has been observed throughout the design process of the above areas. Indeed, steps have already been taken in achieving integrated control with the release of the SPEED switched reluctance control chip (LMB1008) which was produced in collaboration with National Semiconductor. This has been described in detail in Appendix 1.1. It should be noted that the level of integration required for economic manufacture was not implemented in the prototype SR drive systems. However, this would logically be the next phase in the project.

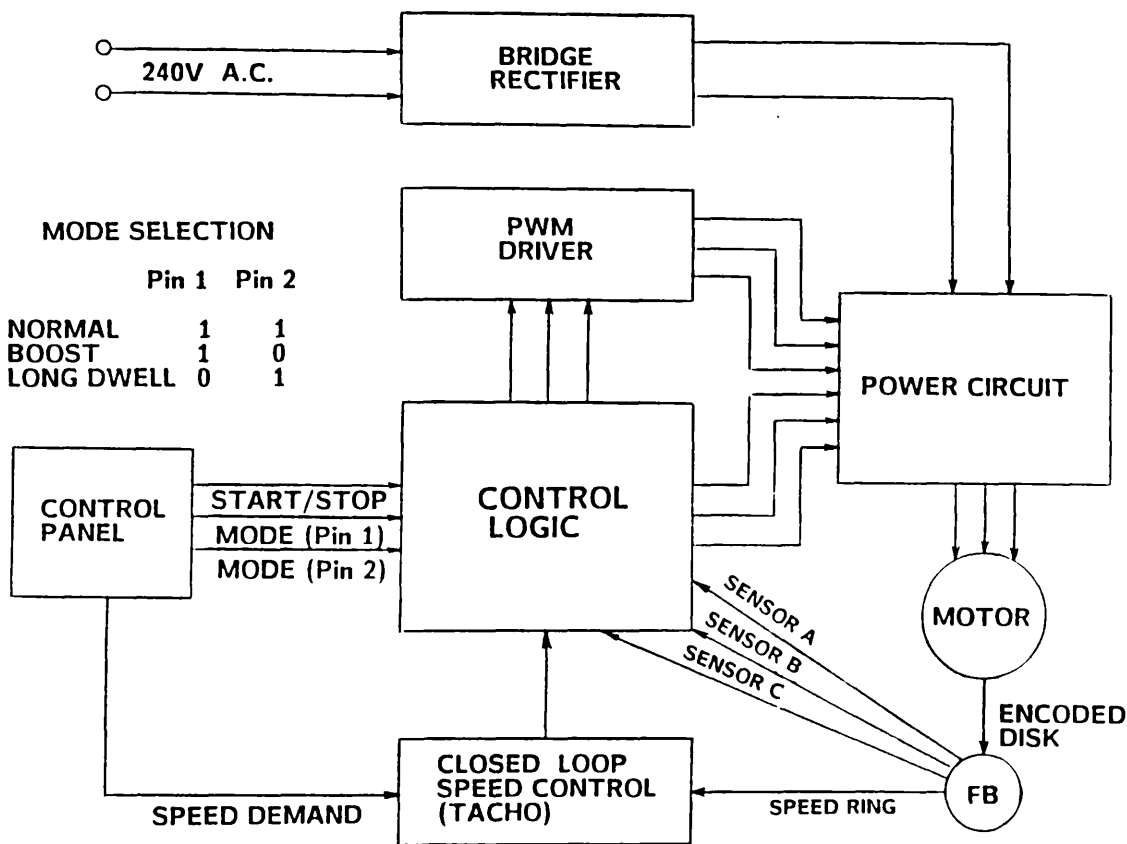


Figure 2.6 Schematic Diagram for SR Drive System

2.3.1 Motor Design

The lamination geometries of the 72mm and 88mm SR motor drives are shown in Appendix 2.3 and 2.4. Figure 2.7 shows the rotor and stator geometry for the 72mm stator diameter motor.

The stator teeth have wide pole tips to help improve the torque ripple, reduce the acoustic noise and increase the unsaturated aligned inductance. The air-gap is machined to 0.02 inches (measured) (Appendix 2.3) and was verified by measuring the rotor and stator diameters separately and calculating the difference. The casing is machined from solid aluminium as shown in Figure 2.8. Excellent access for cooling air is achieved by providing a small air channel in the stator slot between adjacent stator phase windings.



Figure 2.7 Stator and Rotor geometry for 72mm motor.

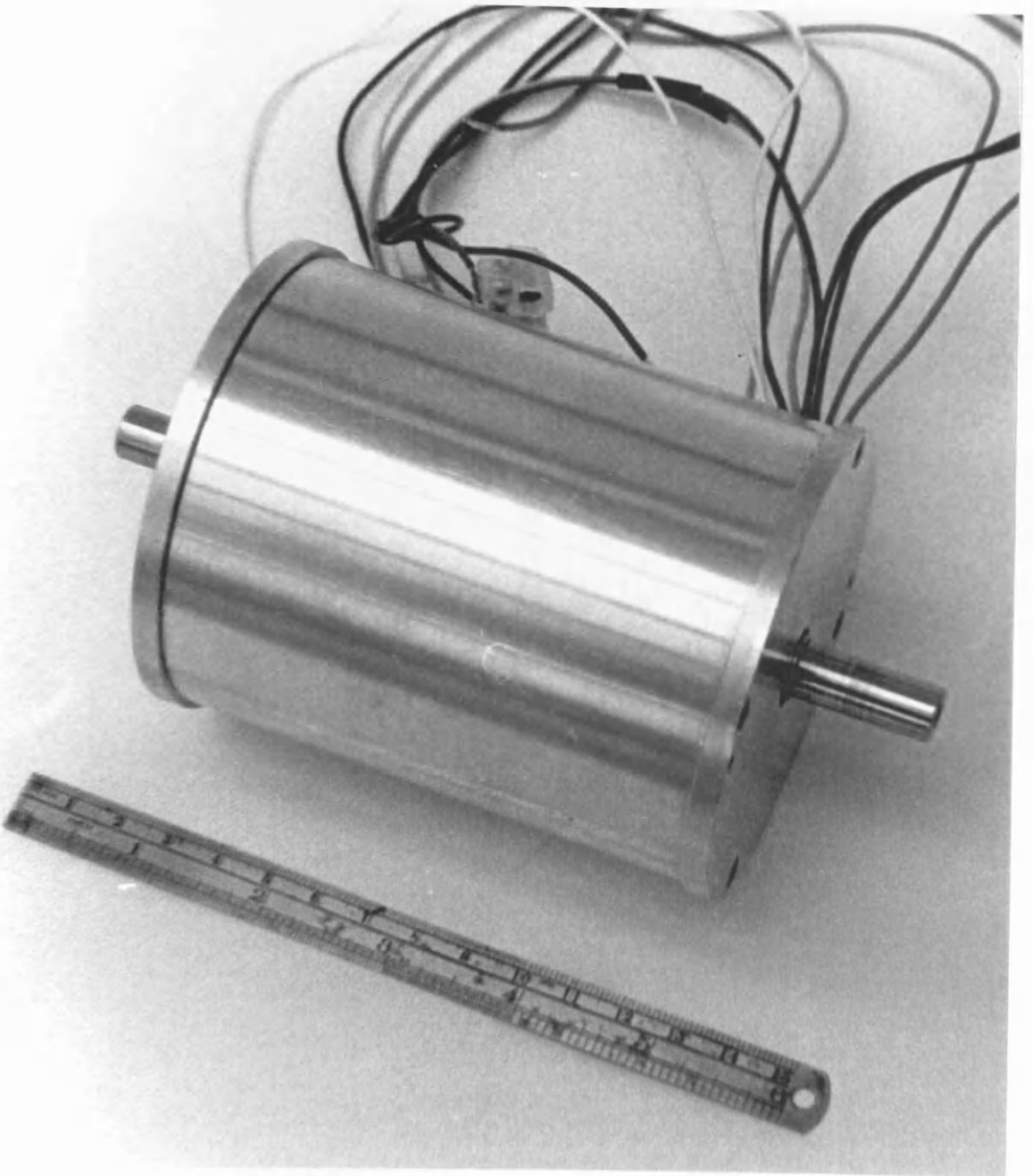


Figure 2.8 Motor Casing for 72mm Stator diameter motor

The 88mm stator diameter motor is shown in Figure 2.9. This larger diameter was chosen to provide greater lateral stiffness under load conditions. The motor was built into the existing series AC commutator motor end frames with the stator laminations fully exposed to the surrounding air.

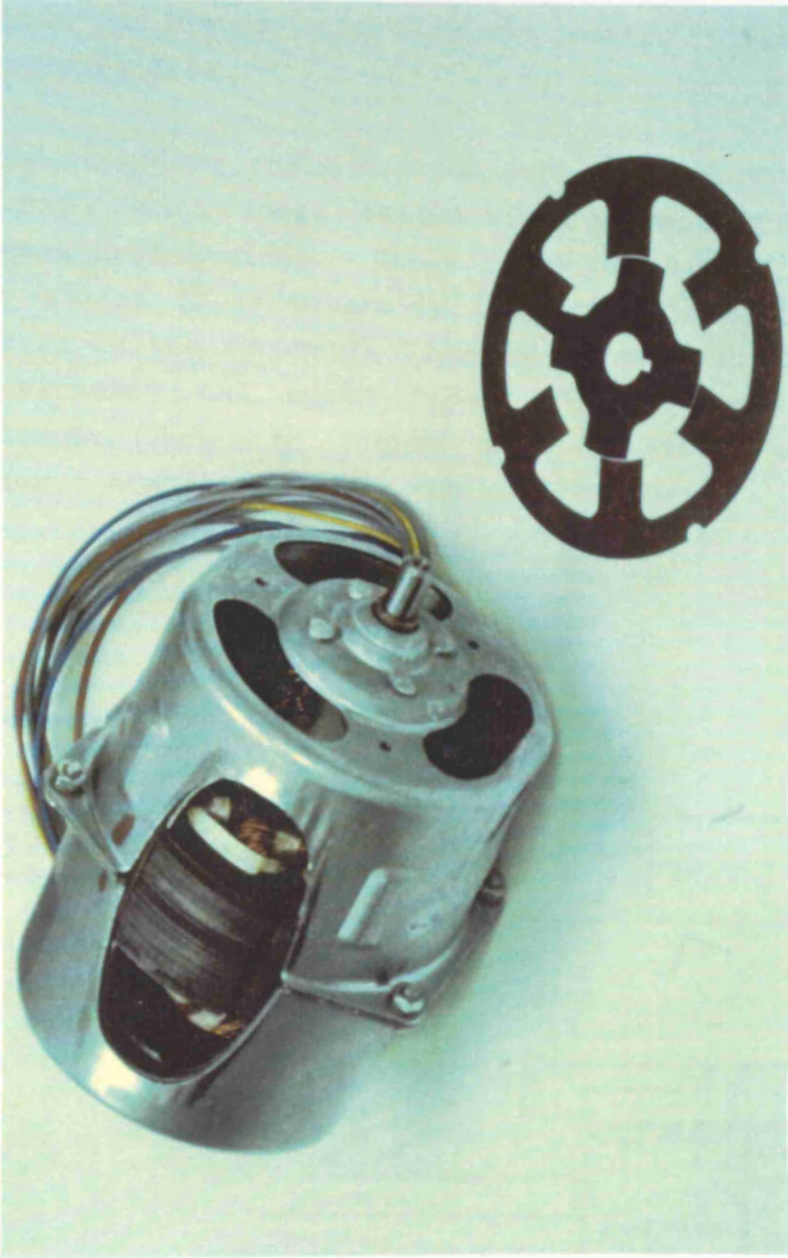


Figure 2.9 Stator Casing for 88mm Stator diameter motor

2.3.2 Control Circuit Design

The control of the SR drive is centered around two mechanisms: first switching angle control and secondly, fixed supply voltage PWM control. This is schematically shown in Figure 2.10 with the control circuit shown in Appendix 2.5a.

The switching angle control employs a programmable logic array with logic selectable 'modes' or fixed firing angle combinations. These modes, described in detail in by Miller [2.3] determine not only the operation of the motor in the forward/reverse direction but also the motor efficiency and speed range. A shaft position sensor circuit shown in Figure 2.11 provides the necessary sensor signal logic for the control board.

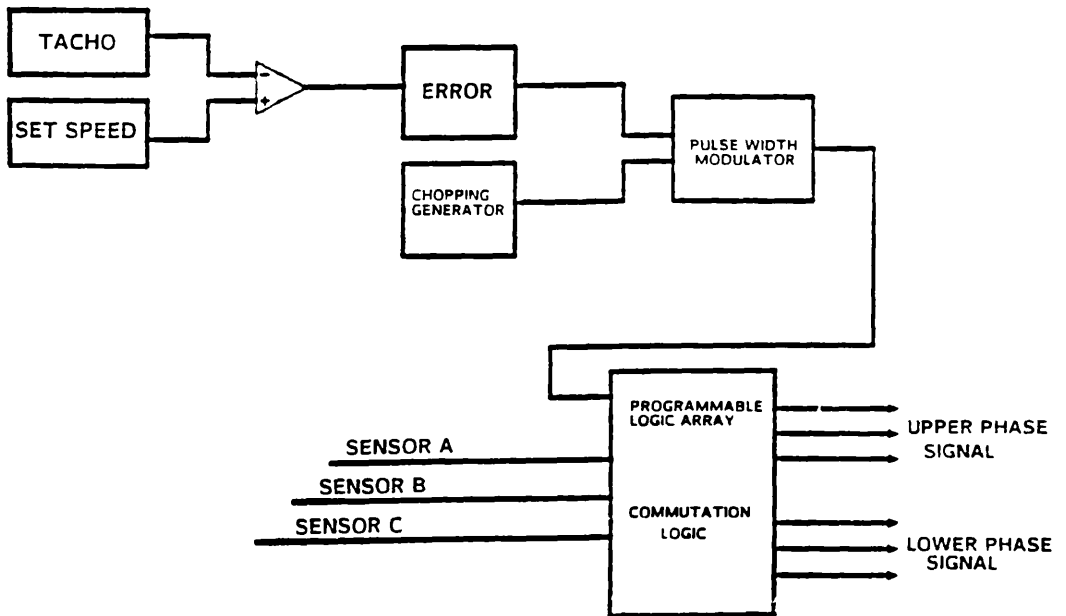
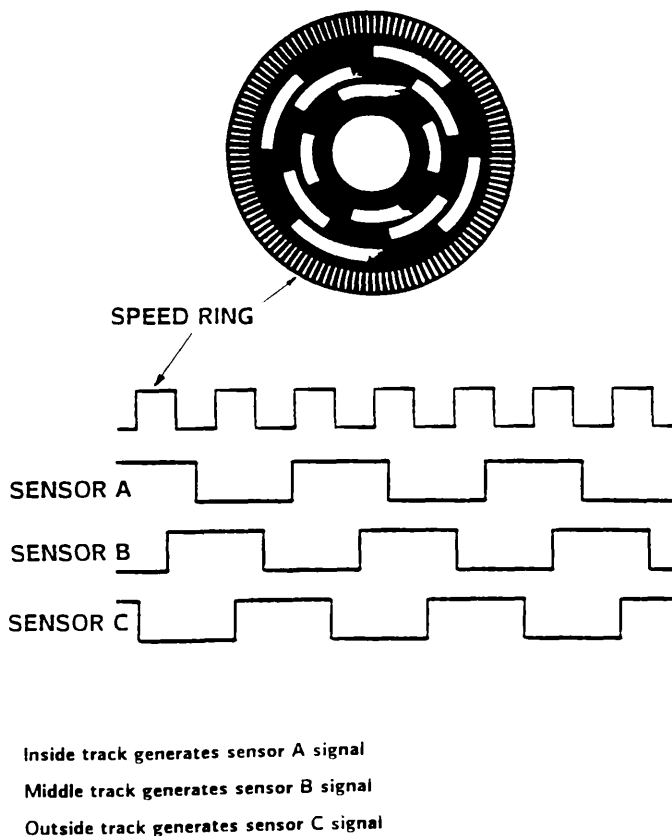


Figure 2.10 Control Board Functions

The output signals from the encoded disk consist of four rectangular waveforms or sensor signals. Three of the signals are shifted 30 degrees out of phase with one another. A logic 0 signal is the result of a window on the sensor disk passing between the transmitter and receiver of the opto-switching devices. Similarly, a logic 1 signal corresponds to the passing of a solid sector. These signals combined with combinational logic held within a programmable logic array (PAL) provide start/stop, current limit, forward/reverse and various operating modes for the motor. These modes are Normal, Boost and Long Dwell and are used to provide different conduction angles during motoring conditions. The logic signals from the three operating modes are converted to a 0-12V swing before being applied to the gates of the lower FET's in the converter circuit.



(not to scale)

Figure 2.11 Shaft Position Sensor Signals

The second control mechanism is the fixed frequency PWM of the supply voltage with variable duty cycle, d . Throughout each phase conduction period the applied voltage across the winding is regulated by chopping using pulse width modulation (PWM). This chopping action controls the amplitude of current through the phase winding. With a sufficiently high chopping frequency the effective applied voltage across the phase winding is the product of the DC source voltage and the duty cycle of the chopping. With the switching angles fixed, this is the basis with which the current and torque are regulated. The PWM control is applied to the upper MOSFET's and is combined with the commutation signal in the PAL. During chopping, when the upper FET is OFF, the lower FET is on and the phase current freewheels through the lower FET and diode (i.e., T2 and D2 of Figure 2.12). Since there is no applied voltage in this loop, the rate of decay of current is much less than it would be if chopping were applied to both FET's, and therefore the ripple current is greatly reduced.

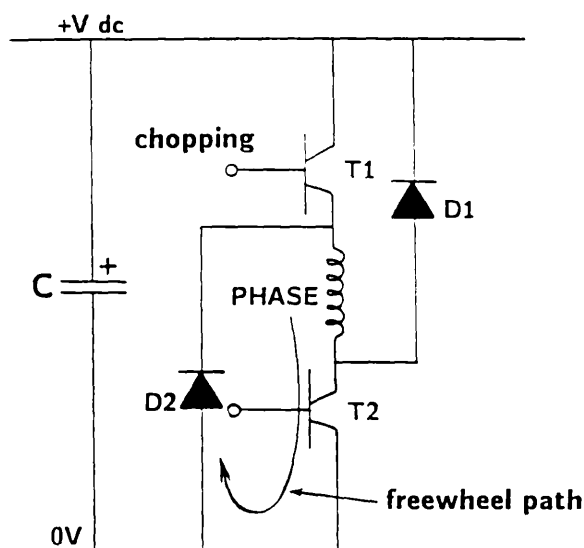


Figure 2.12 One Phase of half H Bridge SR Converter

The duty cycle is proportional to the difference between the speed demand voltage and the speed feedback signal. The DC speed feedback is the output of a frequency-to-voltage converter (LM2917) which converts the speed ring sensor signal from the encoded disk into a DC voltage proportional to the frequency of rotation. This acts to maintain an almost constant speed range for a given load range. This output is compared with the speed demand voltage and fed into a high gain op-amp. This allows the error voltage gain, and consequently the speed loop regulation to be adjusted according to the operating conditions required. With a high gain setting, the motor tends to run very lumpy at no load and low speeds. The gain setting can be selected by an 'on test' adjustment of the gain potentiometer. This needs further investigation to assess the most beneficial gain value. The error voltage is compared with the ramp output of the 555 timer IC using a comparator: LM339. This then produces a TTL signal proportional to the error and is the PWM signal for the PAL. The output logic from the PAL generates the chopping gate drive signal for the upper FET's. When the PWM duty cycle reaches 100% with the maximum phase advance mode i.e., Boost mode, the torque becomes inversely proportional to the speed squared as shown by Figure 2.13.

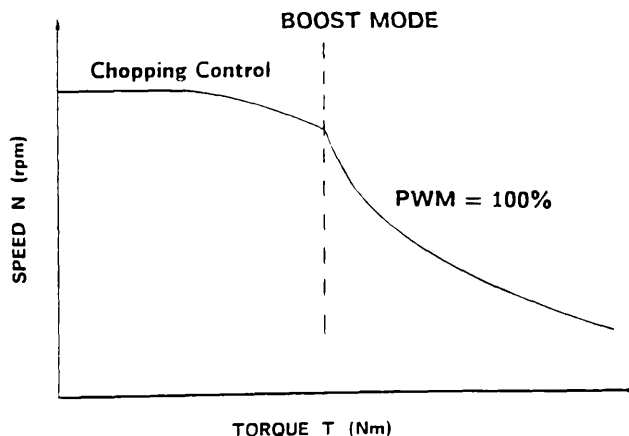


Figure 2.13 Torque/Speed Characteristics in Boost Mode

2.3.3 Power Circuit Design

The schematic diagram for the power converter circuit in the SR drive system is shown in Figure 2.14. Appendix 2.5 shows the circuit for a three phase half H bridge inverter. The circuit consists of six switches, each with an inverse parallel freewheeling diode. The pulse of current into each phase winding coincides with a period of rising inductance, i.e., when a pair of rotor poles is approaching alignment with the stator poles of the excited phase. The amplitude, timing and dwell of the current pulses determine both the torque and speed range: [2.5]. The precise switching angles are controlled by the shaft position sensor described in Section 2.3.2.

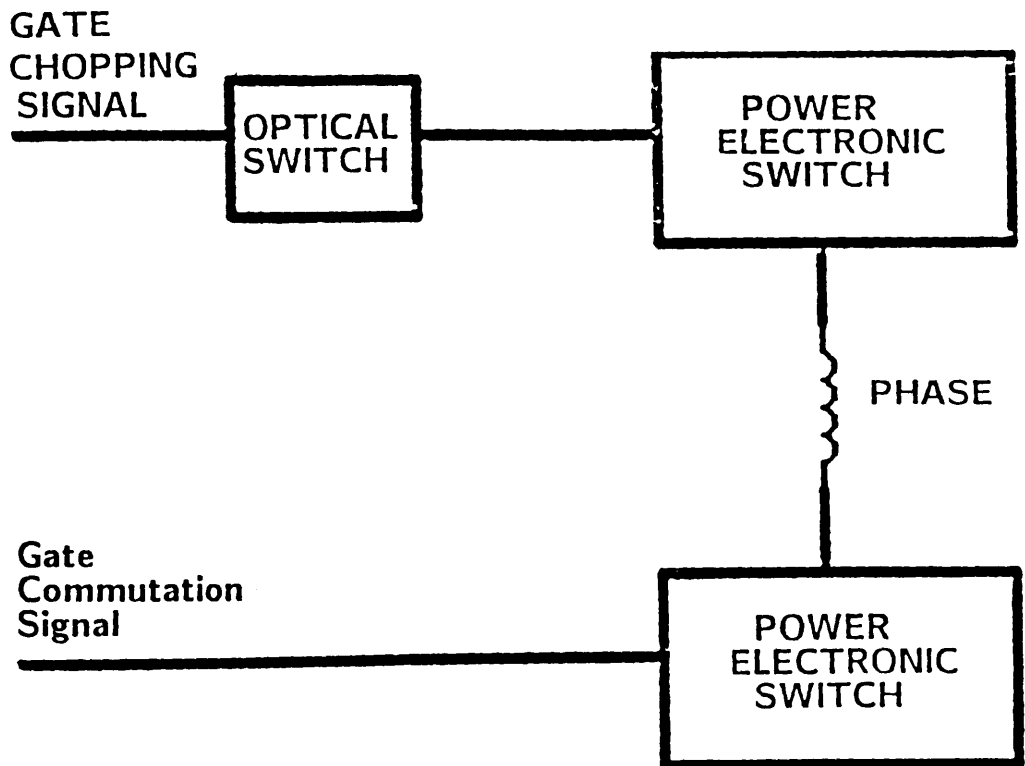


Figure 2.14 Power Board Functions

In a pulse width modulated (PWM) driver circuit, the two most important events are the switch on and off of the power semiconductor devices. This action, combined with an inductive phase load is illustrated in Figure 2.15.

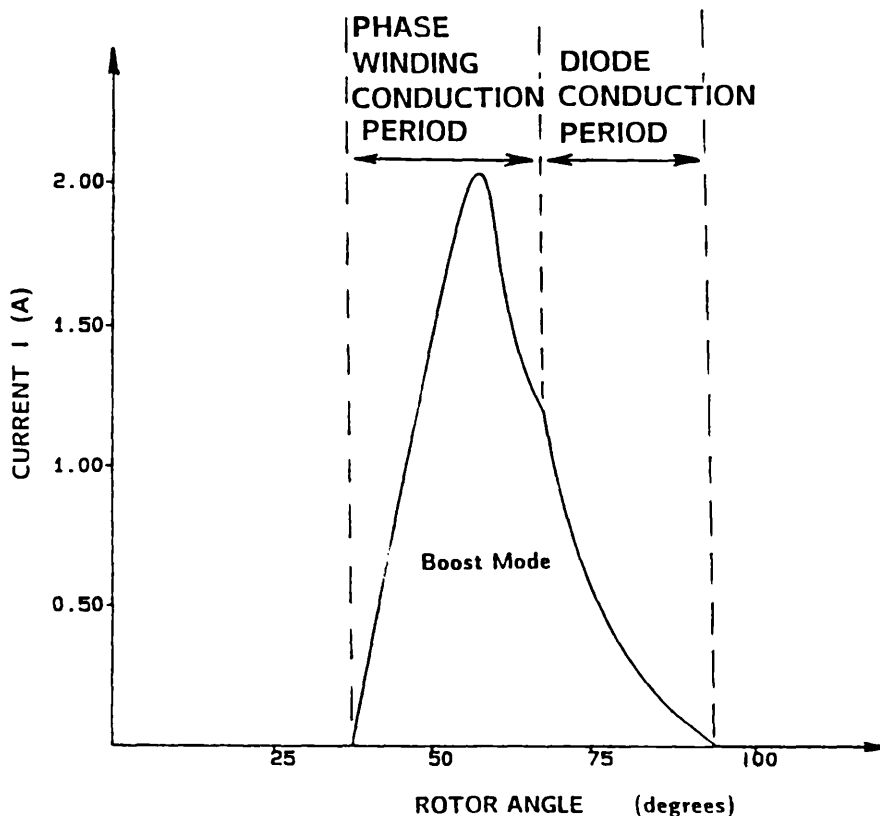


Figure 2.15 Typical Phase Current Waveform in Boost Mode

The phase current is switched on by the switching action of both the upper and lower MOSFET transistors of each individual phase-leg. When both FET's are on, the DC supply voltage is applied to the phase winding, resulting in an approximately linear increase of flux linkage. The current also increases as shown in Figure 2.15. At the end of the conduction period both FET's are switched off. The phase current then freewheels through the two associated diodes and back to the DC link capacitor. During this period the diodes are forward

biased and therefore they connect the negative of the supply voltage across the phase winding resulting in an approximately linear decrease of flux linkage with time. The current also decreases with a waveform typical of Figure 2.15.

The upper FET's of each phase have a floating source terminal with respect to the signal ground and therefore require an isolated drive system. This can be achieved using the opto-coupling device of Figure 2.16. This is basically an optical switch which connects the digital commutation signals with the gate/source connection of the high voltage power FET's. An added feature of the opto-switch is that it provides isolation between the low voltage and high voltage power supplies.

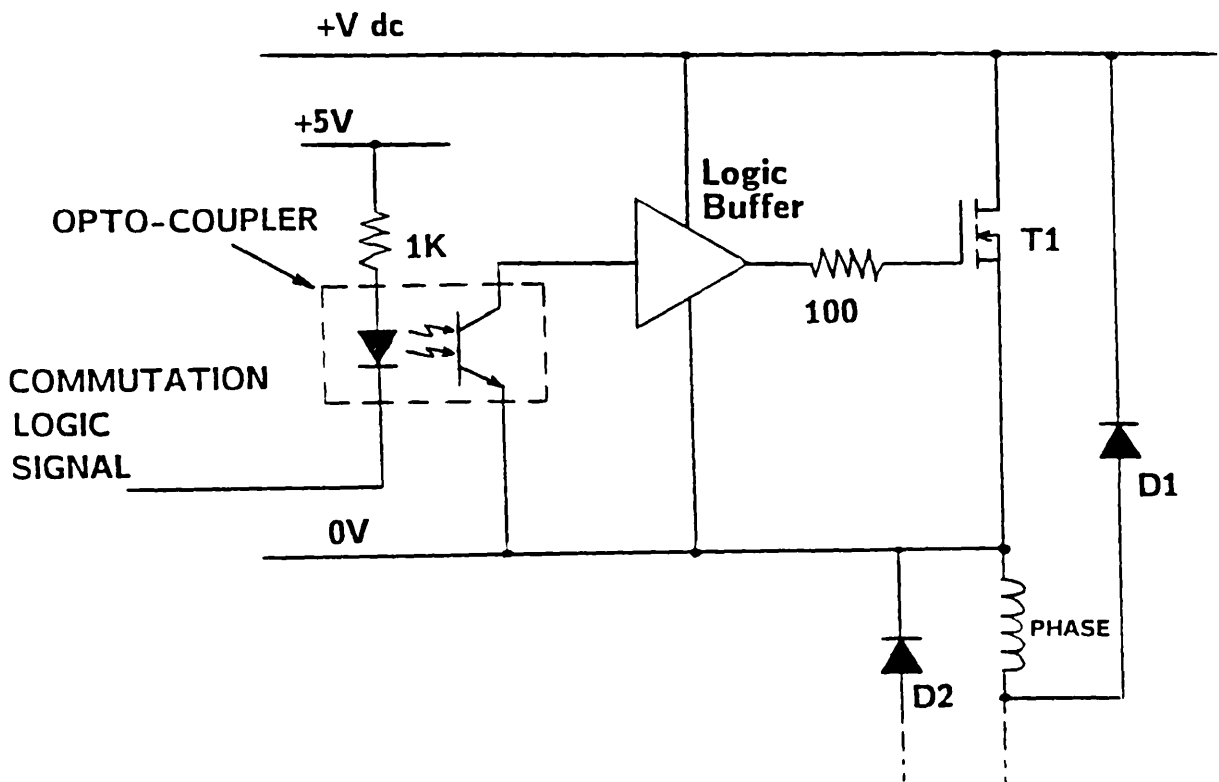


Figure 2.16 Optical Coupler Arrangement to provide isolation between the HV and LV supplies.

Both the upper and the lower FET's are N channel devices since their threshold voltage interfaces easily with logic level integrated circuits. It would have been more appropriate to use a P channel device for the upper drive since a simple level shifting drive transistor could have been used. The main drawbacks of P channel transistors are

- 1) very much larger on-state resistance when compared to N channel devices.
- 2) slower switching speeds and increased losses associated with the transistors.
- 3) poor, uneconomic use of the silicon area for high voltage ratings above 200V DC.

There are stray inductances in the circuit due to wiring inductance and semiconductor device package inductance. During switch ON these inductances will combine to limit the rate of change of current di/dt and cause transient overshoots. During switch OFF, the problem with a fast falling drain current is the presence of transient voltage spikes on top of the drain-source voltage due to stray and parasitic inductance. These are liable to destroy the MOSFET and are therefore suppressed by using a small series resistance on the gate input. This helps to slow down the falling edge of the drain current during switch off. In the circuit of Figure 2.16 a 100 ohm series resistance has been used on the gate of the MOSFET.

2.4 Comparison of Experimental Results

The primary objective of the experimental investigation was to study the torque/speed characteristics and thermal capability of both the 72mm and the 88mm stator diameter SR motors. This would provide valuable information about the capability of each motor under load conditions and consequently allow comparisons to be made with the existing series AC commutator motor.

2.4.1 Torque/Speed Characteristics

Figure 2.17 shows the torque/speed characteristics obtained from both the prototype SR drive systems developed for the food processor. The figure clearly shows the high torque, low speed characteristic with a maximum power output of around 310 Watts. High overall efficiencies are maintained over the wide speed range of loads and speeds. The upper limit has been determined by the thermal capability of the drive systems and it was decided that a maximum speed of 7000rpm was within the capability of both the 72mm and 88mm SR drives.

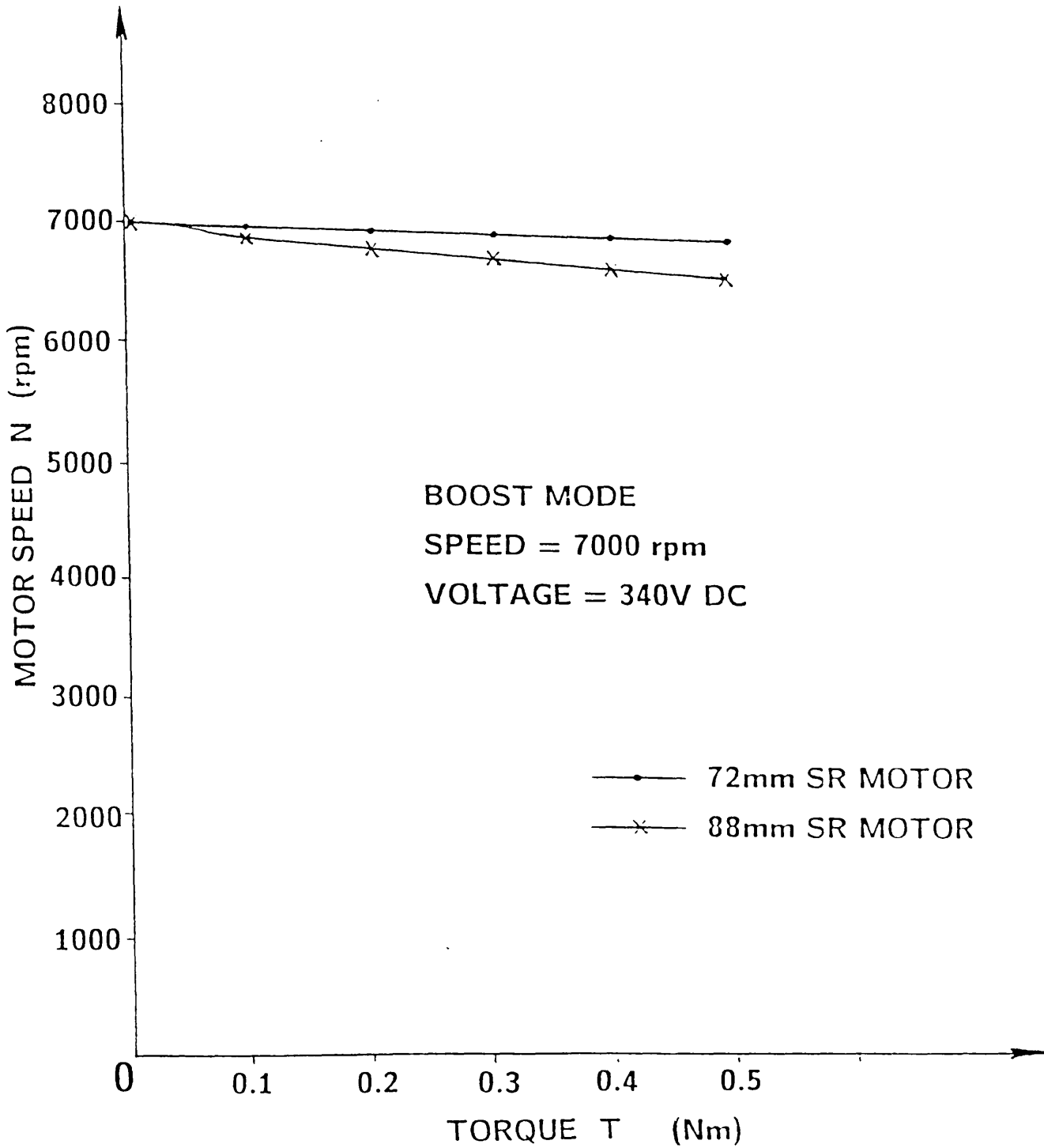


Figure 2.17 Experimental Torque/Speed Characteristics for 72mm and 88mm SR Motors

2.4.2 Thermal Capability

Whenever electrical energy is converted into mechanical energy certain losses occur which appear in the form of heat and raise the temperature of the machine. Because the insulating materials used within the machine have definite temperature limitations then the limiting factor on the motor is the temperature (T). The losses can be divided up into three groups:

- a) Frictional losses
- b) Resistance losses
- c) Iron losses

Frictional losses occur between the shaft and the bearings and from losses due to disturbances of the surrounding air in the stator/rotor geometry, i.e., windage losses. Losses due to resistance in the stator phase windings is a major contributor to the overall losses in the motor. The resistance of an electrical copper conductor is influenced by its temperature and therefore has a positive temperature coefficient of resistivity. This results in the resistance increasing with temperature and is given by

$$R' = R (1 + \alpha \Delta T) \quad (2.11)$$

where R is the resistance at room temperature and R' is the resistance at temperature T, α is the temperature coefficient of resistivity and ΔT is the change of temperature from the ambient. Iron losses occur in all parts of the magnetic circuit which are subject to a changing magnetic field. The two principal effects are

hysteresis and eddy current effects induced in the magnetic steel.

In the period of time just after starting the motor, the power absorbed occurs in the form of a temperature rise. The heat produced passes from the source (stator winding) towards the outer motor frame at a rate which is determined by the difference between the ambient temperature and the temperature inside the motor. As the temperature rises, the rate at which the heat is produced and absorbed decreases and the rate at which the heat is dissipated to the surrounding air increases. Eventually, a final temperature is reached where the rate of heat produced balances the rate of heat dissipated. In this steady state condition (see Figure 2.18) no heat is absorbed and the temperature of the motor levels out until there is a change in load or change in the surrounding air temperature.

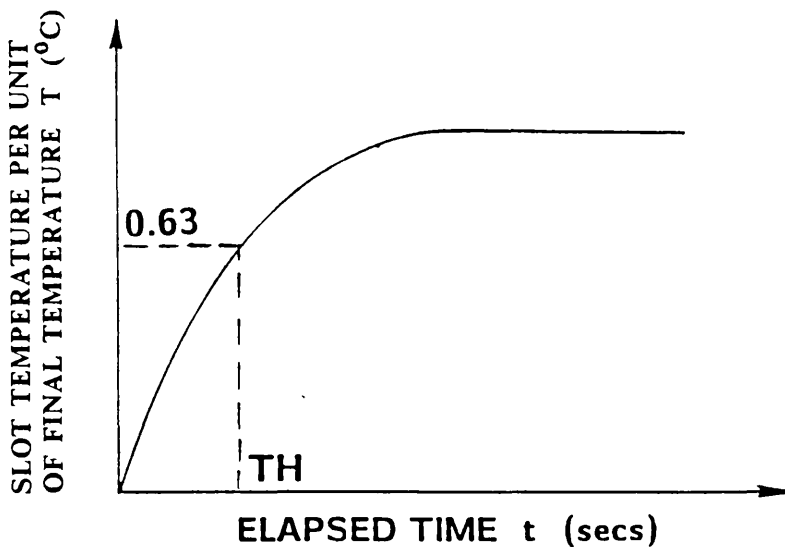


Figure 2.18 Temperature rise versus Elapsed Time for constant level of power dissipation

As the initial motor temperature rises, the heat energy will be stored in the surrounding motor material and, in particular, the metallic parts of the motor construction. This 'stored' thermal energy will be dependent on the mass of the material present within the motor and, as such, will increase with any increase in material used. The thermal capacity of the SR motor can be calculated from

$$H = M \times C \quad (2.12)$$

where H is the thermal capacity, M is the mass of the machine and C is the specific heat of the materials used in the motor construction.

An analogue circuit can be used for the thermal analysis of the motor. This is detailed in Figure 2.19.

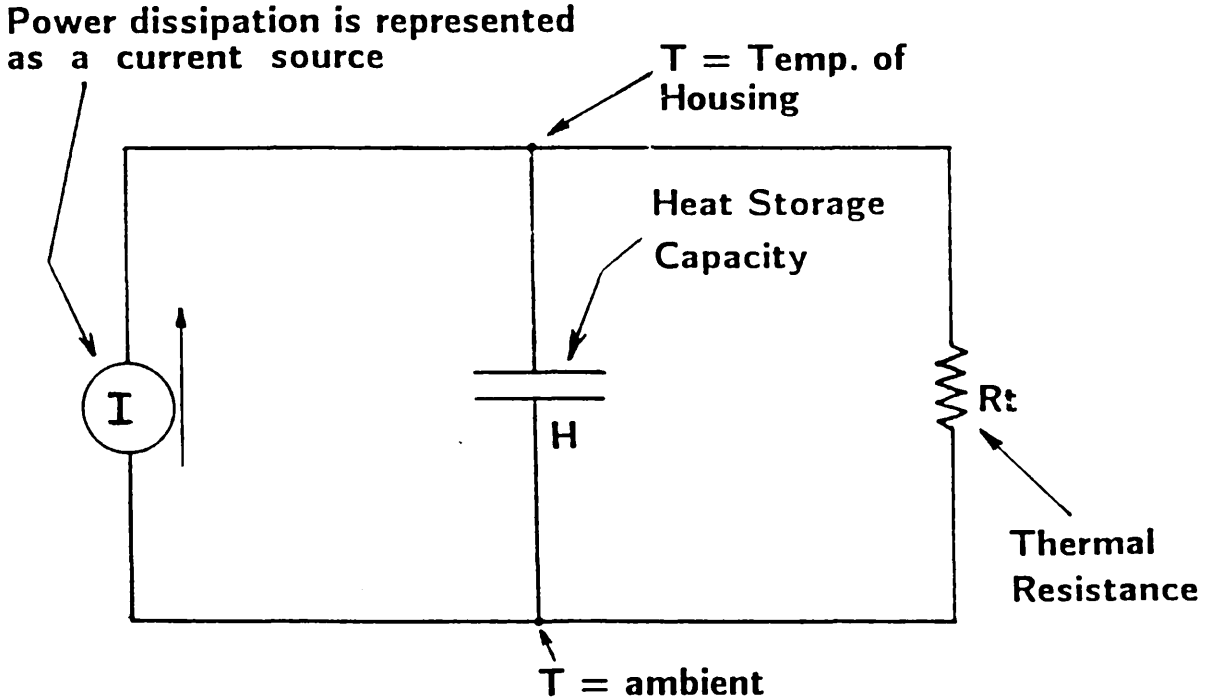


Figure 2.19 Equivalent Analogue Circuit for Thermal Analysis

In this circuit all the motor losses are lumped together and assumed to originate from a single source (I). Similarly, the heat storage and thermal resistance are represented by single elements H and R_t respectively. The thermal resistance can be described according to the equation

$$R_t = \text{steady state temp rise/Motor losses} \quad (^\circ\text{C/Watt})$$

The value of the heat storage capacity, H can be calculated by multiplying the weights of the metals used within the motor by their respective specific heat coefficients: (Appendix 2.6a, 2.6b).

$$H = M_1.C_1 + M_2.C_2 + M_3.C_3 + \dots\dots\dots$$

i.e., $H = M_t.C_t$ where $t = 1$ to n

The value of I in Figure 2.19 is the total value of the motor losses in Watts.

In circuit terms, the current response on the resistor R_t is given by

$$i = I \left[1 - e^{-t/R_t H} \right] \quad (2.13)$$

The voltage dropped across the resistor, i.e., the temperature rise is given by

$$V = iR_t = IR_t \left[1 - e^{-t/R_t H} \right] \quad (2.14)$$

This gives the characteristic exponential curve of Figure 2.18. The time constant associated with this curve is the thermal time constant and is defined by

$$T_H = R_t H \quad (2.15)$$

This is the time taken to reach 63% of the final steady state temperature rise at a constant rate of heat dissipation. The slot temperature rise versus elapsed time curves of Figure 2.21 show the effectiveness of the cooling fan and air blower methods. These curves demonstrate the advantages of rapidly removing the heated air from the inside of the 72mm motor frame. The cooling fan at the end of the 88mm motor is not so effective since the rate of heat removal is dependent on the motor speed. Because of high rotor speeds in the series AC commutator motor, then the cooling fan becomes more efficient and as such enhances the ability of the motor to dissipate the heat. The results of Figure 2.20 provide a comparison between the experimental and calculated values for the phase winding temperature rise in the two SR motors. The theoretical method used is outlined in Appendix 2.7. The results show that the winding temperature rise in the 88mm motor is very much greater than the 72mm motor. This is confirmed by the theoretical calculations. The experimental measurements of slot temperature were therefore inadequate in providing realistic temperature values for the phase winding under load conditions. The reason for this was due to the measuring thermocouple which was placed too close to the incoming cold airflow from the external air blower. The one advantage of the this totally enclosed 72mm motor casing with fan blower was the effective way in which heat could be removed at light loads under 0.3Nm. This was due to the mass of aluminium surrounding the stator frame which acted as a heatsink to provide a good heat transfer. The result was a reduction in the motor power

losses when compared to the 88mm motor. The results are shown in Figure 2.20.

APPLIED TORQUE Nm		0.1	0.2	0.3	0.4	0.5
72mm MOTOR						
Power Loss (Watts)		29	46	73	92	135
T (°C)	Calculated	8.15	12.94	20.53	25.87	37.96
	Measured	8.41	13.34	21.17	26.68	39.15
88mm MOTOR						
Power Loss (Watts)		52	75	86	97	127
T (°C)	Calculated	18.22	26.27	33.98	34.33	44.49
	Measured	19.00	26.62	34.43	34.79	45.08

Figure 2.20 Comparison of Calculated and Experimental Results for Phase Winding Temperature Rise (resistance measured) and Power Losses for 72mm and 88mm SR motors at 7000 rpm.

2.5 Conclusions

Within the bounds of this research project the main objectives which were to design, build and test two prototype SR drives for a food processor, have been achieved.

The 72mm SR motor which was a totally enclosed, fan cooled drive was found to be very efficient under load

conditions when compared to the series AC motor: (Appendix 2.8). The main reason for this was 1) the reduction in the volume of magnetic material used helping to reduce the iron losses within the motor and 2) the tightly wound phase windings which possessed very small end-turns. The ball bearings used had low frictional losses which also helped to improve efficiency.

The 88mm SR motor possessed a totally exposed stator lamination design which was held together with end-plates from the series AC commutator motor. The efficiency of this drive system under load conditions was less than the 72mm motor due to an increase in the copper losses from the large end-turns plus the contribution of increased frictional losses between the shaft and the sleeved bearings used.

Throughout all of the experimental tests, attention was paid to the noise levels from both SR drive systems. It was found that the 72mm SR motor with very stiff aluminium frame was very much quieter than the 88mm SR motor under load conditions. There were two main reasons for this; first, the 72mm motor had wide stator poles which helped to reduce the torque ripple and acoustic noise; secondly, the mechanical construction of the casing was more detailed in design and possessed very good mechanical stiffness. The penalty incurred by reducing the acoustic noise is the increased cost and mechanical complexities involved. . The airgap for the series AC commutator motor was measured to be 0.03 inches. The airgap size for the 72mm and 88mm SR motors was 0.02 inches and 0.015 inches respectively. In practise, manufacturing costs will likely prohibit these very small airgap tolerances. Both the 72mm and 88mm SR motors were quieter than the series AC commutator motor under all load conditions.

The theoretical results obtained for the phase winding temperature rises under load conditions show quite clearly that the temperature rises can be predicted quite accurately from knowledge of the heat storage capacity.

2.6 Future Work

Further work will be undertaken into various issues. In particular, the reduction or possible elimination of the shaft position sensor. Lumsdaine et al. [2.21] and Bass [2.22] have both reported schemes for the operation of SR motors without the need for a shaft sensor. With unidirectional and single mode operation the requirement for only two sensors will be feasible. Another possible future development will be a cost effective high voltage IC controller to eliminate the large transistor requirement. Further development of the mechanical engineering aspects for mass production of the switched reluctance motor drive will be required if the SR technology has any hope of competing with the future generation of motor drives. Further work will be carried out on the noise levels from the various motor configurations.

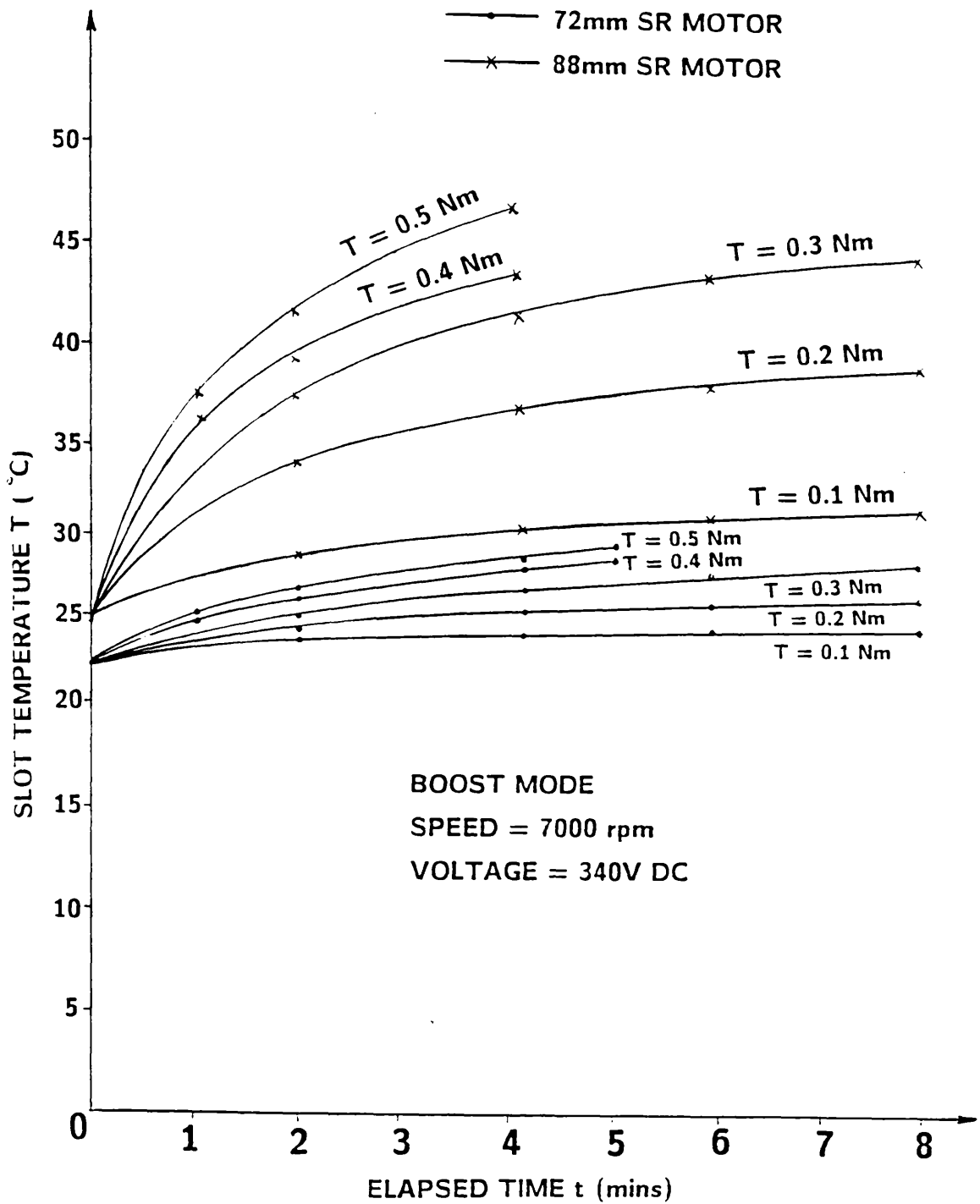


Figure 2.21 Experimental Slot Temperature versus Elapsed Time for 72mm and 88mm SR Motors

CHAPTER 3

FLUX SCREENING METHODS IN A SWITCHED RELUCTANCE MOTOR

3.1 Introduction

The second aspect of this thesis is an investigation into the use of flux screens to improve the specific torque (torque per unit volume) of the switched reluctance motor.

In the last decade there has been rapid development of the SR motor drive. This has been the result of three main lines of development; first, the perfection of motor lamination geometries ; secondly, the advent of more flexible control electronics and the availability of improved power semiconductor devices and thirdly, the increased use of the SR drive not only in industrial applications such as pumping [3.1] and traction drives [3.2] but also in computer peripherals [3.3] and prototype domestic applications. Such developments have, in recent years, found applications for the SR motor both in the high and low horse-power categories. As a result, the SR drive is beginning to deliver on its early promise of high efficiency, high torque per unit volume, etc.: [3.4,3.5]. Our concentration will be focussed in the low horse-power range although the fundamental principles will be applicable to higher power drives.

The objective of this research is to investigate specific techniques which can be implemented to improve the output performance of the switched reluctance motor. Conducting flux-screens is one such area [3.6] which has been investigated in order to reduce the unaligned or minimum phase inductance L_u . This is a key parameter in the torque per unit volume and torque/speed range.

Eddy currents induced in these screens help to dynamically reduce the apparent inductance of the phase winding under transient conditions. If the screening effect persists for a long time relative to the phase conduction period then the induced screen currents will remain 'inductance limited' and will behave as an impermeable barrier to the flux. In this condition the screen surface is like a diamagnetic (zero permeability) boundary and produces the maximum possible reduction in phase inductance. A number of possible screen locations and designs have been identified. Their effects on the unaligned phase inductance have been analysed using a finite-element package. An experimental investigation has been carried out on a 50W SR motor (Appendix 3.1). The principles developed in this Chapter also apply to larger motors where the benefits might be more significant, because of the reduced effect of resistance in the screens. Measurements have also been made to determine the static and dynamic unaligned DC inductances for all the concepts considered. The torque/speed characteristics are also determined to assess the improvement of the speed range for a given torque using the flux screening methods.

3.2 Fundamental Principles

3.2.1 Torque Production using Screening Methods

In the conventional switched reluctance motor the torque is developed by the tendency for the magnetic circuit to adopt a configuration of minimum reluctance or maximum inductance. The energy converted from electrical to mechanical during one step or 'working stroke' of the rotor is equal to the 'conversion area' (W) enclosed by

the maximum inductance and the unaligned or minimum inductance as shown in Figure 3.1. This is the locus of the point whose co-ordinates are the phase current and phase flux linkage, as these vary throughout one complete step. The average electromagnetic torque (T) is given by

$$T = \frac{qN_r}{2\pi} W \quad (3.1)$$

where qN_r is the number of steps per revolution with q the number of phases and N_r the number of rotor poles. In order to gain the maximum available 'conversion area', it is desirable to maximise the area between the aligned and unaligned magnetisation curves for a given phase current.

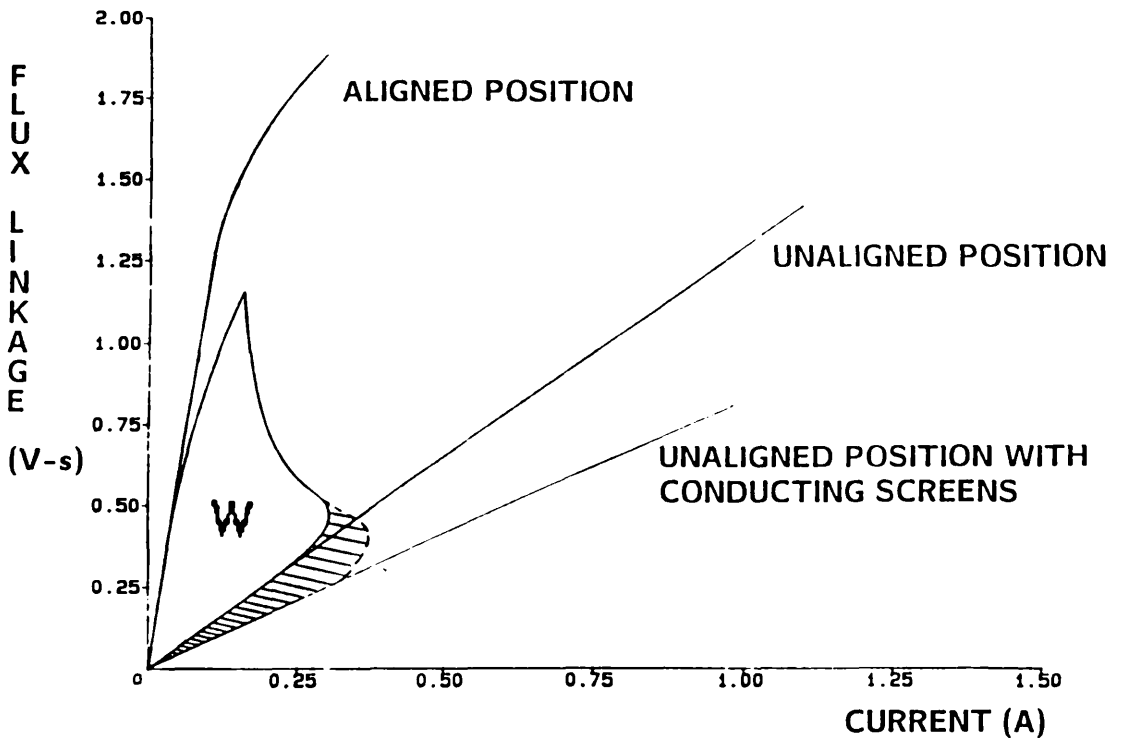


Figure 3.1 Flux Linkage/Current Trajectory

To achieve a high aligned inductance a small air-gap and wide stator poles are needed together with a magnetic steel which possesses a high saturation flux density. The smallest possible unaligned inductance can be derived from a rotor geometry with large interpolar gaps, deep rotor slots and narrow stator poles. These requirements are, in some respects, contradictory to achieving a high aligned inductance and therefore, computer design methods are essential in establishing the optimum geometry.

An alternative approach to reduce the unaligned or effective minimum inductance is through the use of conducting flux-screens. In general, if resistance is neglected, the effective inductance of the phase winding will be reduced by the effect of eddy-currents induced in the screen. Consider the circuit of Figure 3.2.

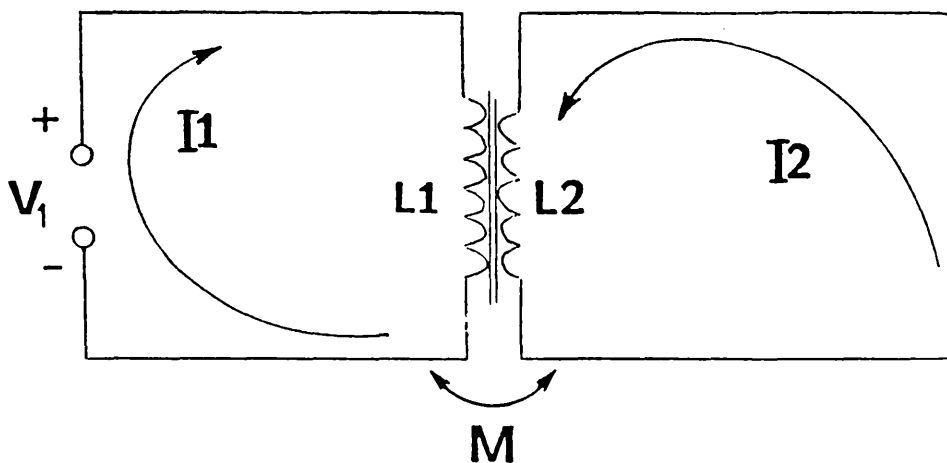


Figure 3.2 Ideal circuit for Rotor with Conducting Flux Screen

The primary voltage (phase voltage) on the stator can be defined by equation 3.2:

$$V_1 = L_1 \frac{di_1}{dt} + M \frac{di_2}{dt} \quad (3.2)$$

and the short circuit voltage across the secondary winding (screen) is

$$V_2 = 0 = L_2 \frac{di_2}{dt} + M \frac{di_1}{dt} \quad (3.3)$$

Using Laplace gives

$$\frac{V_1}{di_1/dt} = L_1 (1 - k^2) \quad (3.4)$$

where k is the coupling coefficient between the winding and the screen ([3.7] and Appendix (3.2)). This then gives

$$L' = L_1 (1 - k^2) \quad (3.5)$$

where L is the 'unscreened' inductance. If the screening effect persists for a long time relative to the phase conduction period, then the induced screen currents will remain 'inductance limited' and will behave as an impermeable boundary to the flux.

In practice, resistance is not negligible but the ideal screened inductance may be obtained for the first few instants under transient conditions, i.e., the conducting screen surface acts like a diamagnetic boundary and produces the maximum possible reduction in phase inductance: [3.8].

The operation of the switched reluctance motor is based on a sequence of current pulses which reactivate the conducting screen at every phase switching operation. The effectiveness of the screen to act as an impermeable boundary will depend heavily on the diffusion time constant of the eddy-currents and the conduction period. These parameters are themselves dependent on the speed

and torque demand. The eddy-currents must be allowed to persist for long enough to provide any benefit.

In the absence of magnetic saturation the instantaneous torque at any rotor position is given by

$$T = \frac{1}{2} i^2 \frac{dL}{d\theta} \quad (3.6)$$

With negligible resistance, the L value is replaced by L' which is actually the leakage inductance between the winding and the screen 'referred' to the terminals of the phase winding: (equation 3.5).

3.2.2 Transients in Coupled Circuits

An understanding of transients in coupled circuits [3.9] is important when studying the effects of conducting screens within the switched reluctance motor. Appendix 3.3 details transients in an RL circuit.

3.3 Methods for Screen Evaluation

To achieve the lowest possible minimum inductance two approaches are possible: one is to minimize L ; the other is to make k as near to unity as possible. Unfortunately, a high coupling coefficient is achievable only when the air-gap is very small and the magnetic flux is highly guided. Similarly, this is when the unscreened flux path is constrained by high permeability magnetic material. This inevitably leads to high value for the unscreened inductance L and tends to offset the benefit of the high

value of k . This research considers two approaches towards achieving these objectives.

There were three methods of evaluation used:

- 1) Finite-element analysis
- 2) Static DC Inductance Measurements
- 3) Torque/Speed Characteristics

The finite-element analysis was used to estimate the maximum reduction in unaligned inductance that could be achieved using perfectly conducting flux screens. The screens were modelled by diamagnetic boundary conditions representing impermeable surfaces around the screen boundaries. The field solution was based on perfectly conducting screens which are optimistic but provide an upper bound to the inductance reduction, and which may or may not be approachable in practice.

The static DC inductance measurements were made with the rotor clamped in the unaligned position and a step of voltage applied to one phase winding. From the phase current waveforms, the initial di/dt can be determined to give a measure of the screened unaligned inductance of the phase winding.

The speed/torque measurements were made at speed under load conditions. The phase current waveform was also recorded to provide a check of the screened inductance value.

3.3.1 Phase Current Expression for Rotor with Conducting Inserts

The equivalent circuit for the stator and rotor configuration is shown in Figure 3.3.

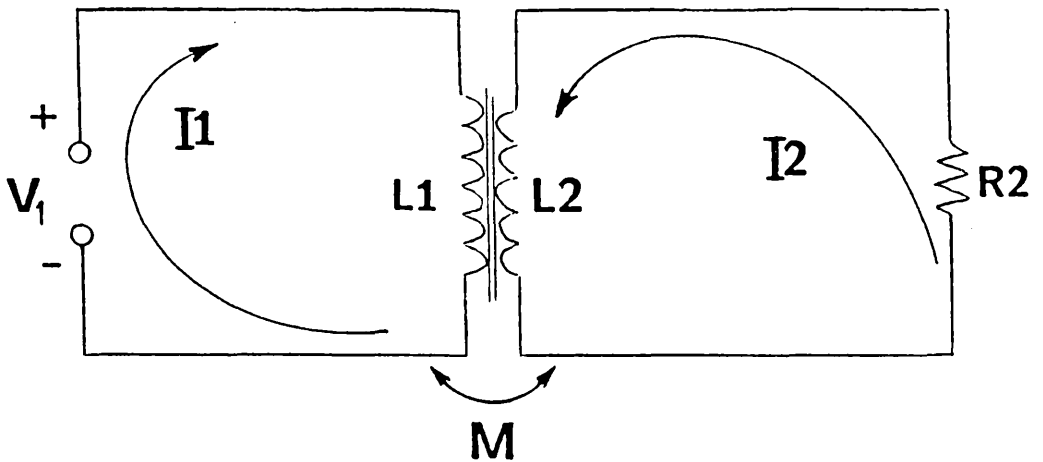


Figure 3.3 Equivalent Circuit for SR motor with Conducting Inserts on the Rotor.

The voltage across the stator winding is given by

$$V_1 = L \frac{di_1}{dt} + M \frac{di_2}{dt} \quad (3.7)$$

The short circuit voltage across the conducting insert is

$$V_2 = 0 = L_2 \frac{di_2}{dt} + M \frac{di_1}{dt} + R_2 i_2 \quad (3.8)$$

Use Laplace transforms to give

$$I_2 = \frac{-sMI_1}{R_2 + sL_2} \quad (3.9)$$

Substitute

$$V_1 = sL_1 I_1 - \frac{s^2 M^2 I_1}{R_2 + sL_2} \quad (3.10)$$

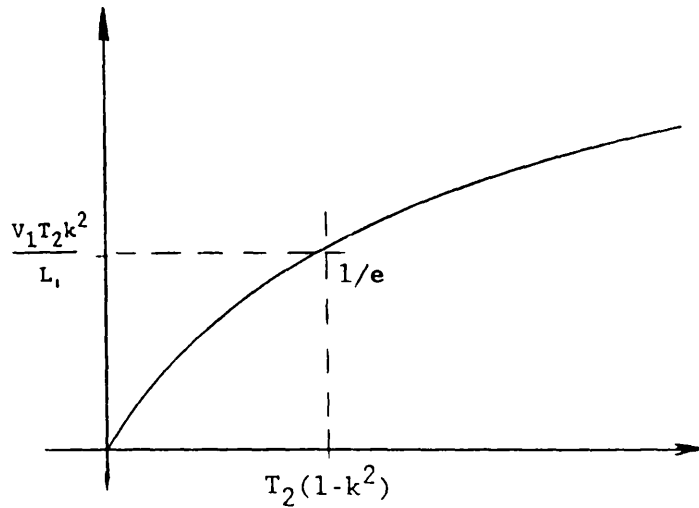
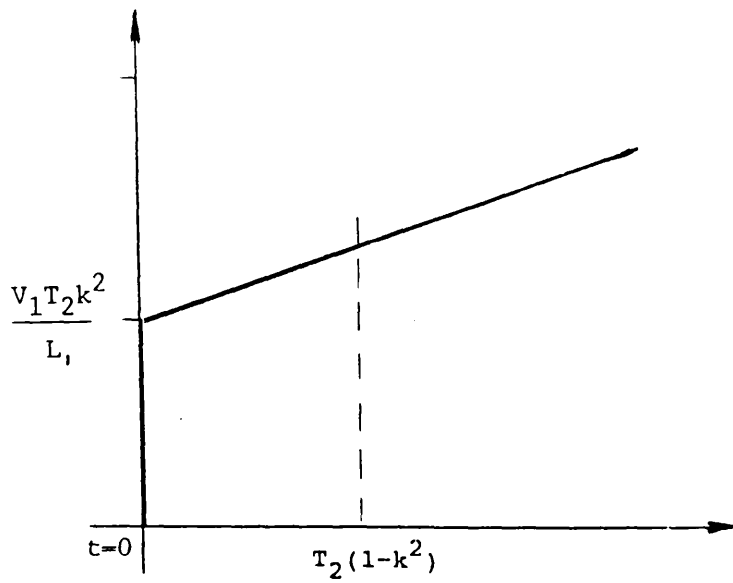


Figure 3.3b Phase Current (I_1) under step voltage input.

3.4 Evolution of Different Rotor/Stator Configurations

Four different screening concepts are summarised in Figure 3.7 and Appendix 3.4.

3.4.1 Conducting Insert Rotor

The rotor of Figure 3.4 is that used in a conventional switched reluctance motor. It is built up from a stack of laminations which are clamped at either end by compressive washers. Figure 3.5 shows the first of four screening concepts to be evaluated. The rotor has conducting inserts filling the interpolar space on the rotor stack. These inserts are made from copper and are insulated from the laminations using slot liners. No electrical connection exists between the conducting inserts. They are supported against centrifugal load by embedded steel pins attached to rebated tufnol extensions. These are encased in steel end-rings at each end of the rotor. Insulating tufnol was used to prevent the steel flanges from shorting the conducting inserts together.

The screening effect is established in the unaligned position due to the incident magnetic flux giving rise to a current distribution within the conducting insert. Consequently, the screen currents exclude all the flux from the insert interior provided that the currents are maintained, i.e., reactance-limited eddy currents in the screen completely exclude all the flux from the interpolar space between the rotor poles. In practice, a finite resistance is present in the screen which causes these eddy-currents to decay and die out. This decay time is called the screen time constant. If this time is too short, the screen currents die out quickly. It is then said that the eddy currents are resistance-limited. With a slow decay rate, the screen currents are said to be inductance (reactance)-limited. A material with a high conductivity (low resistivity) will become more effective as a flux barrier since it tends to make the induced currents reactance-limited.

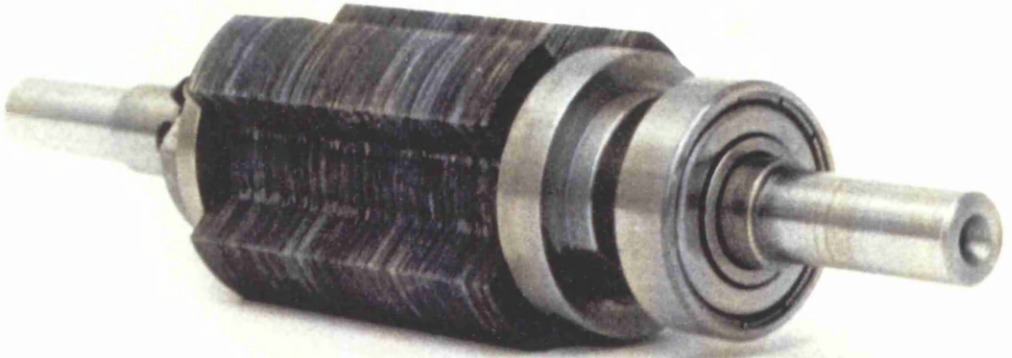


Figure 3.4 Conventional Rotor



Figure 3.5 Conducting Insert Rotor

3.4.2 Copper Bar Rotor

The second screening concept is shown in Figure 3.6. It has a circular cylindrical laminated rotor with four pairs of round slots. Each slot is filled with a copper conductor which has a glass coating to insulate it from the laminations. The conductors are linked, in adjacent pairs at the ends of the rotor to give four screened axes and four unscreened axes. Appendix 3.5 gives the technical aspects of the rotor construction.

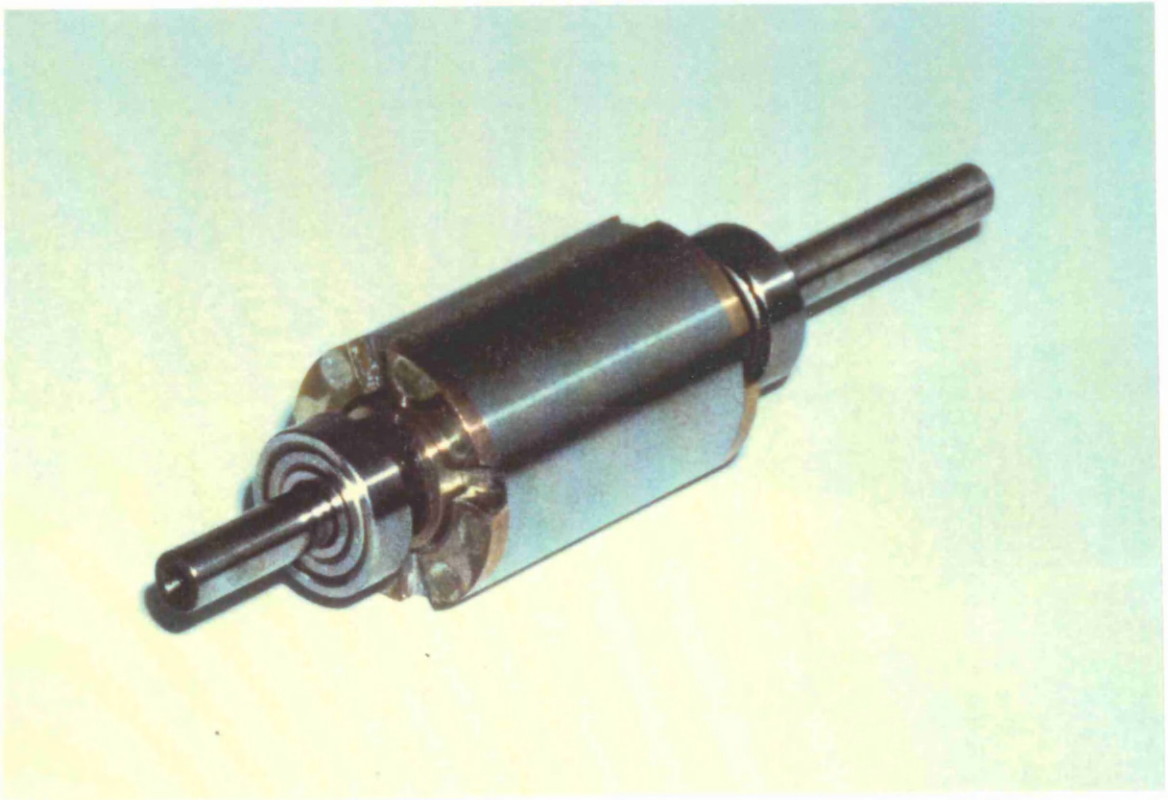


Figure 3.6 Copper Bar Rotor

3.4.3 Conducting Stator Slot Screens

The third concept is shown in Figure 3.7. It has flux screens in the stator slots instead of on the rotor. These have been strategically positioned to limit the stator leakage flux which is a component of the unaligned inductance. The fourth concept is a combination of the rotor interpolar inserts and the stator slot screens.

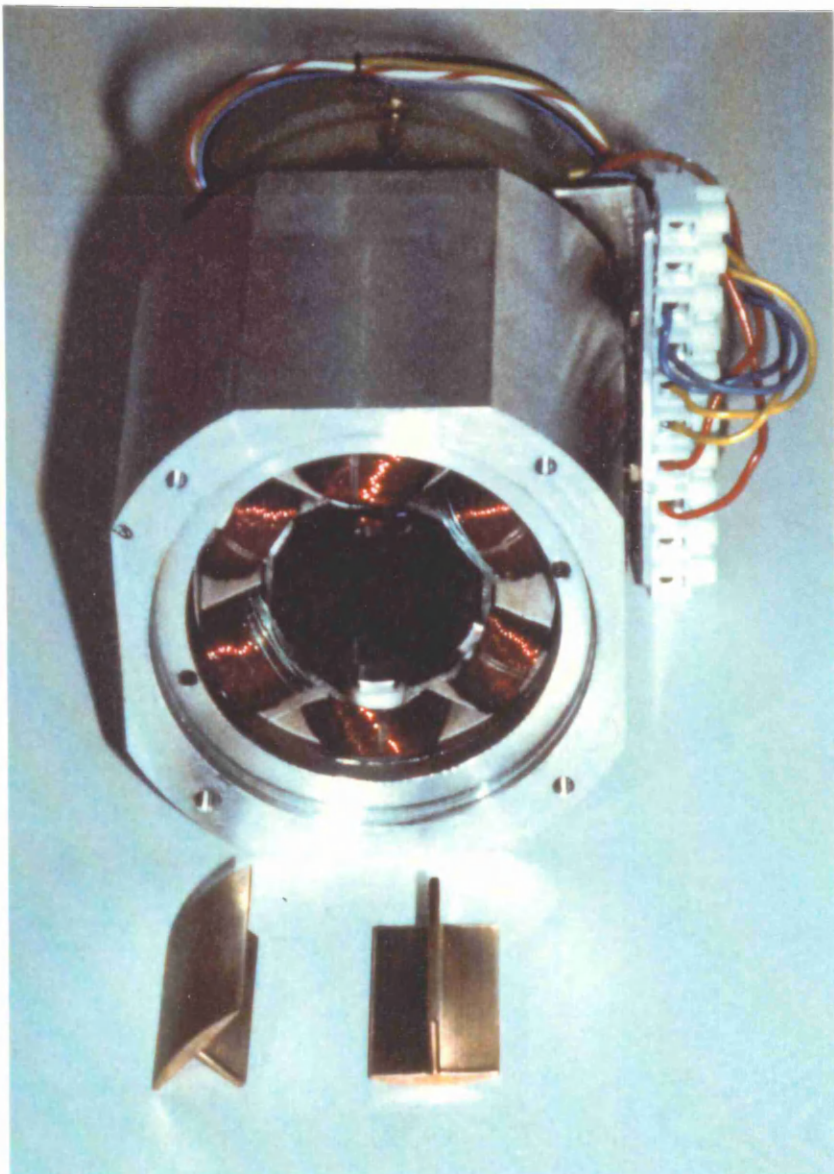
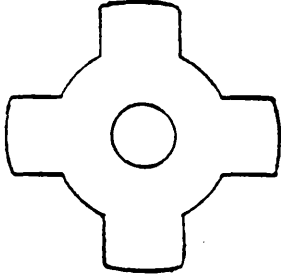
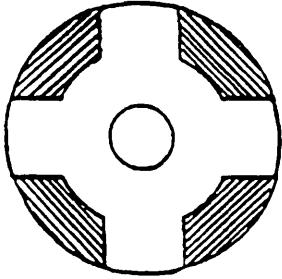
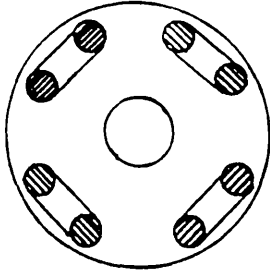
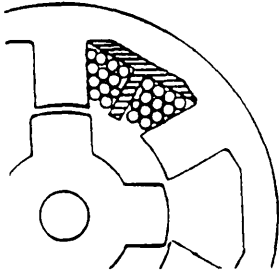
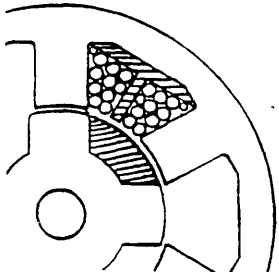


Figure 3.7 Conducting Slot Screened Stator

3.5 Finite-Element Analysis of Screen Concepts

Figure 3.8 provides a comparison for the various results obtained using finite-element analysis and from experimental tests. The unaligned inductance calculated by finite-elements (with a simple end-turn correction) for the conventional rotor is 13.6mH. The aligned inductance in the 72mm test motor was computed to be 125mH, giving an unsaturated inductance ratio of about 9. Figure 3.9 and 3.10 show the flux-plots for the aligned and unaligned positions of the conventional rotor pole with respect to the stator pole. A finite-element analysis was carried out for the rotor with conducting screens. The screens were modelled as impermeable boundaries over the entire surface. The computed unaligned inductance is 7.84mH. This is significantly less than the unscreened inductance value and suggests the possibility of a performance improvement. Figure 3.11 shows the flux-plot from the finite-element calculations illustrating the screening effect of the conducting insert.

ROTOR/STATOR CONCEPT	UNALIGNED INDUCTANCE L_u (mH)	
	FEA	SIM
	13.6	14.0
	7.84	11.3
	-	21.5
	5.71	12.0
	5.63	8.95

FEA: Finite-element analysis
SIM: Static Inductance Measurement

Figure 3.8 Table of Results for Various Screen Concepts

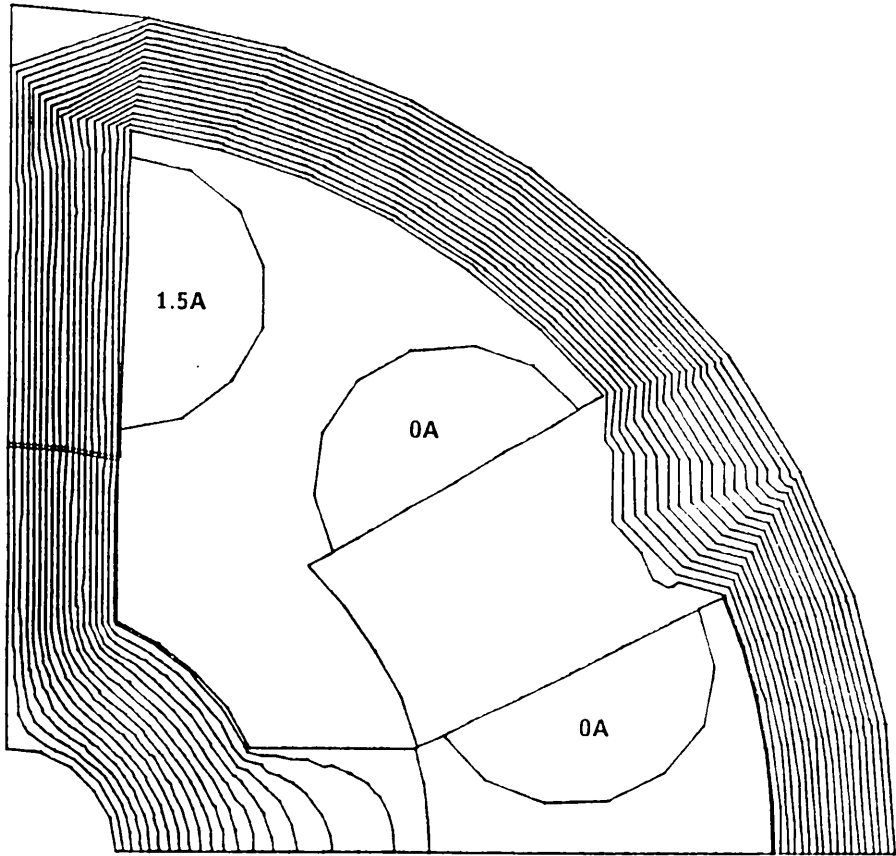


Figure 3.9 Aligned Position Flux Plot for Normal Rotor

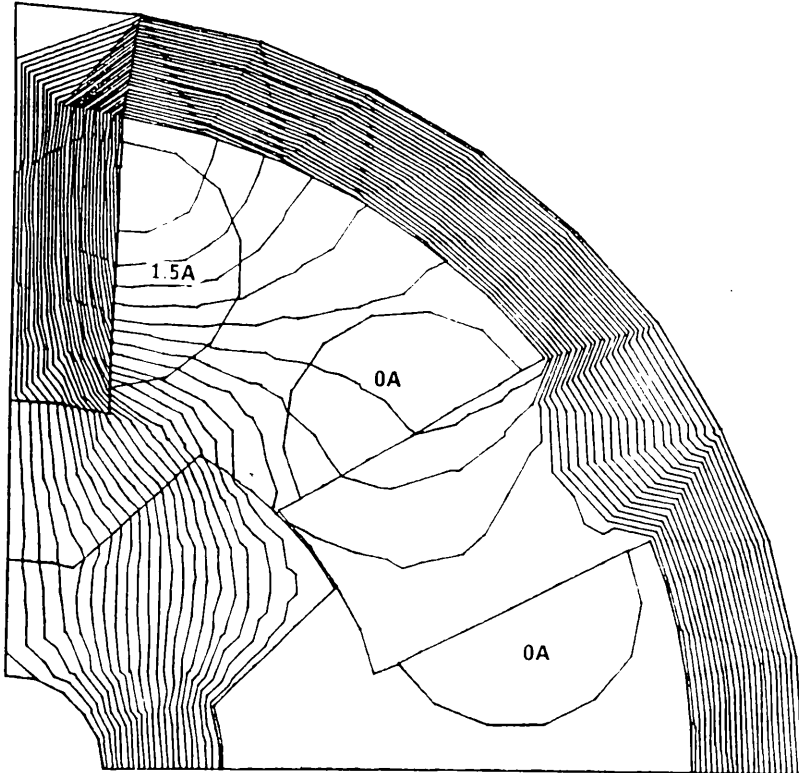


Figure 3.10 Unaligned Position Flux Plot for Normal Rotor

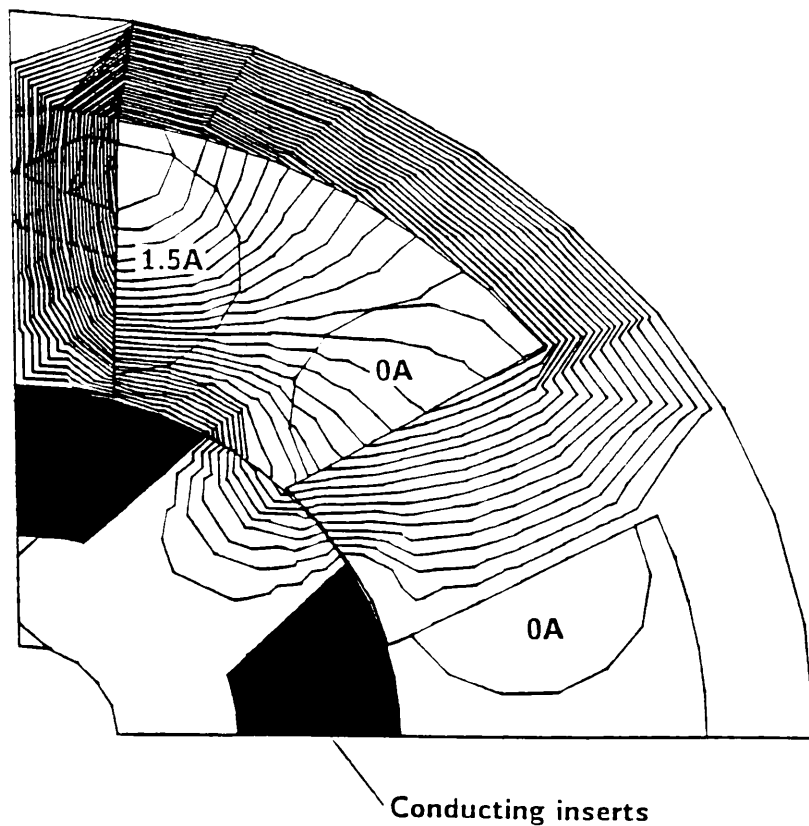


Figure 3.11 Unaligned Position Flux Plot for Conducting Insert Rotor

A magnetostatic analysis cannot strictly be used on the current bar-rotor concept since a predetermined current value is required in the rotor circuits. Therefore the finite-element analysis could not be used to predict the screened unaligned inductance. However, it can be argued that if the rotor circuits span the same arc as the interpolar insert, and if they are equally effective in excluding flux from passing through this arc, then the screened inductance should be comparable to the 7.8mH calculated earlier.

The conducting screens in the stator slot are modelled by impermeable boundaries using the finite-element analysis. These boundaries are placed between the stator slots, i.e., bisecting the slots. The calculated screened inductance is 5.7mH which is 73% of the value obtained

with rotor inserts. This is only 41% of the original unshielded inductance using the conventional rotor. Figure 3.12 shows the flux-plot for the screens on the stator.

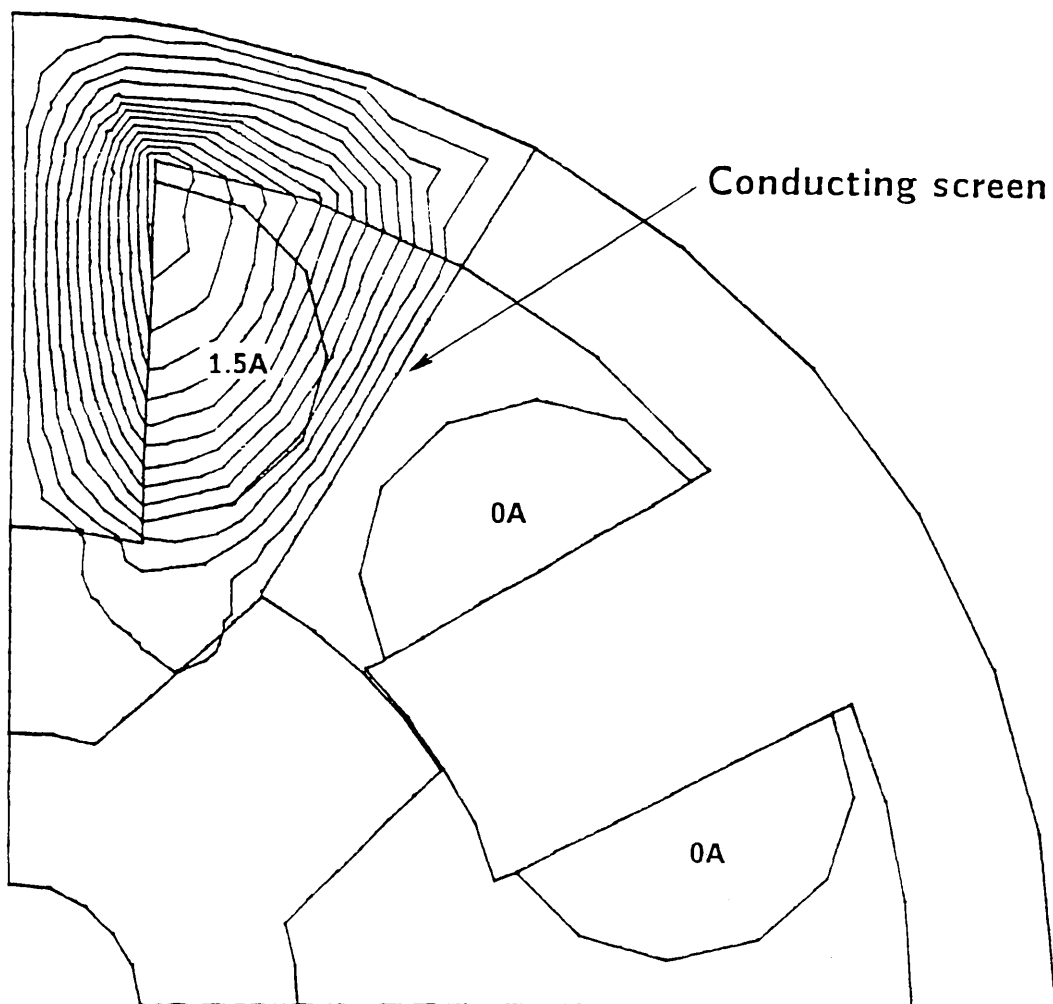


Figure 3.12 Unaligned Position Flux Plot for Conducting Stator Slot Screens

The combination of the inserts on the rotor and screens on the stator was also modelled using finite-elements. The predicted unaligned screened inductance was 5.6mH which was only a small further reduction when compared to the screened stator concept. A flux-plot for this screening combination is shown in Figure 3.13.

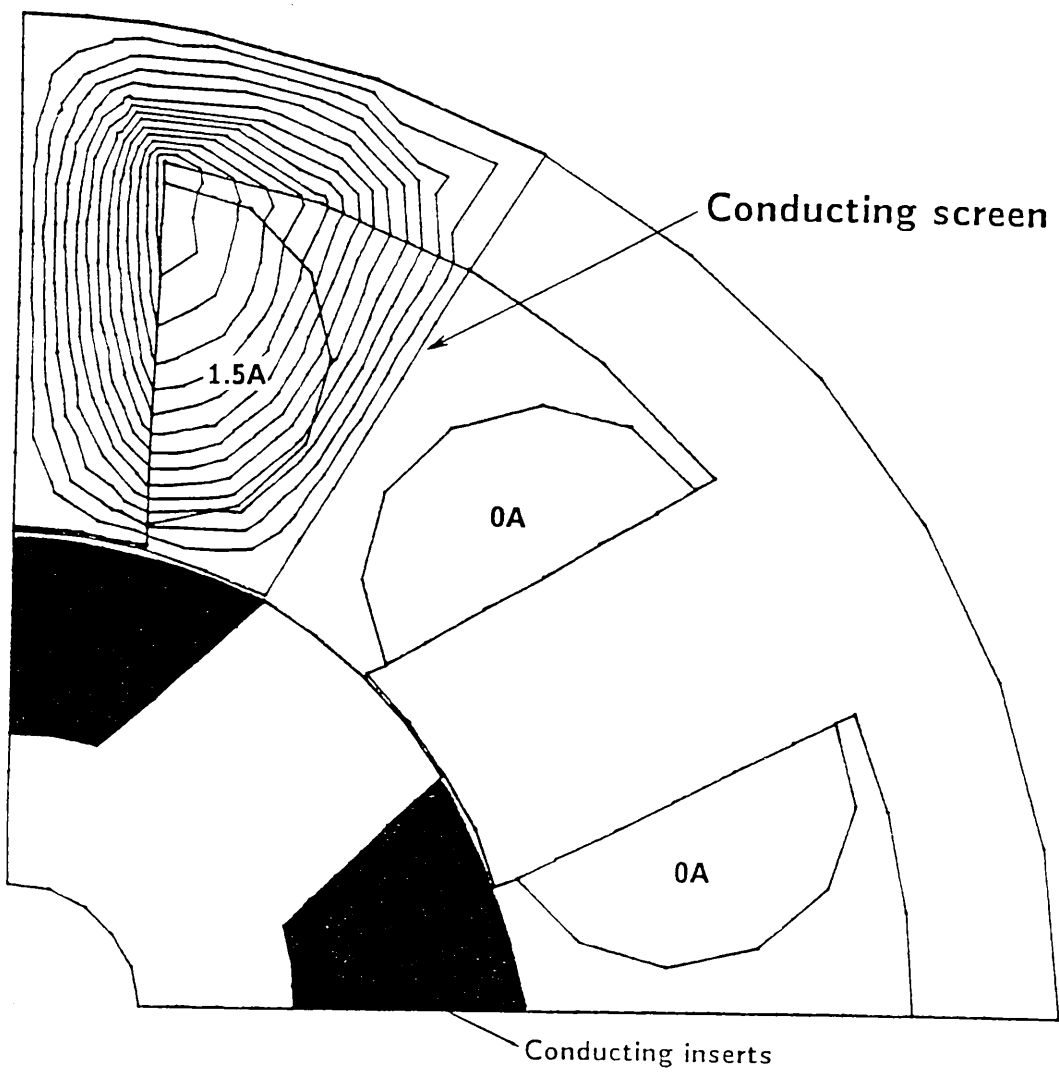


Figure 3.13 Unaligned Position for Stator/Rotor Screens

3.6 Modelling of Diffusion Effects within Rotor Screen using Finite-Elements

The operation of the SR motor depends on a series of current pulses on each alternative phase winding to provide rotation of the rotor. These pulses will re-activate any conducting flux screen present in the rotor/stator construction during phase switching times. However, the effectiveness of the screens will depend on the relative values of the diffusion time constant and conduction period.

A finite-element analysis was used to investigate the diffusion time constant (τ) within different regions of the conducting flux screens on the rotor. Hypothetical current distributions in the rotor inserts were modelled to provide valuable information about the period of time that the screens could remain inductance limited. Values of inductance and resistance were calculated to allow estimates of τ from the L/R ratio. The inductance can be determined from the energy stored in the magnetic field E. It is known that

$$E = 1/2 Li^2 \quad (3.15)$$

and therefore

$$L = \frac{2E}{i^2} \quad (3.16)$$

The energy stored can be determined from the flux density B by the integral

$$E = \int \left[\int B dH \right] dV \quad (3.17)$$

This equation shows that the stored energy can be calculated from the integral of the magnetic energy density taken over the entire volume V of the motor. If

$B = u_o u_r H$, where u_r is the relative permeability of each region within the motor, then this integral can be calculated from B^2 as shown in the finite element command file of Appendix 3.6.

From Figure 3.18, it is clear that the average time constant within the screen is around 0.5ms. This is only 6 degrees of rotation at 2000rpm and is therefore more than likely to be ineffective in screening the flux for the period of time during which the phase winding is excited.

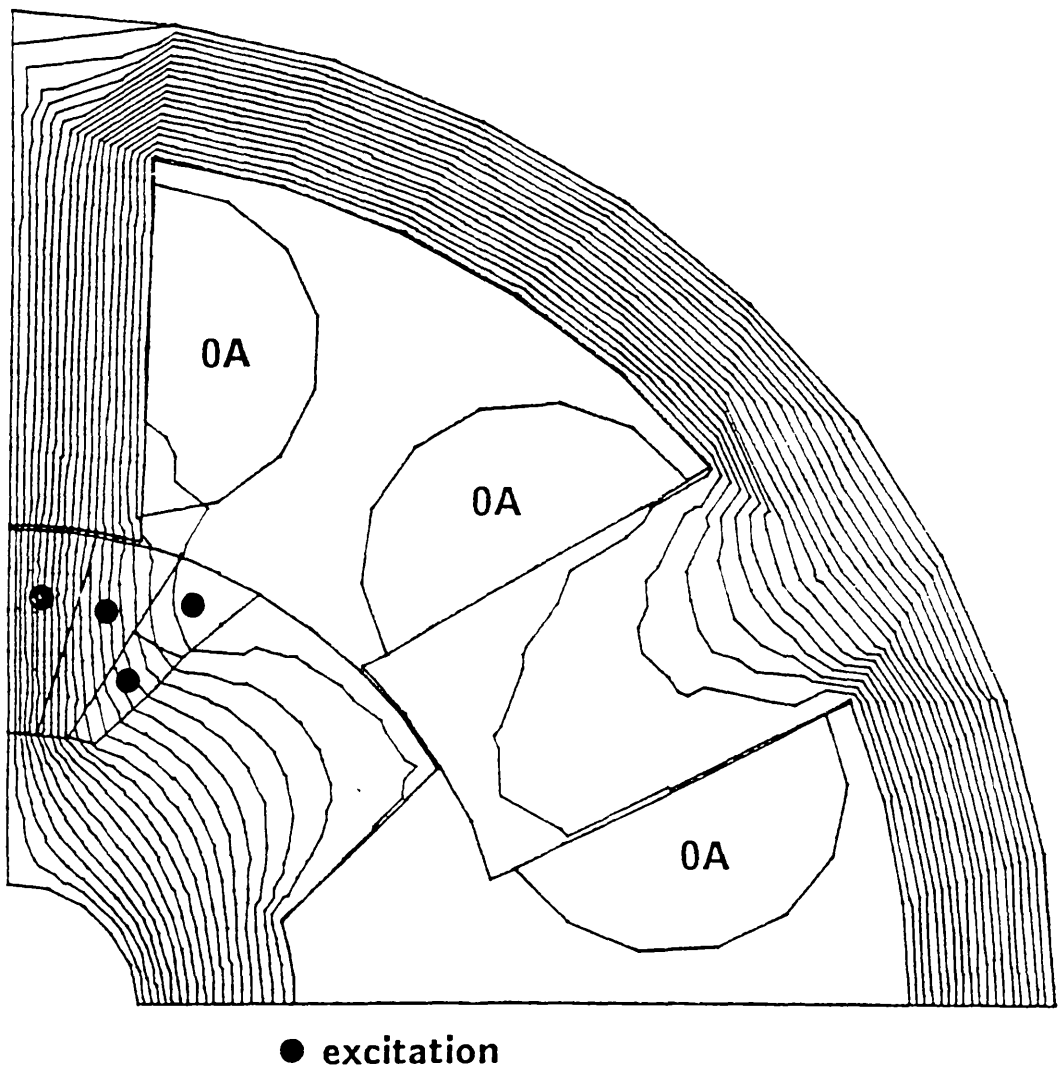


Figure 3.14 Diffusion Flux Plot for Current in Region 1

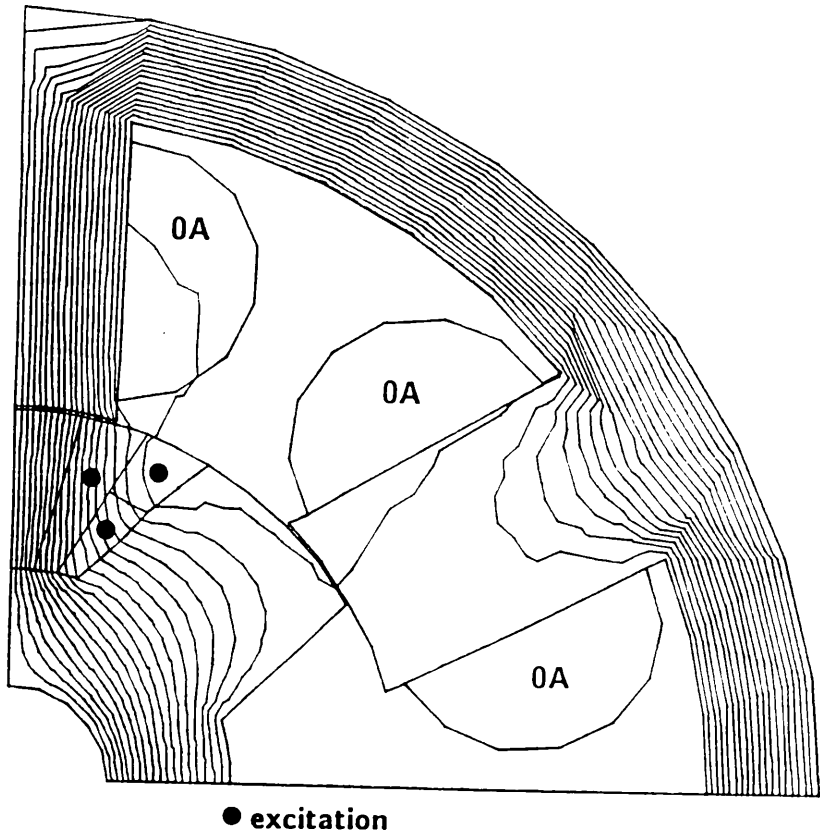


Figure 3.15 Diffusion Flux Plot for Current in Region 2

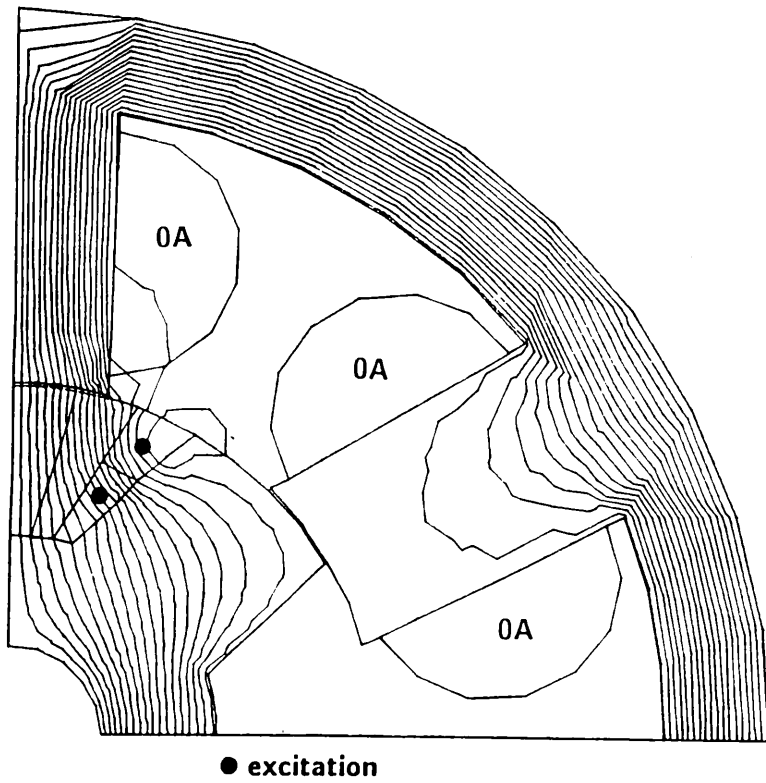


Figure 3.16 Diffusion Flux Plot for Current in Region 3

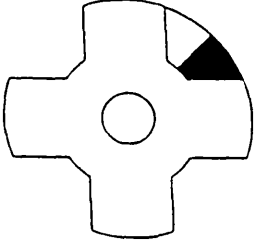
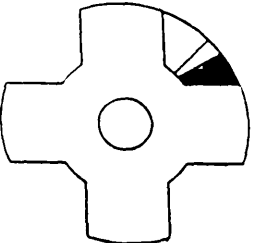
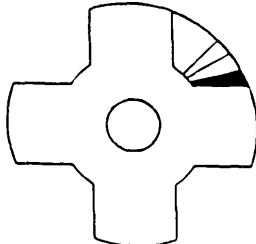
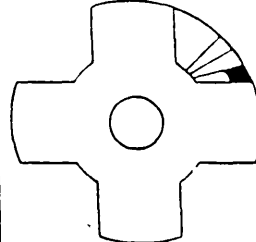
CURRENT DISTRIBUTION		SCREEN CURRENT TIME CONSTANT t (msecs)
REGION 1		0.59
REGION 2		0.54
REGION 3		0.41
REGION 4		0.31

Figure 3.18 Table of Results for Diffusion Time Constant Within Conducting Insert on Rotor.

3.7 Experimental Tests

3.7.1 DC Static Inductance Measurements

Static inductance measurements were made on all the rotor/stator concepts. A square-wave voltage of about 30V was applied to one phase of the stator with the rotor clamped in the unaligned position. The stator phase current waveforms were recorded on a digital processing oscilloscope. The effective (screened) inductance was calculated from the quotient of the applied voltage V and the initial rate of change of current (di/dt) given in equation 3.18.

$$L = \frac{V}{di/dt} \quad (3.18)$$

The measurements of Figure 3.8 agree with the finite-element calculations only to the extent that they confirm the ranking of the screen concepts in the order of inductance reduction which they produce. The greatest reduction is with a combination of the stator slot screens and the rotor interpolar inserts. This combination gives a screened unaligned inductance of 9mH, i.e., 64% of the unscreened value. Acting alone, the rotor inserts give a screened inductance of 11.3mH, which is 81% of the unscreened value. Acting alone, the stator slot screens give a screened inductance of 12mH, i.e., 86% of the unscreened value. From the experimental tests based on DC static inductance measurements, it appears that the combined screens give the lowest unaligned inductance for the switched reluctance motor.

The significant differences between the measured and calculated results require further analysis. The most

important phenomena to be studied concern the distribution of current in both the stator winding and the screens. To improve the agreement of the results, the diffusion effects outlined in Section 3.6 will have to be modelled in more detail. Since the measured inductances are uniformly higher than the calculated ones, end-turn inductance is probably a significant factor which must also be given further analysis.

3.7.2 Open Loop Torque/Speed Characteristics

Dynamometer tests were performed to test the effect of the screens in normal operation. The tests were carried out under open loop conditions. Three operating modes were tested namely, Normal , Boost and Long Dwell which are described in detail in Chapter 2 and by Miller et. al. in [3.12]. Figure 3.19 shows the speed/torque characteristic for the unscreened motor and the motor with copper inserts on the rotor in the Normal mode. There was no chopping of the applied voltage (60V) and the duty cycle was fully opened to 100%. At all speeds the screened motor produced less torque than the unscreened motor. This was also the case for the other modes tested: Appendix 3.7a and 3.7b. The recorded current waveforms of Figure 3.20 showed little difference between the screened and unscreened motors at lower speeds.

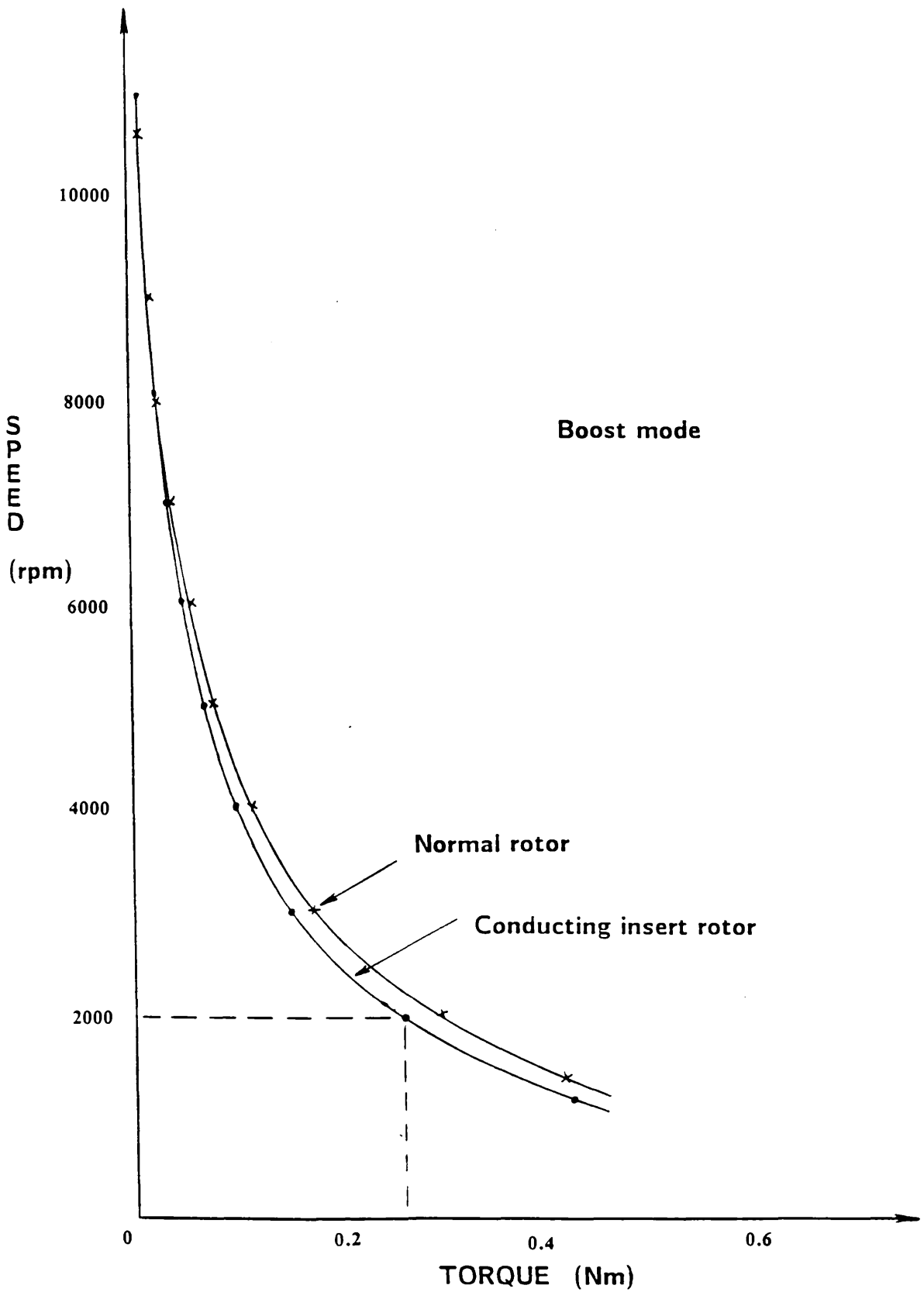
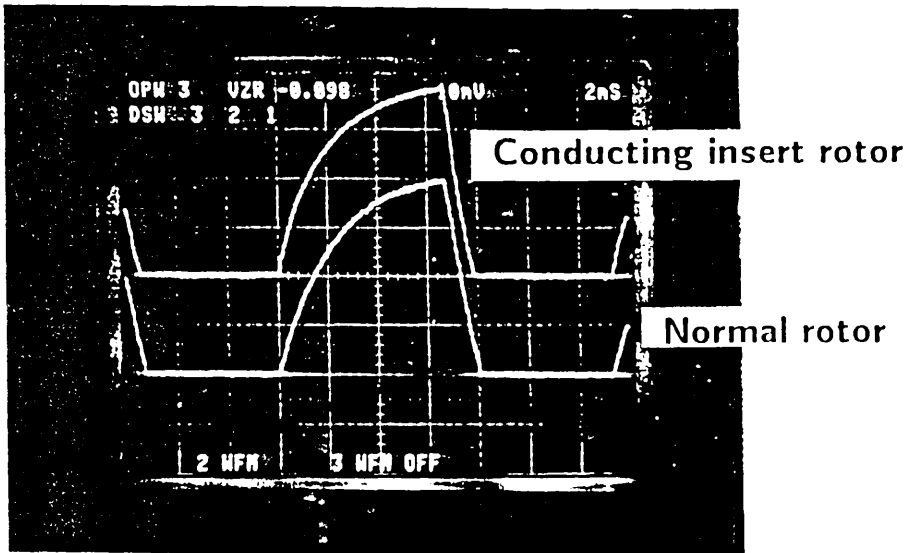


Figure 3.19 Speed/Torque Performance for Normal and Conducting Insert Rotors with Open Loop Control



$V_s = 25V$ $1A/div$ $f = 75Hz$

Figure 3.20 Static Phase Current Waveforms for Normal and Conducting Insert Rotors

The reduction of torque can be explained by considering the resistance of the screens and the diffusion time constant. It appears to be the case that the cross sectional area of the screens is small enough to have an appreciable effect on the resistance. This, in turn, causes the eddy-currents to become resistance-limited in a period that is short compared to the conduction period: (30 degrees of rotation). The net effect is a reduction in the period of time for the 'inductance limited' condition. This creates a drag torque that is more than sufficient to offset any gains that would otherwise be expected. This has been demonstrated by the finite-element analysis of the current distribution within the conducting rotor inserts: Figure 3.18. For this case, the time constant was around 0.5ms which is only 6 degrees of rotation at 2000 rpm. This rapid decay of the screen

currents is also consistent with Figure 3.20, confirming that the screen currents are too resistive to have any beneficial effect. It has been shown that the results are no better at lower speeds or higher speeds. At lower speeds the induced currents may simply not persist long enough, while at higher speeds the I^2R losses in the screen overcome any benefits arising from the reduced inductance.

3.8 Conclusions

Investigations have been carried out into the use of flux screens to improve the specific torque of the switched reluctance motor. Various screening concepts were studied using finite-element analysis and experimental tests. The first of these concepts was a normal SR rotor with conducting inserts in the interpolar air-gap. The finite-element analysis indicated that if the screens were perfectly diamagnetic the unaligned inductance would be 7.8mH, which is only 56% of the value obtained for the conventional rotor. However, the measured value was 11.3mH. The difference in the two results was attributed to the rather idealised way in which the finite-elements distributes the stator conductors within the stator slot. There were also differences due to end-turn effects and the existence of partial flux linkages in the winding. Both of these cannot be modelled using the 2D finite element analysis. Finite-elements could not be used for the copper bar rotor since the current values in the rotor bars are required. However, it can be argued that if the rotor circuits span the same arc as the conducting inserts, and if they are equally effective in excluding flux from passing through, then the screened inductance should be comparable to the 7.8mH calculated earlier. The calculated unaligned inductance for the flux screened

stator concept was 5.7mH. This was 73% of the value obtained with rotor inserts and was only 41% of the original unscreened unaligned inductance in the conventional rotor. The screened stator/screened rotor concept predicts only a small further reduction of the screened inductance to 5.6mH. All of the measurements agree with the finite-element calculations only to the extent that they confirm the ranking of the screen concepts in the order of inductance-reduction which they produce. The greatest reduction is with a combination of the stator slot screens and the rotor interpolar inserts. This combination gives a screened unaligned inductance of 9mH, i.e., 64% of the unscreened value. Acting alone, the rotor inserts give a screened inductance of 11.3mH, which is 81% of the unscreened value. Acting alone, the stator slot screens give a screened inductance of 12mH, i.e., 86% of the unscreened value. It is clear that the combined screens give the lowest unaligned inductance.

The significant differences between measurement and calculation require further analysis. The most important reasons probably concern the distribution of current in both the stator winding and the screen and the end effects. To get better agreement, the diffusion effects will have to be modelled in detail.

The experimental load tests reported here have failed to show any benefit from rotor or stator screens in a small switched reluctance motor, even though the effective unaligned inductance could be reduced by up to 36% with a combination of rotor and stator screens. The diffusive effects of resistance appear to overcome any beneficial effect of the reduced inductance.

From the finite-element analysis of the current distributions with the rotor screen, it seems that the screen currents are extinguished too quickly and that the additional I^2R losses are producing a drag to reduce the

net torque by several percent. A change in the switching angles of the phase currents using different operating modes has been shown to have no effect to the overall speed/torque performance from the motor although there remains considerable scope for further experimentation.

One factor to be considered is the effect of scale on resistance within the conducting screens. With a small screen cross-sectional area there will be short time constants associated with it and so the screening effect will only last for a short period of time. In larger motors, however, the screen time constant scales with the square of the linear dimension. This suggests that the screens would be less resistive permitting them to have their intended effect of increasing the performance results from the motor. In smaller motors, there still exist possibilities for employing rotor screens to assist in the production of torque in motors with very low phase numbers. It is possible that flux screens on the rotor could be utilised for starting single-phase motors. These motors are of interest because of the reduced number of power transistors in the controller, typically only one power switch is required. Further study will be carried out into the most profitable rotor/stator geometry to provide the greatest benefit of output torque.

3.9 Future Work

There is still a lot of further research required before the concept of flux screening within small motors is fully understood. More work will be needed into the current distribution within the flux screens on both the rotor and the stator. Future experimental investigations will be carried out into flux screens on a much larger 4kW switched reluctance motor. It is expected that better

4kW switched reluctance motor. It is expected that better results will be achieved since the screen resistances will be very much smaller and so the screen time constants will last for a longer period of time. Continuing investigations should also consider the finite-element modelling of the various screening concepts to bring them more into line with the experimental results. Finally, the general analysis presented in Appendix 3.3 to obtain expressions for describing the phase current under an applied step of voltage will require further work to include the effects of eddy currents within the conducting screens.

CHAPTER 4

CONCLUDING DISCUSSION

4.1 Discussion

The overall aim of this thesis was to investigate certain applications of the switched reluctance motor and also to improve on its output performance and torque delivery.

Chapter 2 has highlighted the potential commercial capability of the switched reluctance drive in a domestic food processor. Two prototype SR drives were designed, built and tested to provide experience on the entire SR drive system. One of the main issues under investigation was the capability of the SR drive at high speed and under load conditions. In particular, the efficiency, thermal characteristics, power density and noise level were all monitored and compared with the conventional AC series commutator motor with triac control. It was shown that between the two prototype drive systems, the 72mm SR motor was the most efficient drive for the food processor. This was only because it utilised an external air blower which provided a continuous cold airflow across the phase windings, helping to remove the heat and keep the windings cool. However, it should be noted that the power taken by the external blower was not included in this efficiency calculation. The 88mm SR motor, although not as efficient as the 72mm motor, was still capable of meeting the torque requirements of the food processor. This motor was considered to be more of a competitor to the series AC commutator motor since it required no external fan.

The chapter on flux screening methods has introduced several techniques to improve the output electromagnetic torque from a switched reluctance motor. Several

configurations of screens were postulated, analysed by finite-element techniques and tested in an experimental 50W SR motor. Previous work for the SR motor fundamentals established that the torque development was determined by the variation of self-inductance of the phase winding as the rotor rotates. Therefore, in principle, this variation could be increased by dynamically decreasing the minimum self-inductance through the use of eddy current screens. The experimental work has established two major factors in the effectiveness of flux screens. First, the order by which the different flux screening concepts can reduce the unaligned inductance has been established. The experimental investigation clearly showed that the most effective screening method incorporated flux screens both on the stator and on the rotor. Secondly, the diffusive effects of resistance seem to overcome any beneficial effect of reduced unaligned inductance. This may have been a result of the small machine frame size and so the screen currents were dissipated too quickly. Consequently, they produced a small drag torque component which was significant enough to reduce the net output torque by several percent. Useful information has been obtained from this chapter despite the somewhat negative experimental results. It has further confirmed that the flux screening techniques in small motor drives (50W) are ineffective in increasing the output torque and that large motors, above 0.5kW, would probably benefit more from the conducting flux screens.

REFERENCES

CHAPTER 1

- 1.1 Lawrenson, P.J., Stephenson, J.M., Blenskinsop, P.T., Corda, J., Fulton, N.N. : ' Variable-Speed Switched-Reluctance Motors', Proc. IEE, Vol.127, Pt.B, No.4, July 1980, pp253-265.
- 1.2 Miller, T.J.E.: 'Switched Reluctance Motor Drives', PCIM Reference Book, Intertech Communications Inc., Ventura, California, USA, 1988.
- 1.3 Byrne, J.V., Lacy, J.G. : British Patent #132 1110, 1973, based on Irish Patent Application 872, 25th June, 1969.
- 1.4 Byrne, J.V. : 'Tangential Forces in Overlapped Pole Geometries incorporating Ideally Saturable Material', IEEE Trans. on Magnetics, MAG-8, 1972, pp2-9.
- 1.5 Anderson, A.F. : ' Robert Davidson - Father of the Electric Locomotive', Proc. IEE, History of Electrical Engineering Conf., 1975.
- 1.6 Charlish, G. : ' An Idea 100 Years Old Comes to Fruition', Financial Times Technology Section, 26th January, 1983.
- 1.7 Anderson, A.F., Cruickshank, A.J.O. : ' AC Electric Motor having Reluctance-Type Rotor', British Patent, #111 4561, 1968.
- 1.8 Chicken, C.B., Thain, J.H. : US Patent #135 3025, Electrical Signalling Apparatus, 1920.

- 1.9 Ranseen, E.L. : ' Electric Motors', US Patent, #300 5118, 1961.
- 1.10 'Stepping Motor Runs at 8000pps', Control Engineering, 1968, p59.
- 1.11 Unnewehr, L.E., Koch, W.H. : ' An Axial Air-gap Reluctance Motor for Variable-Speed Applications, IEEE Trans. on Power Appl. and Sys., Vol. PAS-93, 1974, pp367-376.
- 1.12 French, P. , Williams, A .H. : ' A New Electric Propulsion Motor', Proc. AIAA 3rd Propulsion Joint Specialists Conf., Washington DC, July 1967.
- 1.13 Bastos, J.P., Goyet, R., Lucidarme, J. : 'Performances Intriseques des Machines a Reluctance Variable a Disque Imbriques', Revue Phys. Appl., Vol.15, January 1980, pp45-54.
- 1.14 Ray, W.F., Davis, R.M.: 'Inverter Drive for Doubly-Salient Reluctance Motor:Its Fundamental Behaviour, Linear Analysis and Cost Implications', IEE Electric Power Appl., Vol.2, No.6, December 1978, pp185-193.
- 1.15 Ray, W.F., Lawrenson, P.J., Davis, R.M., Stephenson, J.M., Fulton, N.N., Blake, R.J. : 'High Performance Switched Reluctance Brushless Drives', IEEE Trans., on Industrial Appl., Vol. IA-22, No.4, 1986, pp722-730.
- 1.16 French, P.S.R. : ' Switched Reluctance Motor Drives for Rail Traction', Proc. IEE, Vol.31, Pt.B, No.5, Sept. 1984.

- 1.17 Regas, K.A., Kendig, S.D. : ' Step Motors that Perform like Servos', Machine Design, December 1987, pp116-120.
- 1.18 Compter, J.C. : 'Microprocessor-Controlled Single-Phase Reluctance Motor', Drives/Motors/Controls, Brighton, 1984. Published by P. Pereguinus Ltd., pp64-68.
- 1.19 Welburn, R. : ' Ultra-High Torque Motor System for Direct Drive Robotics', MOTOR-CON Proc., Atlantic City, April 1984, pp17-24.
- 1.20 Gupta, R.K., Mathur, R.M. : 'Transient Performance of Variable Reluctance Stepping Motors', Conf. on Small Electric Machines, pp109-112.

CHAPTER 2

- 2.1 Fitzgerald et al.: ' Electric Machinery', 3rd Edition, McGraw-Hill Books, 1971, New York, pp539-542.
- 2.2 Corda, J., Stephenson, J.M. : ' An Analytical Estimation of the Minimum and Maximum Inductances of a Doubly-Salient Motor', Proc. of Int. Conf. on Stepping Motors and Systems, University of Leeds, UK, 1979, pp50-59.
- 2.3 Miller, T.J.E., Bower, P., Becerra, R., Ehsani, M.: 'Four Quadrant Brushless Reluctance Motor Drive', IEE Conf. on Power Elec. and Variable Speed Drives, London, July 1988, pp273-276.

- 2.4 MILLER, T.J.E., MCGILP, M.: ' PC CAD for Switched Reluctance Drive': Electric Machines and Drives Conf., December 1987.
- 2.5 MILLER, T.J.E.: 'Brushless Reluctance-Motor Drives', Power Eng. Journal, November 1987, pp.325-331.
- 2.6 MILLER, T.J.E.: ' Small Motor Drives expand their Technology Horizons': Power Eng. Journal, September 1987, pp.283- 289
- 2.7 LINDSAY, J.F., ARUMUGAM, R., KRISHNAN, R.: 'Finite-Element Analysis Characterization of a Switched Reluctance Motor with Multitooth per Stator Pole': Proc. IEE, Vol.133, Pt.B, No.6, November, 1986, pp.347-353.
- 2.8 ARUMUGAM, R., LOWTHER, D.A., KRISHNAN, R., LINDSAY, J.F.: ' Magnetic Field Analysis of a Switched Reluctance Motor using a 2-Dimensional Finite -Element Model': IEEE Trans. on Magnetics, Vol.MAG -21, No.5, September 1985, pp.1883-1885.
- 2.9 EASTHAM, A.R., DAWSON, G.E., MIZIA, J.: ' Switched Reluctance Motor Torque Characteristics: Finite -Element Analysis and Test Results': IEEE Trans. on Ind. Appl., Vol.IA-23, May/June, 1987. pp864-869.
- 2.10 EL-SHERBINY, M. K.: ' Representation of the Magnetization Characteristics by a Sum of Exponentials': IEEE Trans. on Magnetics, Vol.MAG-9, No.1, March 1973, pp60-61.
- 2.11 BYRNE, J.V., O'DWYER, J.B. .: ' Saturable Variable Reluctance Machine Simulation using Exponential Functions', Proc. of Int. Conf. on Stepping Motors and Systems, University of Leeds, July 1976, pp11-16.

- 2.12 PICKUP, I.E.D., TIPPING, D. : 'Method of Predicting the Dynamic Response of a Variable Reluctance Stepping Motor', Proc. IEE, Vol.120, No.7, July 1973, pp757-765.
- 2.13 CHAPPELL, P.H.: ' Winding Current in a Switched Reluctance Motor', Proc. IEE, September, 1987, pp277-283.
- 2.14 RAY, W.F., LAWRENSON, P.J., DAVIS, R.M., STEPHENSON, J.M., FULTON, N.N., BLAKE, R.J.: 'High Performance Switched Reluctance Brushless Drives': IEEE Trans. on Ind. Appl., Vol.IA-22, No.4, July/August 1986, pp722-730.
- 2.15 HARRIS, M.R. , ANDJARGHOLI, V. , LAWRENSON, P.J., HUGHES, A.: 'Unifying Approach to the Static Torque of Stepping Motor Structures': Proc. IEE, Vol.124, No.12, December 1977, pp1215- 1224.
- 2.16 RAY, W.F., DAVIS, R.M.: ' Inverter Drive for Doubly -Salient Reluctance Motor: its Fundamental Behaviour, Linear Analysis and Cost Implications': IEE Elec. Power Appl., Vol.2, No.6, December 1979, pp185-193.
- 2.17 DAVIS, R.M., RAY, W.F., BLAKE, R.J.: 'Inverter Drive for Switched Reluctance Motor: circuits and component ratings: Proc. IEE, Vol.128, Pt.B, No.2, March 1981, pp126-136.
- 2.18 KAUFFMANN, J.M. , GUDEFIN, E.: ' Moteurs pas a Reluctance Variable', RGE, Vol.3, March 1981, pp183-188.

- 2.19 LUMSDAINE, A., LANG, J.H., BALAS, M.J. : ' A State Observer for Variable Reluctance Motors', Proc. of the Incremental Motion Control System Symposium, June 1986, Urbana-Champaign, Illinois, USA, pp267-273.
- 2.20 BASS, J.T., MILLER, T.J.E., Ehsani, M. : ' Robust Torque Control of Switched Reluctance Motors without a Shaft Position Sensor', IEEE Trans., Vol.IE-33, 1986, pp212-216.

CHAPTER 3

- 3.1 Lawrenson, P.J. : 'Switched Reluctance Motor Drives', Electronics and Power, February, 1983, pp144-147.
- 3.2 French, P.S.R. : 'Switched Reluctance Motor Drives for Rail Traction', Proc. IEE, Vol.131, Pt.B, No.5, Sept. 1984.
- 3.3 Regas, K.A., Kendig, S.D. : ' Step Motors that Perform like Servos', Machine Design, December 1987, pp116-120.
- 3.4 Drives and Controls Magazine, March 1989, p7.
- 3.5 RAY, W.F., LAWRENSON, P.J., DAVIS, R.M., STEPHENSON, J.M., FULTON, N.N., BLAKE, R.J.: 'High Performance Switched Reluctance Brushless Drives': IEEE Trans. on Ind. Appl., Vol.IA-22, No.4, July/August 1986, pp722-730.
- 3.6 Wigington, R.L., Nahman, N.S.: 'Transient Analysis of Coaxial Cables considering Skin Effect', Proc. IRE, February 1957, pp166-174.

- 3.7 Miller, T.J.E. : ' Brushless Permanent Magnet and Reluctance Motor Drives', Oxford University Press, April 1989.
- 3.8 Stoll, R. : ' Eddy Currents in Solids', Oxford University Press,
- 3.9 Welsby, V.G.: 'The Theory and Design of Inductance Coils', MacDonal and Co., London, 1960.
- 3.10 McConnell, H.M.: 'Eddy-Current Phenomena in Ferro-Magnetic Materials', AIEE Trans., July, 1954, pp226-235.
- 3.11 Agarwal, P.D.: ' Eddy-Current Losses in Solid and Laminated Iron', AIEE Trans., No.78, Pt.2, May 1959, pp169-181.
- 3.12 Miller, T.J.E., Bower, P., Becerra, R., Ehsani,M.: 'Four Quadrant Brushless Reluctance Motor Drive', IEE Conf. on Power Elec. and Variable Speed Drives, London, July 1988, pp273-276.
- 3.13 Hammond, M.A. : 'The Calculation of the Magnetic Field of Rotating Machines', IEE Monographs, No.514, April 1962, pp508-515.
- 3.14 Wood, A.J.: 'An Analysis of Solid Rotor Machines', AIEE Trans., February 1960, pp1657-1665.
- 3.15 Kesavamurthy, N., Rajagoplan, P.K.: 'Rise of Flux in Solid Iron Cores due to Impact Excitation', IEE Monographs, No.336, June 1959, pp189-192.
- 3.16 Glennie, E.B., Miller, T.J.E. : 'Inductive Detection of Underground Metallic Pipes', IEE Proc., Vol.122, No.4, April 1975, pp345-348.

- 3.17 Hughes, A., Miller, T.J.E. : 'Analysis of Fields and Inductances in Air-Cored and Iron-Cored Synchronous Machines', Proc.IEE, Vol.124, No.2, February, 1977, pp121-126.
- 3.18 Hore, D.L. : 'An AC Induction Stepping Motor', IEE Conf.on Small and Special Electrical Machines, 1981 pp34-38.
- 3.19 Chalmers, B.J., Mulki, A.S. : 'New Reluctance Motors with Unlaminated Rotors', Proc.IEE, Vol.117, No.12, December 1970, pp2271-2272.
- 3.20 Nasar, S.A.: 'An Axial Air-gap, Variable Speed, Eddy-Current Motor', IEEE Trans. on Power App. and Systems, Vol.PAS-87, No.7, July 1968, pp1599-1603.



National
Semiconductor
Corporation

PRELIMINARY
May 1989

LMB1008 SPEED Switched Reluctance Motor Control Circuit

General Description

The LMP1008 contains all the necessary control and motor drive phase decoding to give the appropriate output waveforms to drive a switched reluctance motor in programable normal, boost, long dwell, advanced long dwell and brake modes for both forward and reverse rotation. In addition a rapid stop mode and operation with 2 sensors are supported.

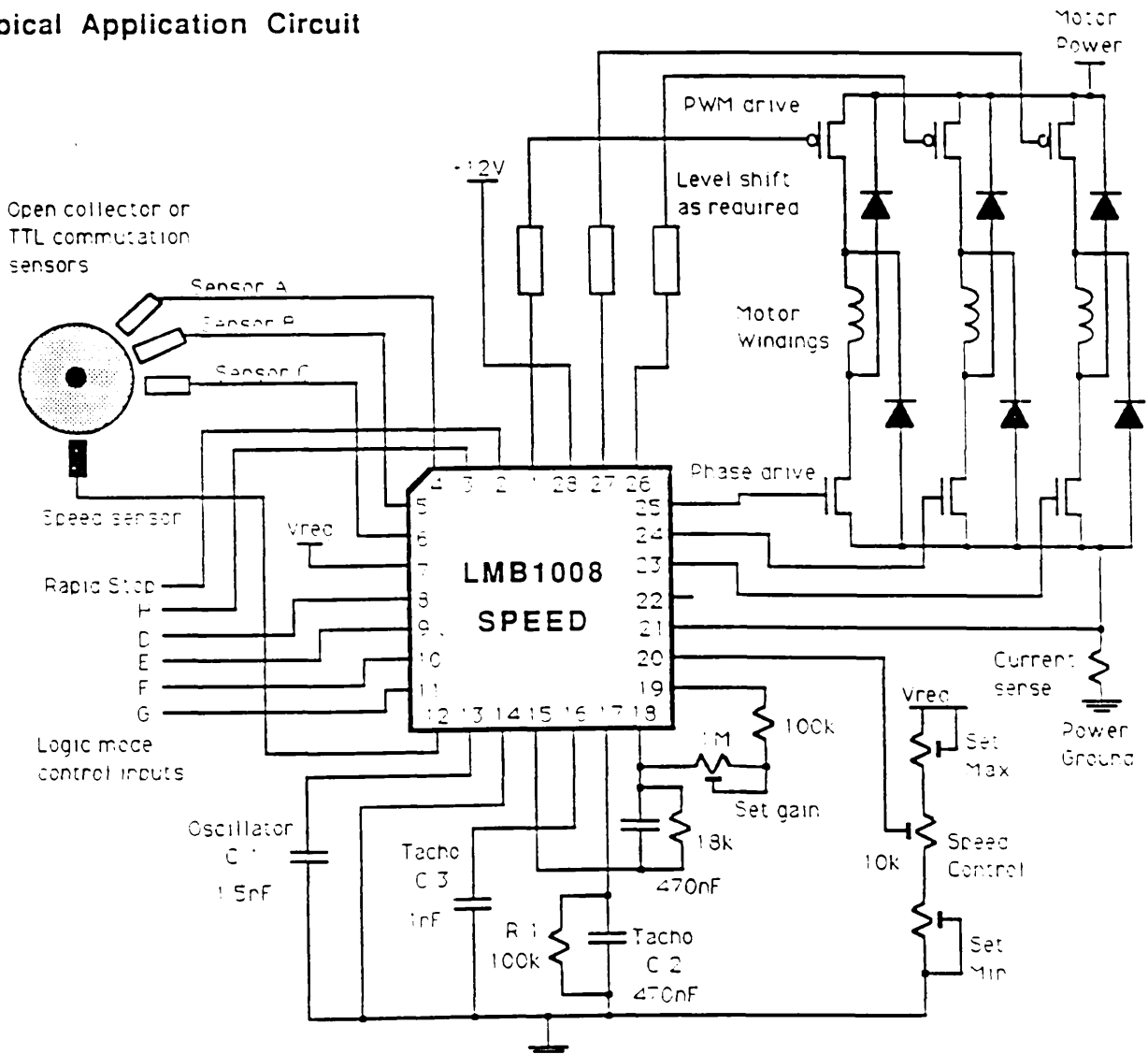
For closed loop speed control an internal tacho, oscillator, error amplifier and PWM generator are provided.

A comparator is provided for excess current detection and current limiting.

Features

- TTL compatible logic inputs with internal pullups
- 3 high level phase outputs to drive power mosfets
- 3 High level PWM modulated phase outputs for speed control
- Full decoding logic to support 5 modes of operation in both forwards and reverse
- Rapid stop feature
- 2 sensor operation supported
- On chip tacho, oscillator and PWM comparator for closed loop speed control
- Externally adjustable error voltage amplifier
- Current limit sense input
- Internal supply regulator

Typical Application Circuit



Absolute Maximum Ratings (Notes 1&2)

If Military / Aerospace specified devices are required, contact the National Semiconductor Sales Office / Distributors for availability and specifications.

Supply Voltage (Vdd)	24V
Package Dissipation at T = 25 °C (Note 3)	1.0W
Voltage at control and signal inputs	-0.3V to Vdd +0.3V
Output Current Phase and PWM Outputs	10mA
Input Current per Pin	5.0mA
Input Current per Package	20mA

Storage Temperature range	-65°C to +150°C
Lead Temperature	
Surface Mount Package	
Vapor Phase (60 seconds)	215°C
Infrared (15 seconds)	220°C
ESD Susceptibility (note 8)	2000V

Operating Ratings (Notes 1&2)

Supply Voltage (Vdd)	7.0V to 24.0V
Temperature Range	-40°C ≤ T _A ≤ 85°C

Electrical Characteristics (Note 4)

PARAMETER	CONDITIONS	Typical (Note 5)	Tested Limit (Note 6)	Design Limit (Note 7)	Units
LOGIC CONTROL INPUTS					
Low Level Input Voltage	0V (Internal 40k pullup to Vreg)	5		0.8	V(min)
High Level Input Voltage				2.0	V(min)
Input Current				150	μA(max)
Input Capacitance					pF
PHASE AND PWM OUTPUTS					
Output voltage	2mA source 10mA sink			9 0.5	V (min) V (max)
TACHO					
Input Threshold	Vout = 2V	2.5			V
Input Current				1	μA(max)
Output Current				±10	mA(min)
Output Voltage Swing				0	V(max)
				Vreg-1.5	V(min)
Vout = Vreg x frequency x C3 x R1					
ERROR VOLTAGE AMPLIFIER					
Bandwidth	gain =1	1			MHz
Input CMR				0	V(max)
				Vreg-1.5	V(min)
Output Current	Vout = 2V			±10	mA(min)
Output Voltage Swing				0	V(max)
				Vreg-1.5	V(min)
OSCILLATOR					
Frequency	Oscillator capacitor C1 = 1.5nF	17			kHz
CURRENT LIMIT COMPARATOR					
Input Current				5	μA(max)
Internal bias on reference input		200			mV
Reference Input Resistance		2			kΩ
Vreg		5			V
Supply Current		50			mA

Note 1: Absolute Maximum Ratings indicate limits beyond which damage to the device may occur. Electrical specifications do not apply when operating the device beyond its specified operating conditions.

Note 2: All voltages are measured with respect to Gnd.

Note 3: For operation at elevated temperatures derate based on 150°C maximum junction temperature and a package thermal resistance of 70°C/W junction to ambient.

Note 4: Unless otherwise noted these specifications apply for : T_A = 25°C, V_{dd} = 12V

Note 5: Typicals are at 25°C and represent most likely parametric norm.

Note 6: Tested and guaranteed to National's AOQL (Average Outgoing Quality Level)

Note 7: Design limits are guaranteed to National's AOQL (Average Outgoing Quality level), but are not tested.

Note 8: Human body model, 100pF discharged through a 1.5kΩ resistor.

Operating Truth Tables

FORWARD, REVERSE, AND RAPIDSTOP OPERATION

D	H	Rapid Stop	Mode
X	0	X	Outputs disabled low
0	1	0	Forward Motion
1	1	0	Reverse Motion
X	1	1	Phase outputs forced high

CURRENT LIMIT action disables PWM drives

3 SENSOR OPERATION

E	F	G	Mode
0	0	0	Normal
0	1	0	Boost
1	1	0	Long Dwell
1	1	1	Advanced Long Dwell
1	0	0	Brake

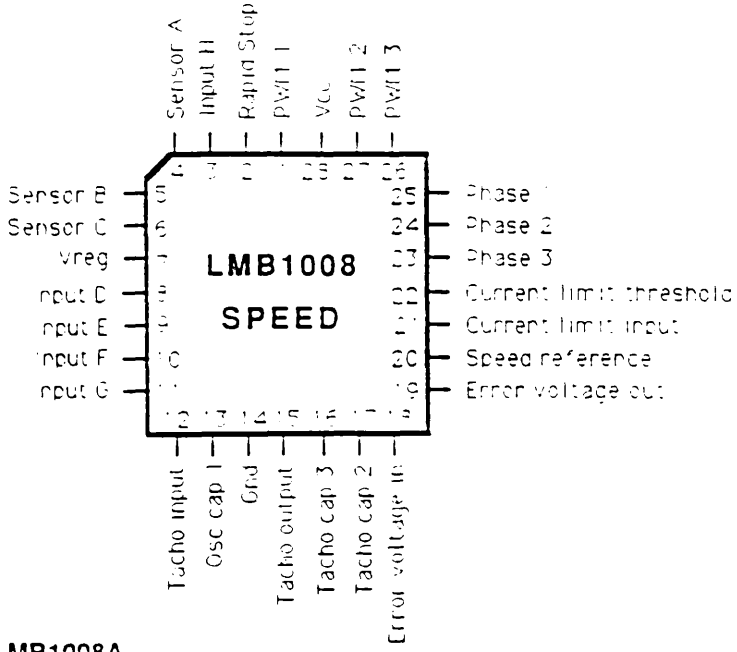
2 SENSOR OPERATION

SENSOR C input is don't care with an internal pull up and need not be connected.

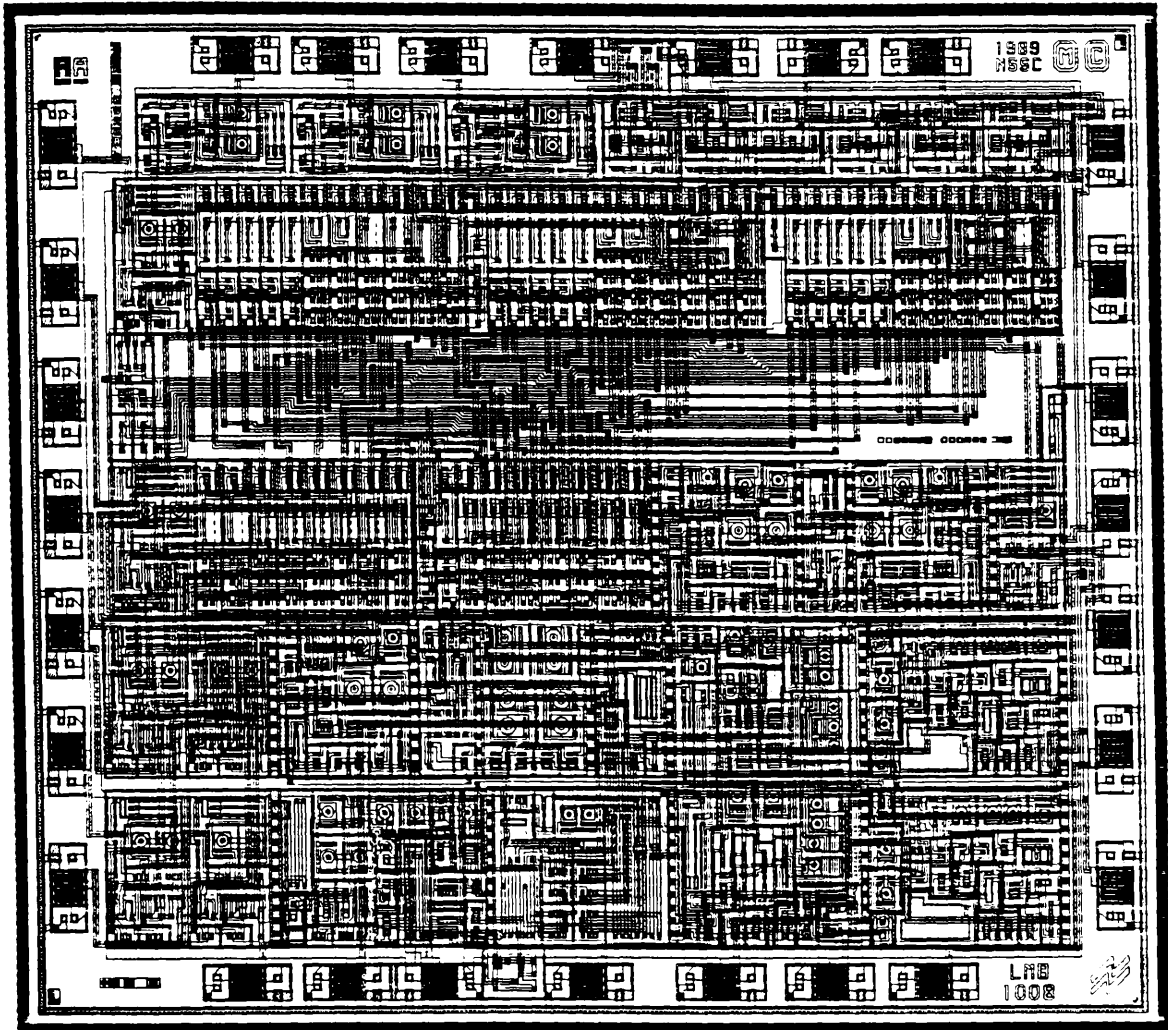
E	F	G	Mode
0	0	1	Normal
1	0	1	Brake

Connection Diagram

28 pin PCC

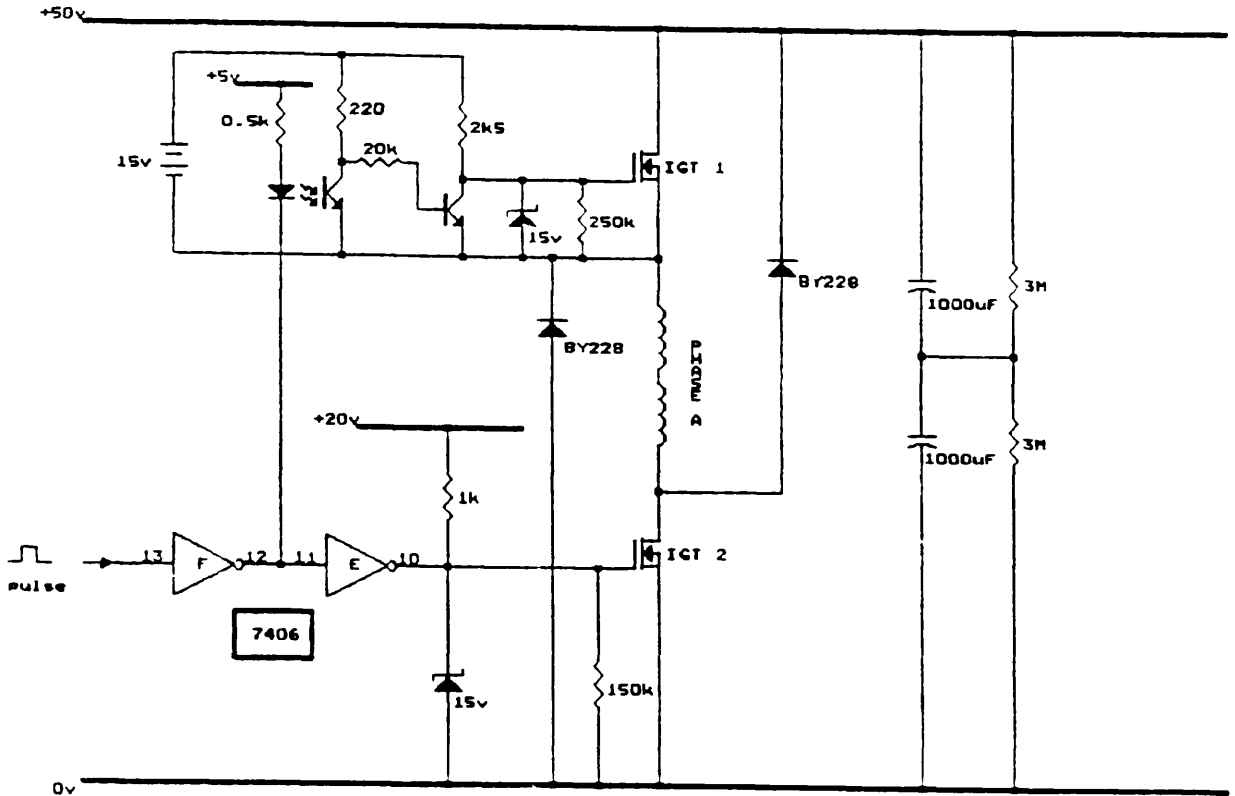


Order Number LMB1008A
NS Package V28A



Multi-mode Commutation and Speed Control
Circuit developed by SPEED and designed
by National Semiconductor UK as a
a monolithic integrated circuit: LMB1008

EXPERIMENTAL TEST CIRCUIT FOR MEASURING FLUX LINKAGE VERSUS TORQUE CHARACTERISTICS FOR DIFFERENT SR MOTOR GEOMETRIES



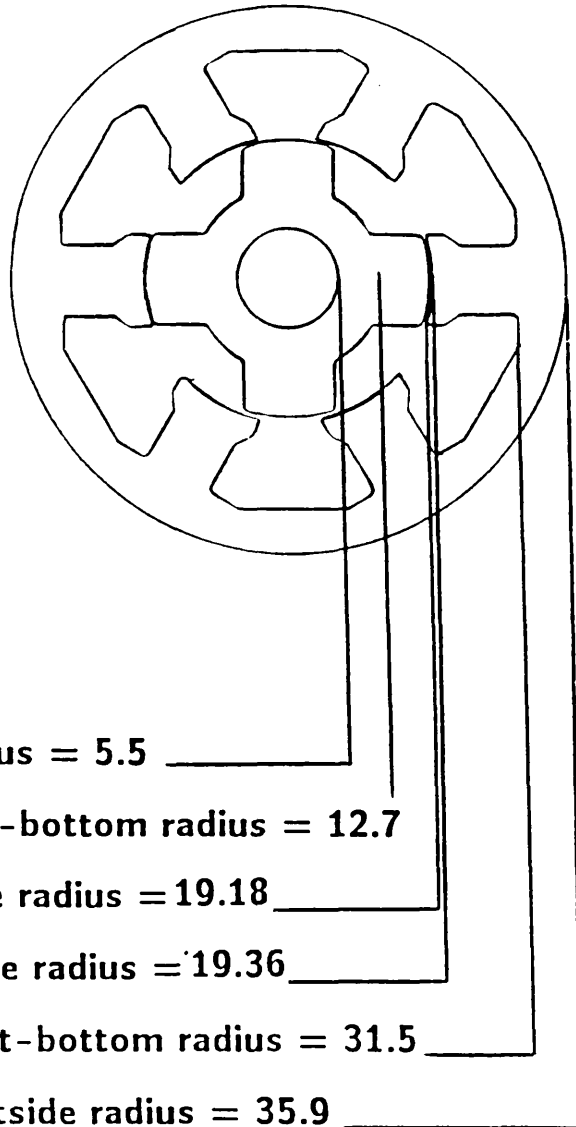
**COMMAND SEQUENCE USED WITH TEKTRONICS
OSCILLOSCOPE TO MEASURE THE FLUX
LINKAGE/CURRENT CHARACTERISTICS**

00 PROG ENTER
01 f LN 01
02 LEFT AQR 1 f WFM
03 RIGHT AQR 2 f WFM
04 2 WFM
05 2 CNS *
06 2 f WFM
07 1 WFM
08 1 CNS *
09 1 f WFM
10 2 WFM
11 1 WFM -
12 4 f WFM
13 TIME
14 STOP

{ set the cursors for one period of}
{ the waveform }
15 MEAN
16 ENTER
17 4 f CNS
18 4 WFM
19 4 CNS -
20 5 f WFM
21 INTG

22 6 f WFM
23 PAUSE
24 8 f VS
25 STOP

72mm SR MOTOR



Shaft radius = 5.5

Rotor slot-bottom radius = 12.7

Rotor pole radius = 19.18

Stator pole radius = 19.36

Stator slot-bottom radius = 31.5

Stator outside radius = 35.9

Rotor pole arc = 34 degrees

Stator pole arc = 32 degrees

Stack length = 55.0

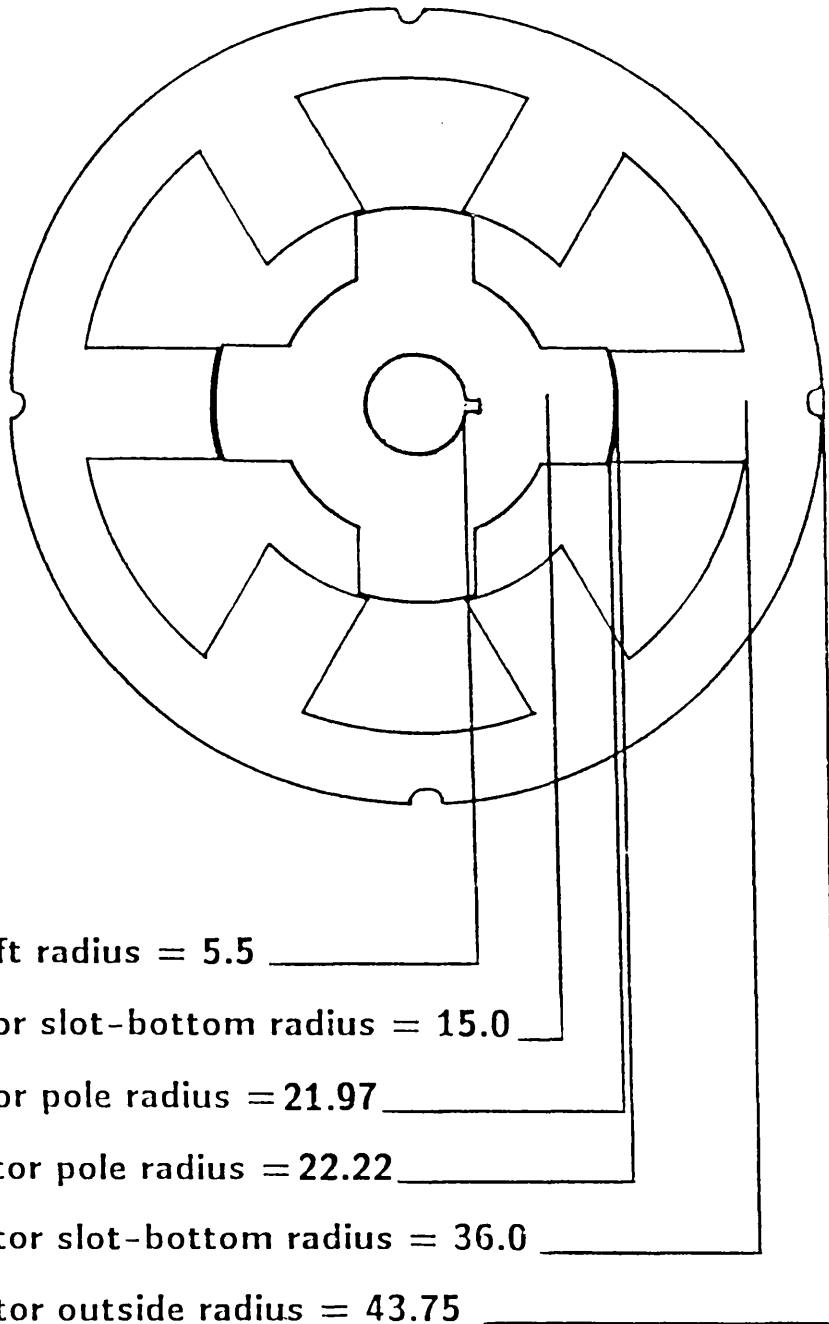
Measured air-gap = 0.020 inches

Number of turns/pole = 150

Wire Size = 0.457mm

Material = Losil 800, varnite coated (0.5mm thick)

88mm SR motor



Rotor pole arc = 34 degrees

Stator pole arc = 32 degrees

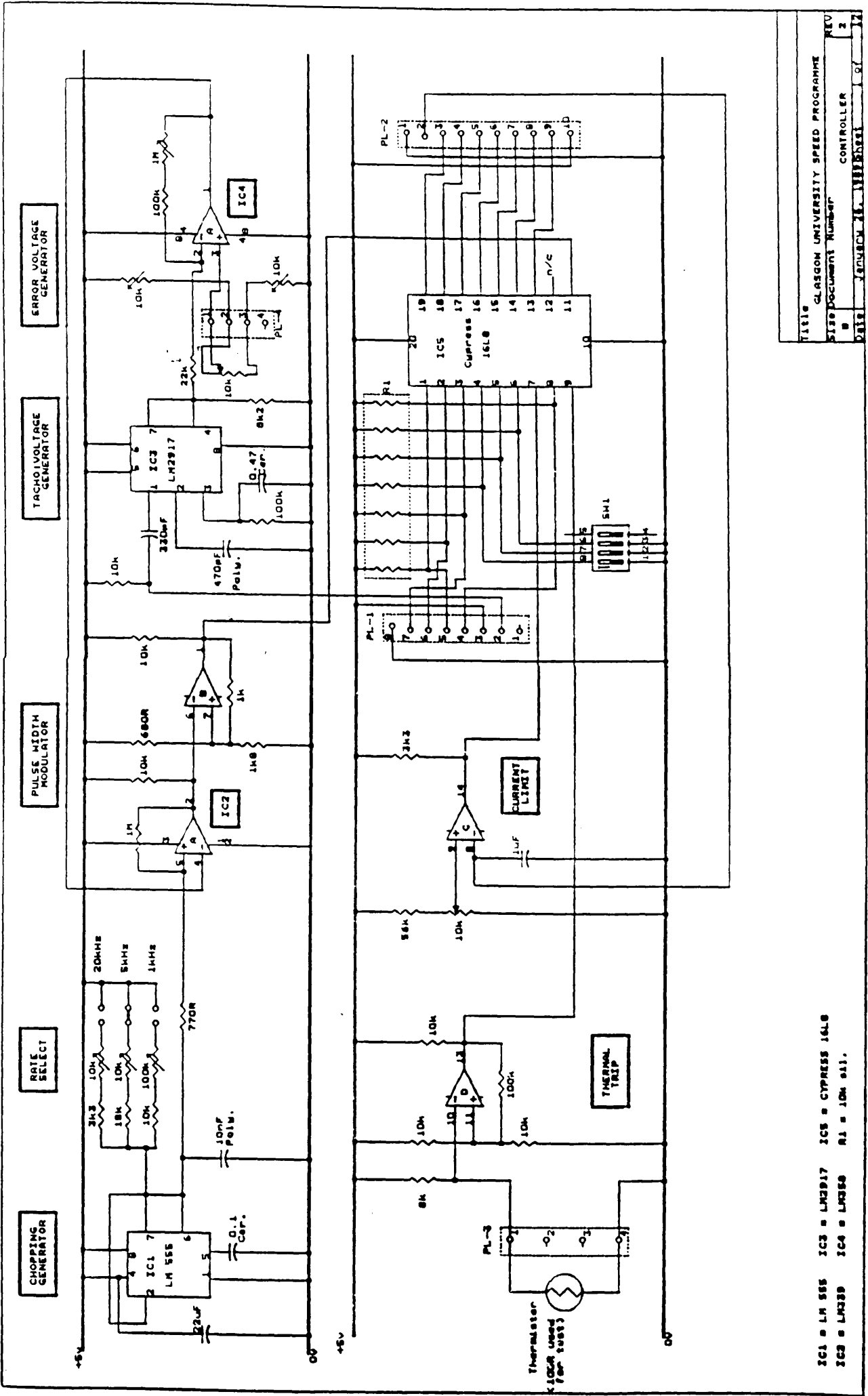
Stack length = 35

Measured air-gap = 0.015 inches

Number of turns/pole = 200

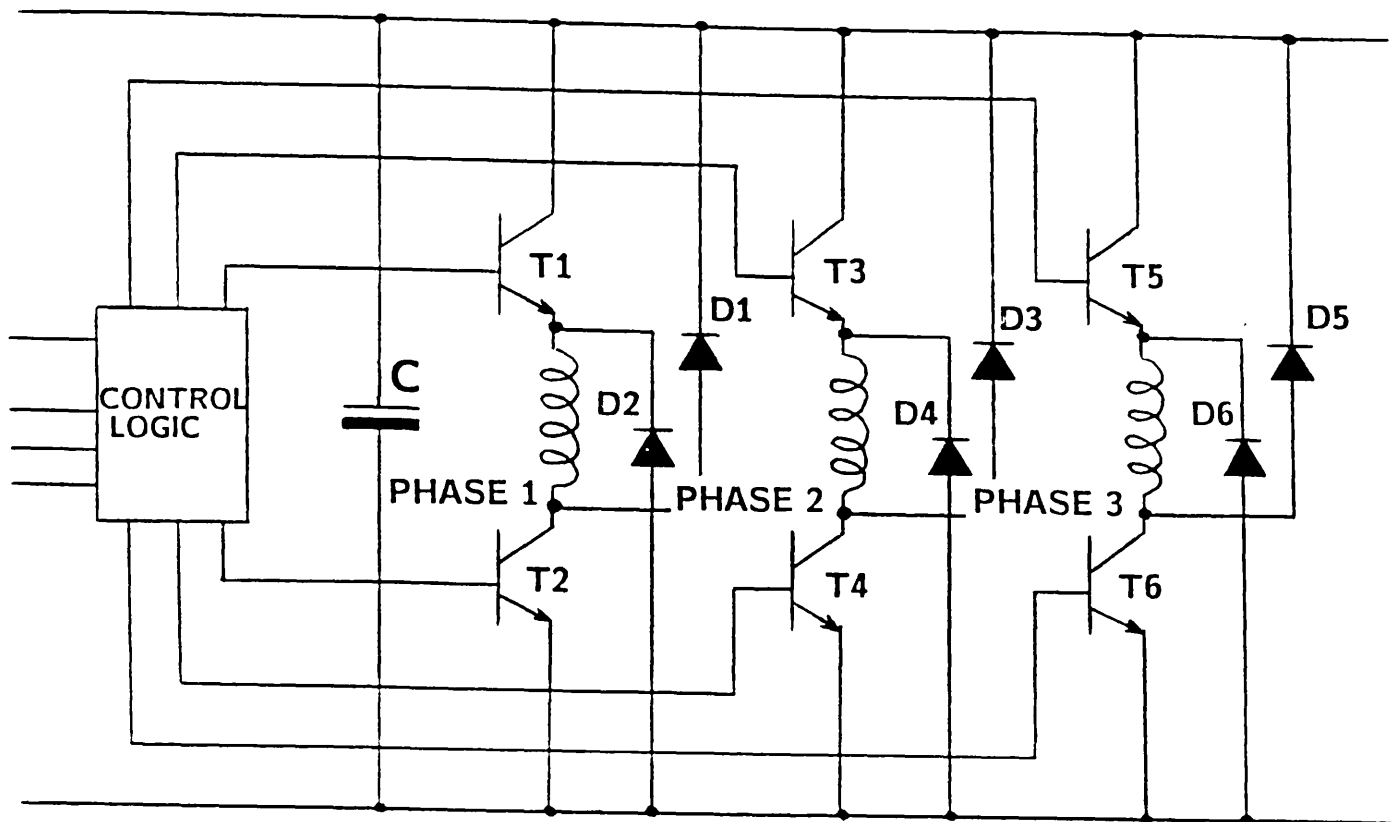
Wire Size = 0.478 mm

Material = Losil 800, varnite coated (0.5mm thick)



IC1 = LM 555 IC3 = LM2917 IC5 = CYPRESS 16L8
 IC2 = LM339 IC4 = LM339 R1 = 10K 0.1.

TABLE	GLASGOW UNIVERSITY SPEED PROGRAMME
REV	2
SHEET	2
DATE	28/05/81
BY	ST

THREE PHASE HALF H BRIDGE INVERTER CIRCUIT FOR SWITCHED RELUCTANCE MOTOR

THEORETICAL CALCULATION OF HEAT STORAGE CAPACITY FOR 72MM SWITCHED RELUCTANCE MOTOR

Total Mass of Losil 500 used = 1388.9g

Total Mass of Copper used = 203g

Total Mass of Aluminium used = 608.1g

$$\begin{aligned}
 \text{Total Heat Storage} &= M_{\text{copper}} C_{\text{copper}} + M_{\text{losil}} C_{\text{losil}} \\
 &\quad + M_{\text{aluminium}} C_{\text{aluminium}} \\
 &= 203 * 0.093 + 1388.9 * 0.107 + 608.1 * 0.211 \\
 C &= 295.8 \text{ Watt secs/ } ^\circ\text{C}
 \end{aligned}$$

THEORETICAL CALCULATION OF HEAT STORAGE CAPACITY FOR 88MM SWITCHED RELUCTANCE MOTOR

Total Mass of Losil 800 used = 1026.7g

Total Mass of Copper used = 194g

Total Mass of Motor Casing = 627.5g

$$\text{Heat Storage Capacity} = M_{\text{casing+losil}} C_{\text{casing+losil}} + M_{\text{copper}} C_{\text{copper}}$$

$$= 1654.2 * 0.107 + 194 * 0.093$$

$$C = 194.9 \text{ Watt secs/ } ^\circ\text{C}$$

Theoretical Calculation of Phase Winding Temperature Rise in 72mm and 88mm Switched Reluctance Motors

Total losses in the motor: $P_{loss} = P_{i/p} - P_{o/p}$

Thermal resistance : $R_t = \text{Final temperature}/P_{loss}$
 $R_t = \quad (\text{ }^\circ\text{C/Watt})$

Heat Storage Capacity = C $\quad (\text{ Watt secs/ }^\circ\text{C})$

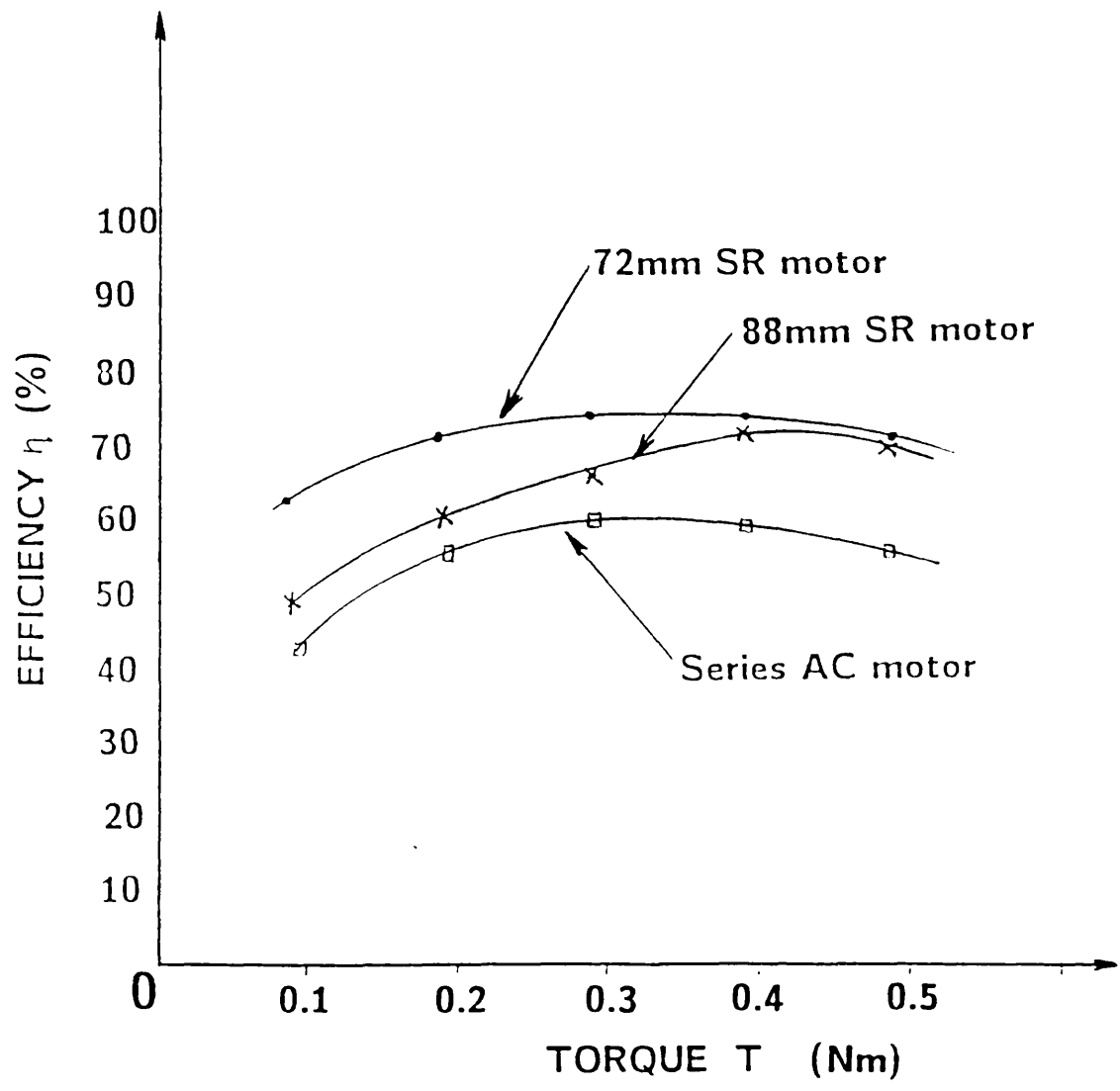
Thermal time constant = TH = CR_t $\quad (\text{ secs })$

If V = Temperature Rise and total losses = I then

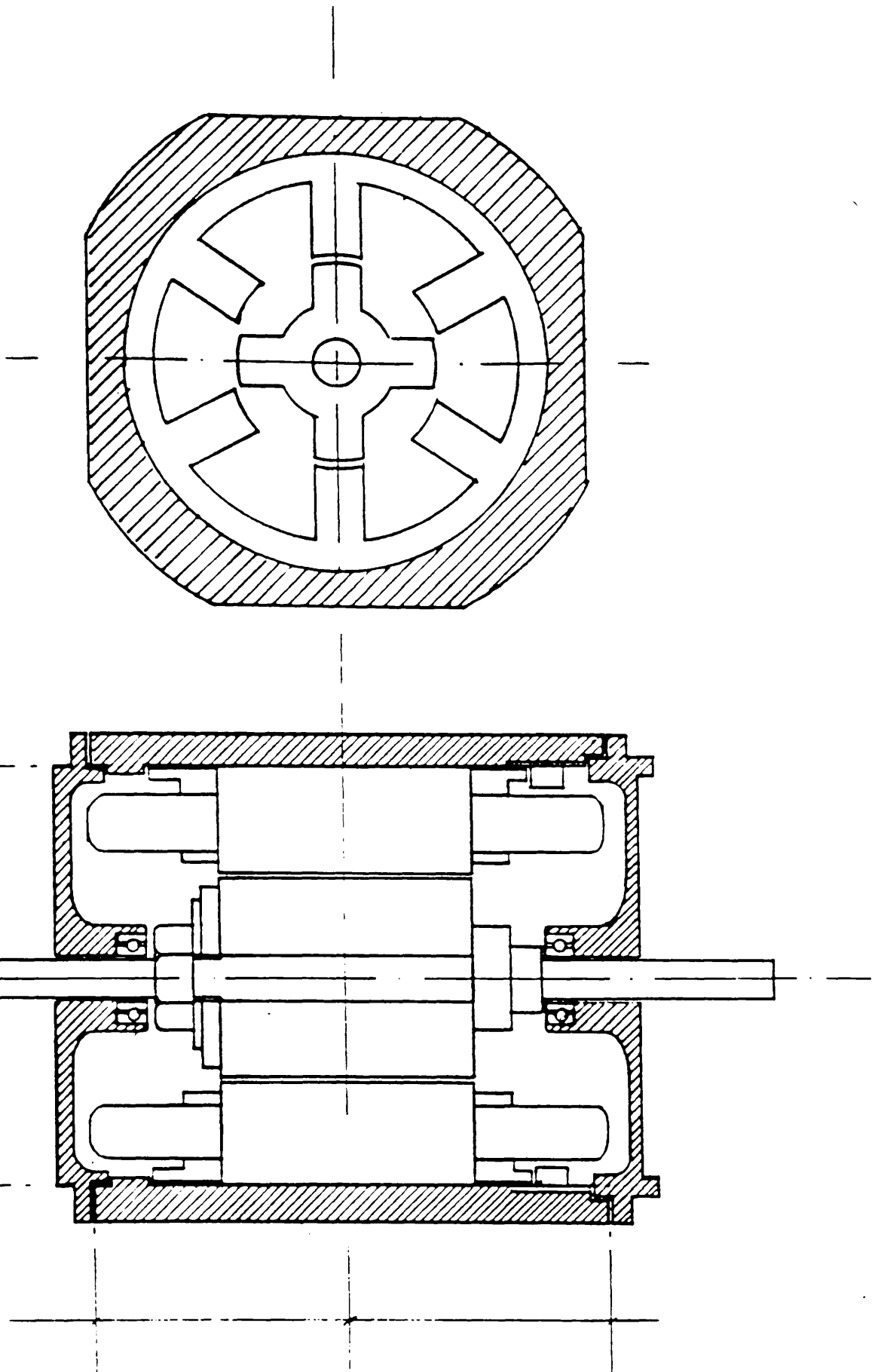
$$V = R_t I \left(1 - e^{-\frac{\text{time elapsed}}{R_t C}} \right)$$

$$V = R_t I \left(1 - e^{-\frac{t}{TH}} \right)$$

Experimental System Efficiency versus Applied Torque for the Series AC Commutator Motor and the 72mm & 88mm SR Motors.



EXPERIMENTAL SR TEST MOTOR LAMINATION CROSS SECTION



SUB-TRANSIENT INDUCTANCE

Consider two coupled circuits with $R=0$

$$V_1 = L_1 \frac{di_1}{dt} + M \frac{di_2}{dt}$$

$$V_2 = 0 = L_2 \frac{di_2}{dt} + M \frac{di_1}{dt}$$

In Laplace form

$$V_1 = sL_1 I_1 + sMI_2$$

$$0 = sL_2 I_2 + sMI_1$$

This then gives $I_2 = - \frac{MI_1}{L_2}$

$$V_1 = sL_1 I_1 - \frac{sM^2 I_1}{L_2}$$

Rearrange to give

$$V_1 = sL_1 I_1 [1 - k^2]$$

Since $M^2 = k^2 L_1 L_2$

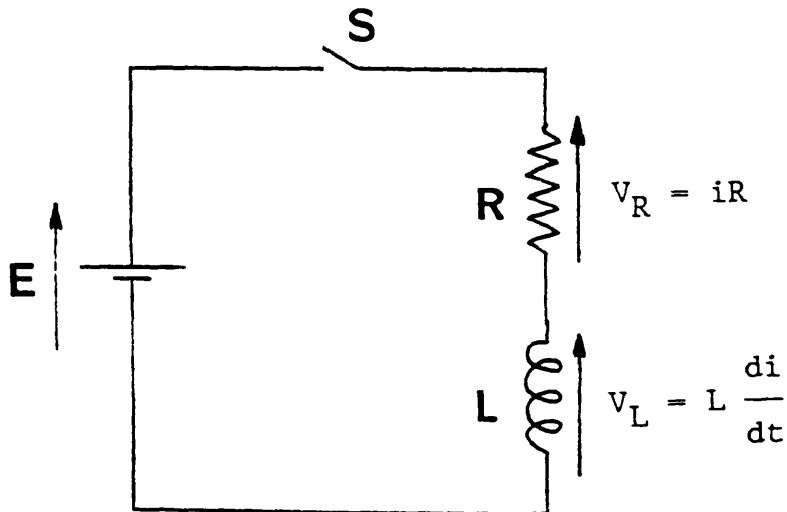
$$V_1 = L_1 \frac{di_1}{dt} [1 - k^2]$$

And since $\frac{V_1}{di/dt}$ is the definition for inductance

$$L' = L (1 - k^2)$$

TRANSIENTS IN SERIES RL CIRCUITS

Consider the series RL circuit below;



With switch S closed;

$$E = iR + L \frac{di}{dt} \quad (1)$$

where i is the instantaneous value of the current.

Rewrite (1) as

$$\frac{R}{L} dt = \frac{di}{E/R - i} \quad (2)$$

so that

$$\int \frac{R}{L} = \int \frac{di}{E/R - i} \quad (3)$$

Integrating both sides gives

$$\frac{R}{L} t = - \ln \left[\frac{E}{R} - i \right] + \ln A \quad (4)$$

where $\ln A$ is a constant of integration.

If $i=0$ when $t=0$ then

$$0 = - \ln \frac{E}{R} + \ln A \quad (5)$$

so

$$A = \frac{E}{R} \quad (6)$$

Substitute back into (4) to give

$$\frac{R}{L} t = - \ln \left[\frac{E}{R} - i \right] + \ln \frac{E}{R} \quad (7)$$

$$\frac{R}{L} t = \ln \left[\frac{E/R}{E/R - i} \right]$$

or in terms of the exponential;

$$e^{Rt/L} = \frac{E/R}{E/R - i} \quad (8)$$

Solving for i

$$i = \frac{E}{R} \left[1 - e^{-Rt/L} \right] \quad (9)$$

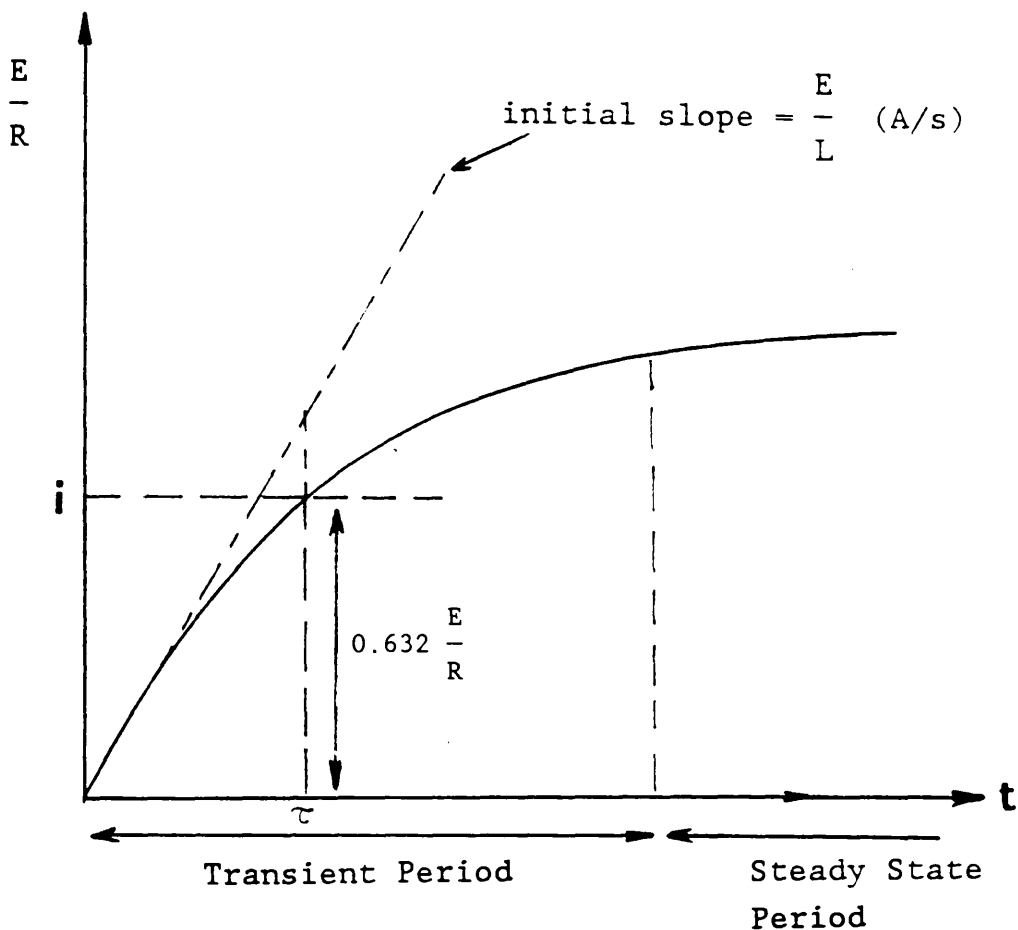
The voltage across the resistor (V_R) is given by

$$V_R = iR = E \left[1 - e^{-Rt/L} \right] \quad (10)$$

The voltage across the inductor (V_L) is given by

$$V_L = E - V_R = E e^{-Rt/L} \quad (11)$$

A plot of the current rise against elapsed time shows the characteristic exponential build up. This is shown in the figure below.



The final value if the current i : i.e., $t = \infty$

$$(i)_{t = \infty} = \frac{E}{R} \left[1 - e^{-\infty} \right] = \frac{E}{R} \quad (12)$$

The initial rate of rise of current i : $(i)_{t = 0} = 0$

$$E = R (i)_{t=0} + L \left[\frac{di}{dt} \right]_{t=0} \quad (13)$$

And so

$$\left[\frac{di}{dt} \right]_{t=0} = \frac{E}{L} \quad (\text{A/s}) \quad (14)$$

If the initial rate of rise of current were maintained, it would reach a value for i of E/R in τ seconds.

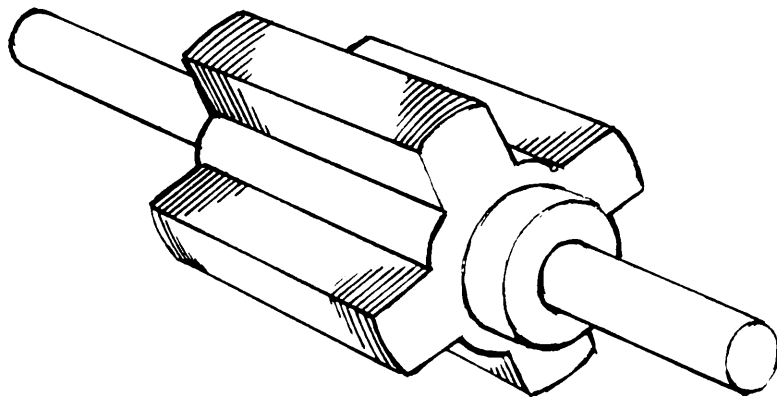
$$\text{where } \tau = \frac{\text{Final Value of } i}{\text{Initial rate of rise}} = \frac{E/R}{E/L} = \frac{L}{R} \quad (15)$$

When $t = \tau$

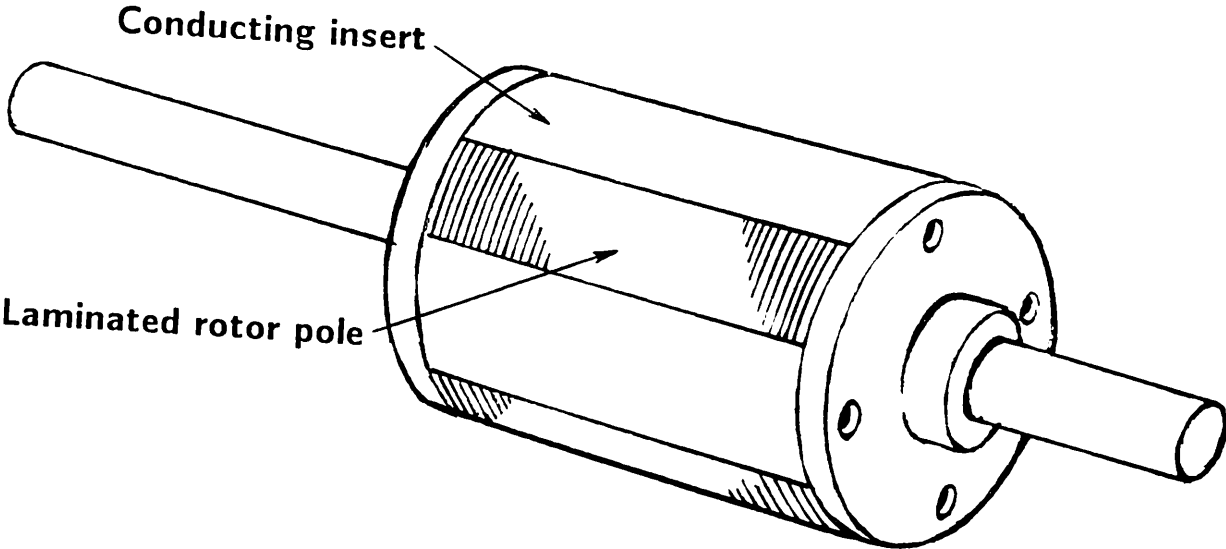
$$(i)_{t=\tau} = \frac{E}{R} \left[1 - e^{-1} \right] = \frac{E}{R} \left[1 - 0.368 \right] \quad (16)$$

$$(i)_{t=\tau} = 0.632 \frac{E}{R} \quad (17)$$

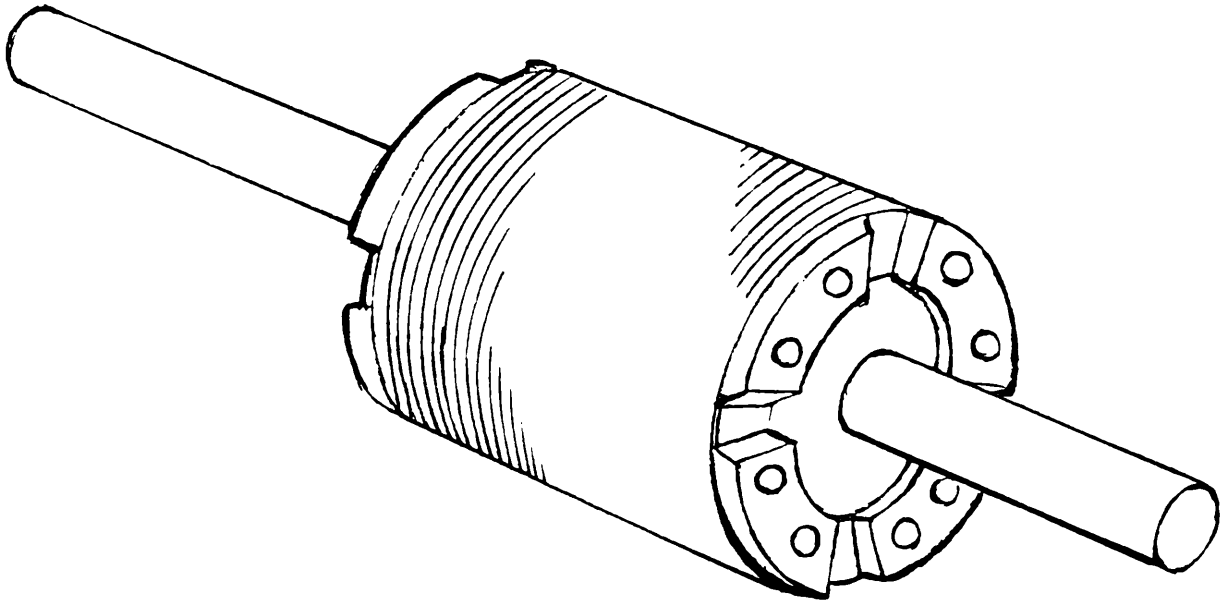
CONVENTIONAL SRM ROTOR



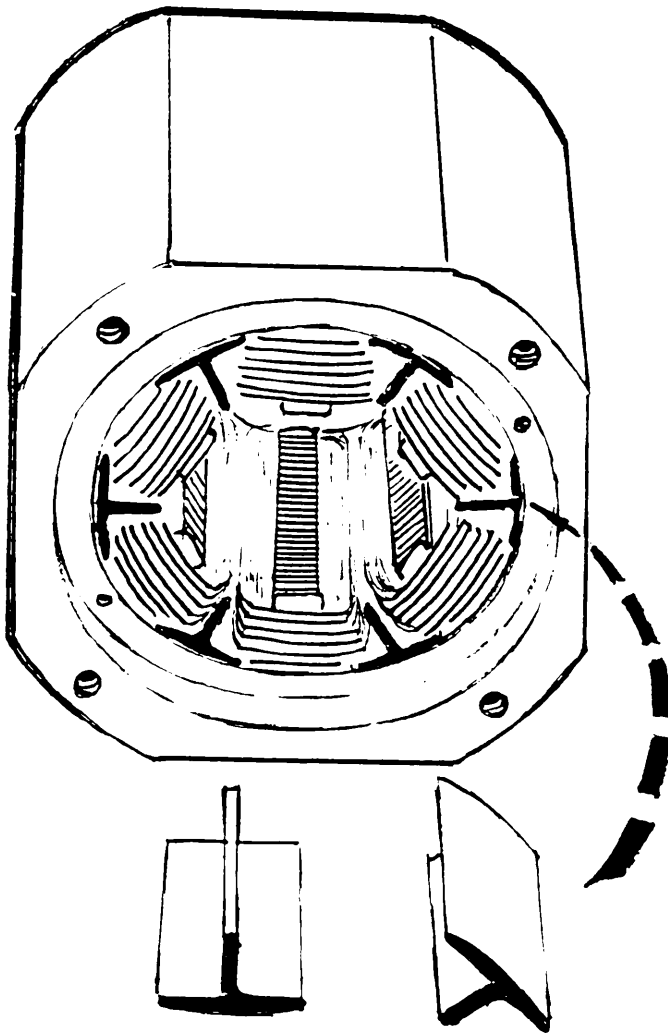
CONDUCTING INSERT ROTOR



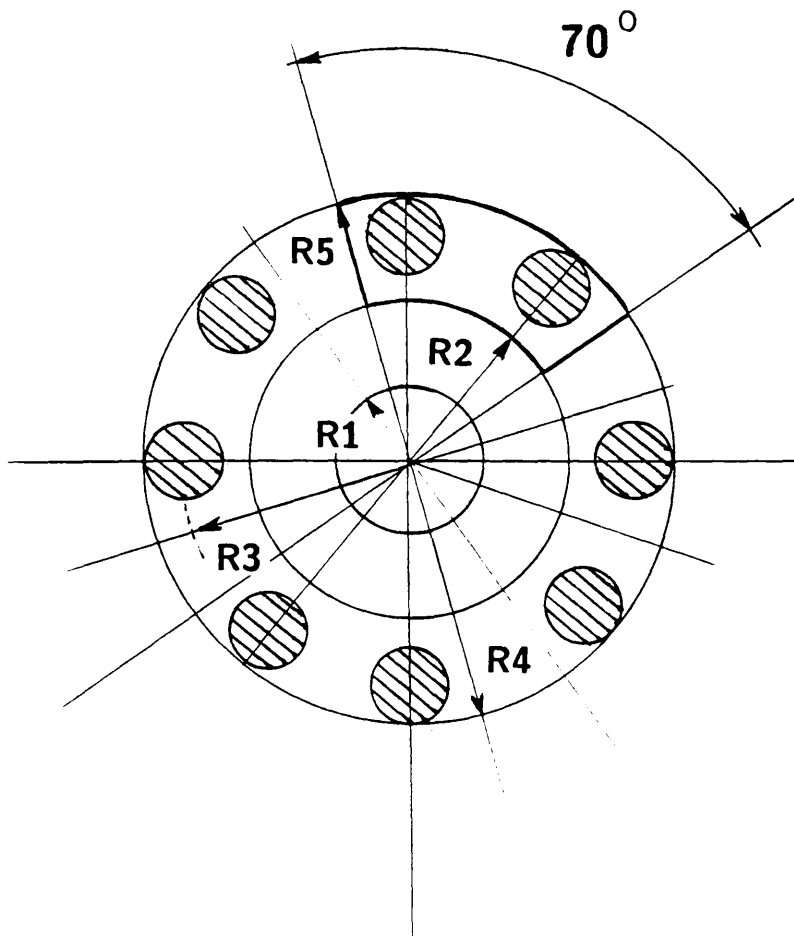
COPPER BAR ROTOR



CONDUCTING STATOR SLOT SCREENS



COPPER BAR ROTOR CONSTRUCTION



R1 = SHAFT RADIUS = 4.76mm

R2 = LINK INNER RADIUS = 10.35mm

R3 = PITCH CIRCLE RADIUS = 15.22mm

R4 = ROTOR RADIUS = 17.6mm

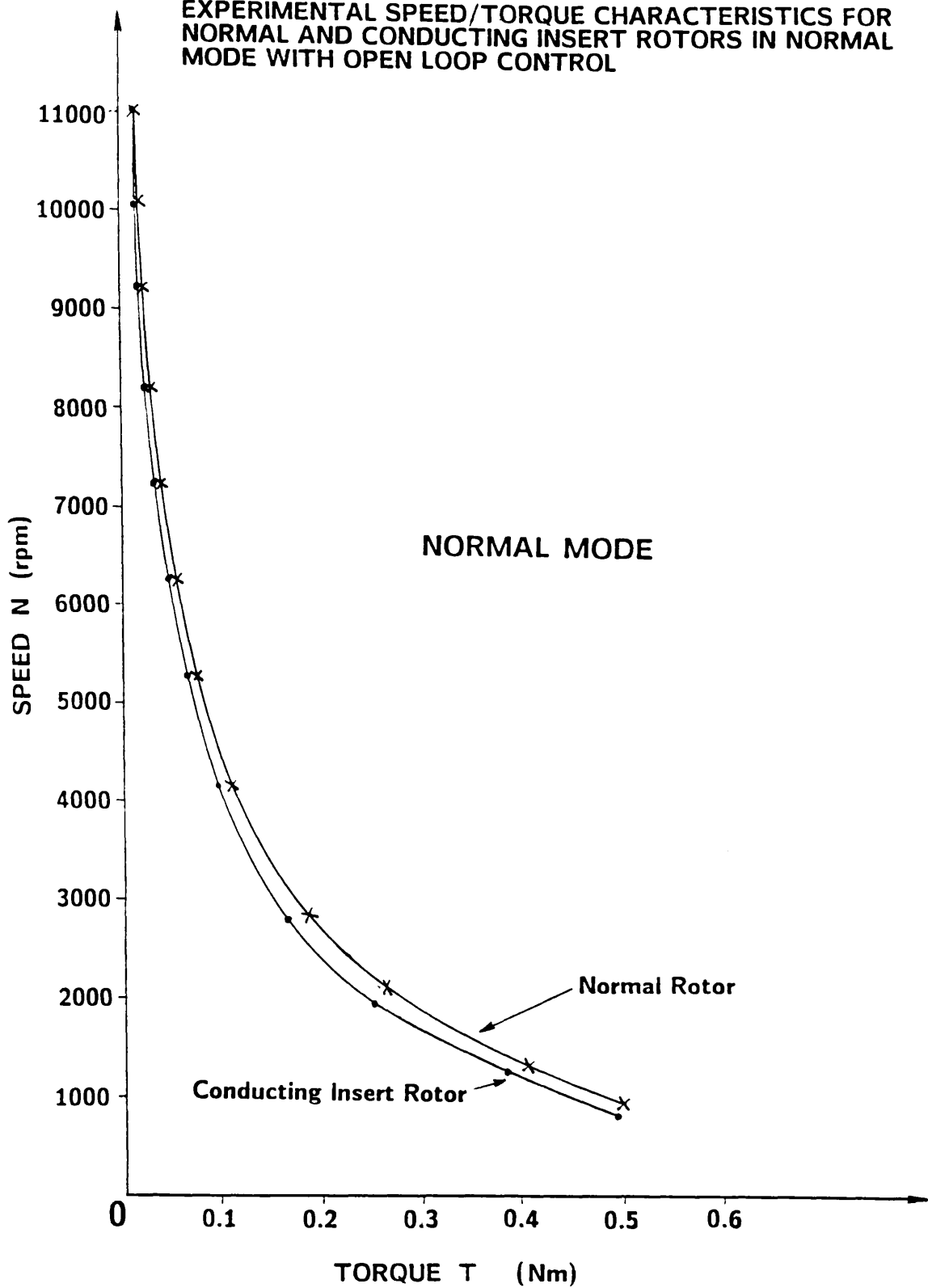
R5 = LINK OUTER RADIUS = 17.6mm

RING THICKNESS = 2.1mm

COMMAND PROCEDURE FOR FINITE-ELEMENT PACKAGE

<DUPL>	Duplicate the field stack entry
<MULT>	Multiply both entries to get B^2
<DUPL>	Duplicate
<VALU C007 MAIN>	Obtain the value of $1/u_r$
<MULT>	Multiply $1/u_r$ by B^2
<INTE>	Integrate this product over each element and make it accessible to the numeric stack
<DISC>	Discard the above integral from the field stack
<STAC NUME>	Activate the numeric stack
<PUSH>	Place the total surface integral in the numeric stack
<ENTE 397888>	Enter the value of $1/2xu_0$
<PUSH>	Place it in the numeric stack
<MULT>	Multiply 397888 by above integral
<STAT>	Display the contents of the numeric stack. Obtain the energy value under "REAL COMPONENT". The units are in Joules (J).

EXPERIMENTAL SPEED/TORQUE CHARACTERISTICS FOR
NORMAL AND CONDUCTING INSERT ROTORS IN NORMAL
MODE WITH OPEN LOOP CONTROL



EXPERIMENTAL SPEED/TORQUE CHARACTERISTICS FOR
NORMAL AND CONDUCTING INSERT ROTORS IN LONG
DWELL MODE WITH OPEN LOOP CONTROL

